DESIGN, ANALYSIS AND APPLICATION OF FLUX-MODULATED MACHINES

YULONG LIU

Ph. D

The Hong Kong Polytechnic University

2016

The Hong Kong Polytechnic University

Department of Electrical Engineering

Design, Analysis and Application of Flux-modulated Machines

Yulong Liu

A thesis submitted in partial fulfilment of the requirements for the degree of Doctor of Philosophy

May, 2016

Certificate of Originality

I hereby declare that this thesis is my own work and that, to the best of my knowledge and belief, it reproduces no material previously published or written, nor material that has been accepted for the award of any other degree or diploma, except where due acknowledgement has been made in the text.

<div style="text-align: right;">

_____

Name of student: Yulong Liu

</div>

Abstract

Electric machines have a history of nearly 200 years. They have played a key role in the electrification of our society and they are widely used nowadays both in industry and our everyday life. A basic rule for designing an electric machine is that the pole number of the stator and the pole number of the rotor should be equal. However, the emergence of flux-modulated (FM) machines breaks this rule. In a FM machine, the excitation field and the armature field interact over their harmonic components, which is the so-called flux modulation effect or magnetic gearing effect since it was first used in magnetic gears. Due to their special working principle, the FM machines own some different characteristics from conventional electric machines such as more flexible pole number combination and the possibility of realizing multi-port design. These features of FM machines make them suitable for a number of certain applications. In this thesis, the design, analysis, and the potential applications of FM machines are introduced.

The thesis mainly includes the following contents.

a) A literature review on the development of different types of FM machines is presented. These machines include the basic FM machines (BFMMs), the vernier permanent-magnet (PM) machines (VPMMs), the doubly-fed reluctance machines (DFRMs), and the dual-excitation PM machines (DEPMMs).

b) The magnetics gears and the flux modulation effect are introduced. A unified theory for FM machines is proposed. Using the proposed

theory, the operating principles of different FM machines are explained in a unified way.

c) The general design rules for different components, namely the winding, the PM and the flux modulation poles, in a FM machine are introduced.

d) A quantitative performance comparison among different types of FM machines is conducted. Based on the comparison result, the potential applications of these machines are identified.

e) Two FM machines are designed for electric vehicle propulsion and wind power generation, respectively, to showcase the potential applications of FM machines. The performance of these two machines are analyzed using FEM. Prototypes are made and tested for validation.

List of Publications

[1] Y. Liu, S. L. Ho, and W. N. Fu, "Novel electrical continuously variable transmission system and its numerical model," *IEEE Trans. Magn*, vol. 50, no. 2, Feb. 2014.

[2] Yulong Liu, Shuangxia Niu, S. L. Ho, and W. N. Fu, "A New Hybrid-Excited Electric Continuous Variable Transmission System," *IEEE Trans. Magn.,* vol. 50, no. 11, Nov. 2014.

[3] Shuangxia Niu, Yulong Liu, S. L. Ho, and W. N. Fu, "Development of a Novel Brushless Power Split Transmission System for Wind Power Generation Application," *IEEE Trans. Magn.,* vol. 50, no. 11, Nov. 2014.

[4] Y. Liu, S. L. Ho, W. N. Fu, "A Novel Magnetic Gear with Intersecting Axes," *IEEE Trans. Magn.,* vol. 50, no. 11, Nov. 2014.

[5] Yulong Liu, S. L. Ho, W. N. Fu and Xiu Zhang, "Design Optimization of a Novel Doubly Fed Dual-Rotor Flux-Modulated Machine for Hybrid Electric Vehicles," *IEEE Trans. Magn.,* vol. 51, no. 3, Mar. 2015.

[6] Yulong Liu, Shuangxia Niu, S. L. Ho, W. N. Fu, and T. W. Ching, "Design and Analysis of a New HTS Double-Stator Doubly-Fed Wind Generator," *IEEE Trans. Appl. Supercond.,* vol. 25, no. 3, Jun. 2015.

[7] Yulong Liu, W. N. Fu, S. L. Ho, Shuangxia Niu, and T. W. Ching, "Electromagnetic Performance Analysis of Novel HTS Doubly-Fed Flux-Modulated Machines," *IEEE Trans. Appl. Supercond.,* vol. 25, no. 3, Jun, 2015.

[8] Yulong Liu, Shuangxia Niu, and W. N. Fu, "A Novel Multi-Phase Brushless Power Split Transmission System for Wind Power Generation," *IEEE Trans. Magn.*, vol. 52, no. 2, Feb. 2016.

[9] Yulong Liu, W. N. Fu, Wei Li, and Mingui Sun, "Design and Analysis of a Shoe-embeded Power Harvester Based on Magnetic Gear," *IEEE Trans. Magn.*, Accepted.

Acknowledgement

I would like to express my best gratitude and appreciation to my chief supervisor Dr. W. N. Fu for his great guidance and supervision on my study during the last four years. His attitude and dedication to research always inspire me.

I would also like to express special thanks to Dr. S. Niu. She provided so much help on my work and I learned a lot from her.

I am grateful to my co-supervisor Dr. C. Y. Chung. Without his help, I could not come to study in PolyU.

I wish to thank Prof. M. Sun for hosting and supervising me during my attachment program. His enthusiasm on research will always motivate me.

In addition, many other members in our research group helped me a lot on both my work and life. It has been a great experience working with them and I am grateful to all of them.

My special gratitude goes to my mother who always supports me for every choice I make. I wish all the best for her.

Finally, I would like to acknowledge the Hong Kong Polytechnic University for supporting me to finish my project.

Contents

Chapter 1

Introduction

1.1 Electric machines

An electric machine is an electromagnetic device for energy conversion from electrical to mechanical, in which process it is usually called a motor, or from mechanical to electrical, in which process it is usually called a generator. For over a century, electric machines have been the most important type of devices for energy conversion concerning electricity. They are used in most electricity generation processes and about half of the electricity generated globally is consumed by electric motors [A1]. Recently, with the fast development of power electronics, the accurately controlled electrical drive is becoming more and more popular as it is efficient and provides good control properties for various applications [A2]. Due to the large power flow related to electric machines, it is of great significance to improve the efficiency of electrical machines for energy saving and environmental protection, which gives electrical engineers a good reason to design new and efficient electric machines.

The induction machines, especially the squirrel-cage induction machines (SCIMs), have been dominant in the electric machine market for a long time because they are rugged, reliable and their costs are low [A3]. However, the induction machines have some inherent drawbacks, namely relatively low efficiency, low power density (power capacity per volume),

low power factor and their accurate control is complex. Since the late 20th century, benefiting from the fast development of permanent magnet material, the performance of PM machines has been significantly improved while their cost is getting lower. Compared with SCIMs, these permanent magnet machines usually have advantages in consideration of efficiency, power density, and power factor [A4]. The PM motors with power electronic drivers also provide good control property. Nowadays, a trend in both industrial and civilian applications is to replace the SCIMs with permanent magnet machines.

In recent years, the environmental and energy problems are drawing more and more attention and many solutions have been proposed to address them. Some of these solutions raise new requirements on the performance of electric machines. For example, in a wind power generation system, the generator needs to have a low operation speed and high torque density (torque capacity per volume). In a single-motor electric vehicle powertrain, the electric motor needs to have a wide operation range and high power density. Although the conventional machines can be used in these applications, their performance is not so satisfactory, which give rise to the development of new types of electric machines.

1.2 Flux-modulated machines

Recently, a new kind of electric machine, namely the FM machine, has drawn much attention from researchers and engineers. As the FM machines use asynchronous field harmonics to realize energy conversion, they break the basic principle for conventional machine design which requires the stator and the rotor to have the same pole number. The FM

machine makes the machine design more flexible, which is especially significant when a high pole number is required in low-speed applications.

The fact that FM machines work on harmonic field makes them quite different from conventional machines. Although the working principles and performance of different FM machines have been reported in a number of references, a systematic and comprehensive study is still desirable. The working principles and design methods for FM machines need to be studied. The performance of different FM machines also need to be quantitatively compared together with that of the conventional synchronous machines. Considering the pros and cons of them, the suitable applications for FM machines need to be clarified and studied.

1.3 Thesis outline

The thesis aims to study the working principle, design method, and performance of FM machines. The pros and cons are concluded through the study and the suitable applications are identified accordingly. Chapter 2 gives an overview of various types of FM machines. The historical development and brief working principles of these machines are introduced. In Chapter 3, a unified theory of FM machines is derived from a coaxial magnetic gear model. Using this unified theory, the working principles of different types of FM machines are explained. In Chapter 4, the general principles for the design of FM machines are introduced. Particularly, the winding design, the PM design, and the design of the flux modulation pole-pieces are introduced. In Chapter 5, a comparison among different FM machines and a conventional PM synchronous machine (CPMSM) is performed. All these machines are designed and optimized under the predetermined constraints. Based on the comparison results, the

potential applications of FM machines are classified. In Chapter 6, a FM machine with wide speed range is designed for in-wheel EV drive. A prototype is made and tested for validation. Chapter 7 presents a doubly-fed dual-rotor FM machine which is designed for wind power generation. This FM machine is also prototyped and tested for performance validation. A brief summary and recommendations for further study are presented in Chapter 8.

References - part A

[A1]   H. Pyrhonen, etc, *Design of rotating electrical machines*, Wiley, UK, 2008.

[A2]   S. K. Sul, *Control of electric machine drive systems*, John Wiley & Sons, New Jersey, 2011.

[A3]   S. J. Chapman, *Electrical Machinery Fundamentals*, McGraw Hill, New York, 2005.

[A4]   J. F. Gieras, *Permanent magnet motor technology: design and applications*, CRC Press, USA, 2010.

Chapter 2

Overview of flux-modulated machines

2.1 Introduction

In recent years, several kinds of non-conventional electric machines emerged or re-emerged to draw much attention with their special features. These machines include a basic FM machine (BFMM), a vernier permanent-magnet (PM) machine (VPMM), a dual-excitation PM machine (DEPMM), and a doubly-fed reluctance machine (DFRM). An outstanding feature that differs these machines from the conventional synchronous electric machines is that, the pole-pair number of the stator can be different from that of the rotor, which breaks the basic rule of conventional electric machines. Although the working principles of these machines are explained in different ways in literature, some inherent similarities clearly exist among them and they all can be summarized as general FM machines.

Generally, the FM machines refer to the category of electric machines whose working principles are based on the flux modulation effect. The flux-modulation effect is also called the vernier effect or the magnetic gearing effect as it is first used in coaxial magnetic gears. In these coaxial magnetic gears or FM machines, the magnetic field path is non-even, which causes asynchronous flux harmonics to realize the speed variation and torque transmission.

2.2 Magnetic gears, magnetic-geared machines and basic flux-modulated machines

The magnetic gear concept is an electromagnetic counterpart of the mechanical gear. The gears are a very basic yet important type of components and they are used everywhere. However, the mechanical gears have some inherent drawbacks, such as vibration, acoustic noise and wear, which limit their applications. The magnetic gears are proposed to replace mechanical gears because of their non-contact elements. The early magnetic gears have a poor usage of PM material. The coaxial magnetic gear, which is based on the flux modulation effect, is then proposed, which significantly improves the torque performance.

The first try to introduce the flux modulation effect into electric machines is realized by the magnetic-geared machine. As is shown in the name, a magnetic-geared machine is essentially a combination of a conventional PM machine and a magnetic gear. A magnetic gear is incorporated into the machine so as to amplify the output torque and fractionalize the speed of the machine. By simplifying the structure of the magnetic-geared machine, namely removing one of the two PM rotors, the basic FM machine is proposed.

2.2.1 Magnetic gears

Since the early 20th century, a number of magnetic gears have been proposed. The early magnetic gears use magnetizing coils for the excitation field. Later on, permanent magnets are used to substitute the coils. However, these magnetics gears usually have a poor utilization of

the PM material because only a small number of PMs take effect at any one time. A typical example is a magnetic spur gear as shown in Fig. 2.1.

In 2001, a coaxial magnetic gear with slotted intermediary ferromagnetic pole-pieces (FMPs) was proposed [B1]. In this magnetic gear, different numbers of PMs are mounted on the inner rotor and the outer rotor and a specific number of steel pole pieces are fixed between the two rotors. As is shown in Fig. 2.2, the magnetic gear has two rotors with PMs mounted on the back iron. Due to the existence of the FMPs between the rotors, the airgap permeance is uneven and asynchronous harmonics of the PM field are generated. The PM rotors can hence interact with each other over the common harmonics to realize stable torque transmission and speed variation. When the losses are neglected, the torque and speed relationships between the PM rotors are,

$$\frac{T_1}{T_2} = \frac{\omega_2}{\omega_1} = \frac{P_1}{P_2} = G_r \tag{2.1}$$

where; T_1 and T_2 are the torque of the PM rotors, respectively; ω_1 and ω_2 are the speeds; P_1 and P_2 are the pole-pair numbers; G_r is defined as the gear ratio, which is similar to the concept in a mechanical gear.
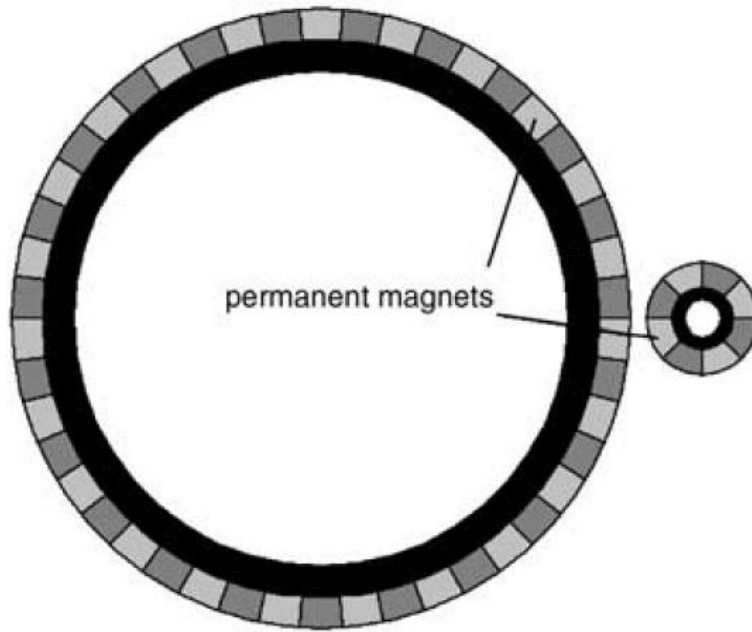
Fig. 2.1. A magnetic spur gear [B1].
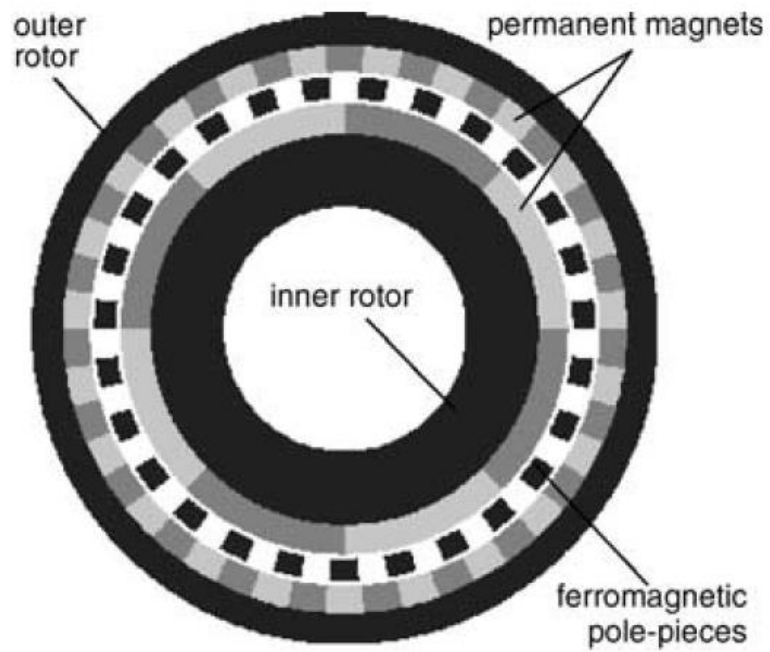
Fig. 2.2. A coaxial magnetic gear [B2].

2.2.2 Magnetic geared machines

In [B3], a magnetic-geared machine is proposed by combining a coaxial magnetic gear with a conventional permanent magnet machine as shown in Fig. 2.3. This machine has two rotors with permanent magnet. The inner rotor has two layers of permanent magnets which are separated by stainless steel. The inner layer of PM interacts with the stator windings like a conventional permanent magnet machine with outer rotor configuration. The outer layer of PM on the inner rotor constitutes a coaxial magnetic gear with the steel pole-pieces and the outer rotor. In this way, the torque on the inner rotor is amplified by the gear ratio through the magnetic gear.

In [B4], another magnetic-geared machine which uses the steel pole-pieces as the low speed rotor is proposed. The magnetic gear and the electric machine are combined both mechanically and electromagnetically since the magnetic flux path is continuous. But the airgap between the windings and the high speed rotor is large in this machine, which makes its airgap reluctance high. In [B5], a magnetic-geared machine is constructed by embedding windings among the slots between the steel pole-pieces. The windings directly drive the inner high-speed rotor and the outer low-speed rotor is driven accordingly through magnetic gearing. This design is expected to achieve better utilization of PM material and save space inside the machine.
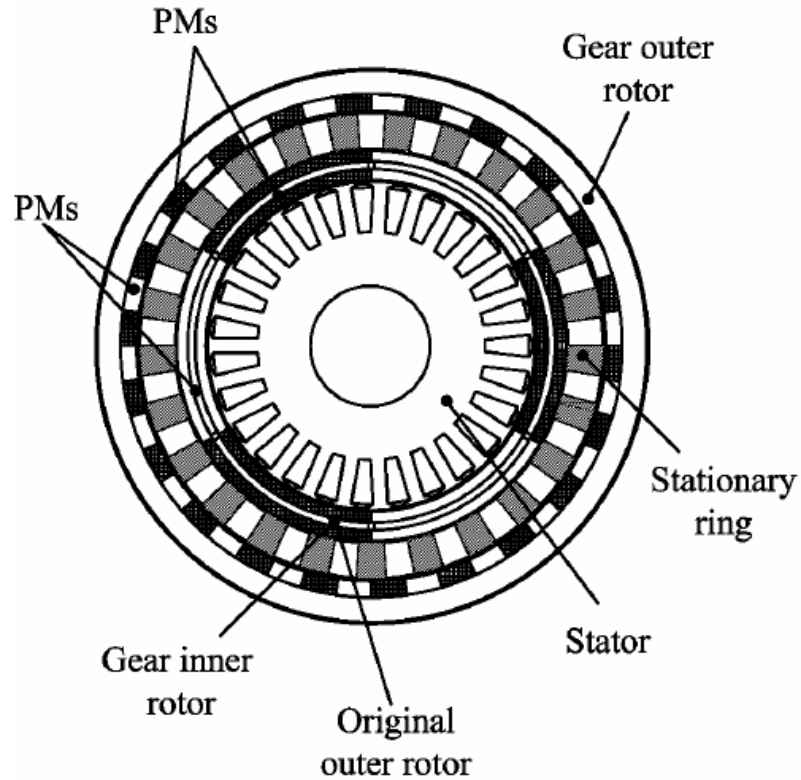
Fig. 2.3. A MG integrated machine [B3].

2.2.3 Basic FM machines

To simplify the structure, the BFMM is proposed with the shared rotor omitted so that the winding field can directly interact with the PM field of the rotor.

As shown in Fig. 2.4(a), the basic magnetic FM motor has a stator with a set of three-phase windings and a rotor with PMs [B6]. Between the stator and rotor, a set of stationary ferromagnetic segments is sandwiched. The magnetic field produced by the PMs is modulated by the ferromagnetic segments and reacts with the magnetic field produced by the armature.

In [B7], a BFMM with a consequent-pole PM rotor is proposed as shown in Fig. 2.4(b). An axial flux type BFMM is proposed in [B8] as shown in Fig. 2.4(c). To improve the power density, the stator is sandwiched by the two parts of the outer rotor and the corresponding ferrite segments. When the ferrite segments and the rotor PMs on the two sides of the stator are placed in alignment respectively, the torques from the two parts of the rotor add up to the output torque. A recent research [B9] shows that, as the free space between the ferrite segments naturally forms ventilating ducts, the axial flux BFMM has better heat dissipation, which is very meaningful for improving the power density.
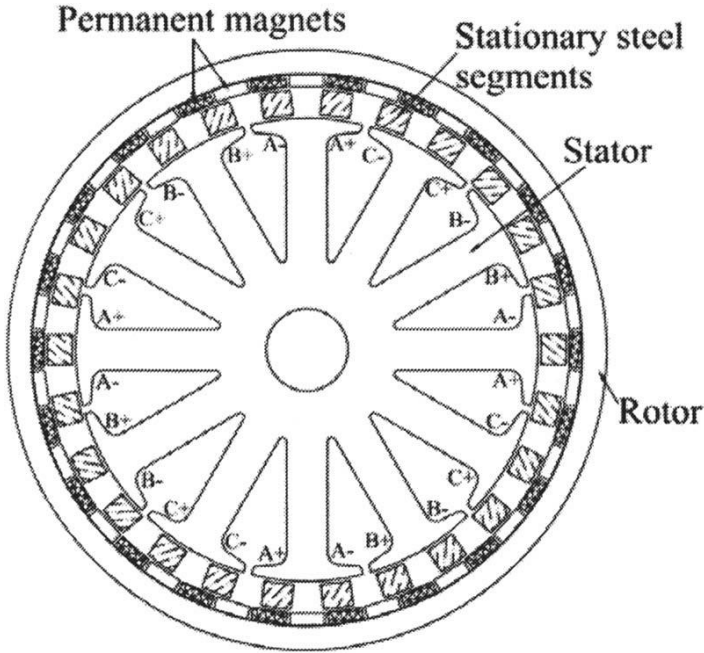
(a)
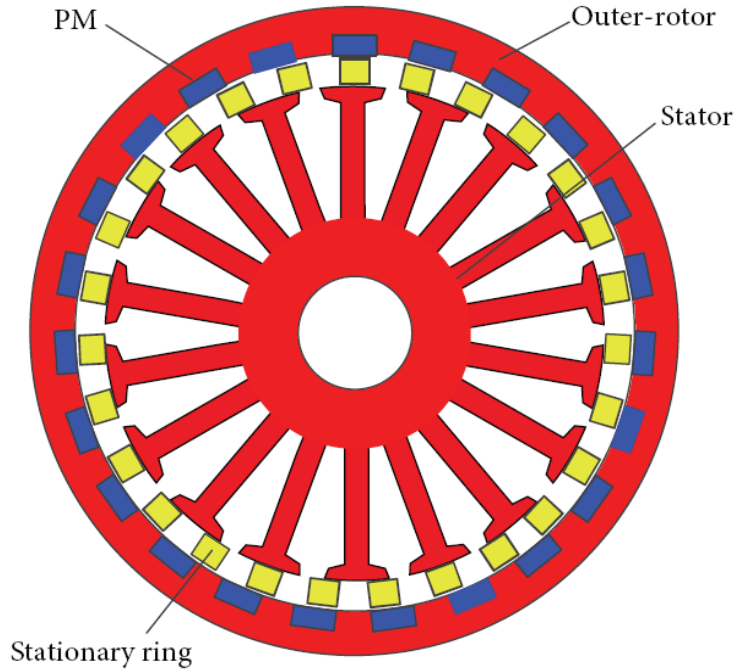
(b)
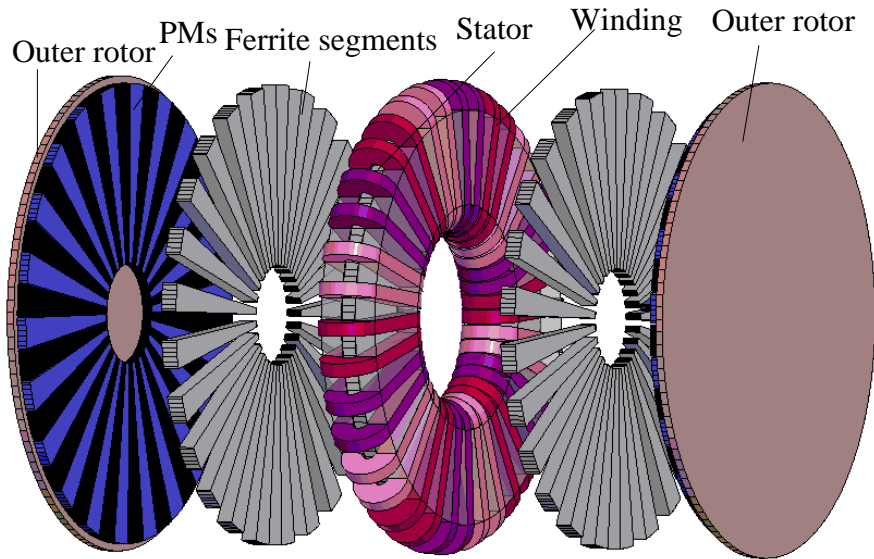
(c)

Fig. 2.4. (a) Radial-flux BFMM I [B6]. (b) Radial-flux BFMM II [B7]. (c) An axial-flux BFMM [B8].

2.3 Vernier PM machines and dual-excitation PM machines

2.3.1 Vernier PM machines

The idea of VPMM comes from the vernier reluctance motor which is designed for very-low-speed applications. As shown in Fig. 2.5(a), the vernier reluctance motor has an open-slot type stator and a rotor which is similar to that of switched reluctance motor [B10]. The particular feature of the vernier reluctance motor is that, a small displacement of one-half slot pitch of the rotor will cause a 90 degrees displacement of the permeance axis, which is depicted in Figs. 2.5(b) and (c). As a result, the rotor rotates at a much slower speed than the winding field speed.

The VPMM is developed based on the vernier reluctance motor by replacing the reluctance rotor with a PM rotor. As it is similar to the principle of the vernier reluctance motor, in the VPMM shown in Fig. 2.6(a), a displacement of one pole pitch of the PM rotor will cause a 90 degree displacement of the permanent magnetic flux in the stator. Due to the introduction of PMs, the power density and efficiency are significantly improved [B11].

As shown in Fig. 2.6(b), the stator of VPMM also can be designed as the split-pole type besides the open-slot type [B12]. In [B13], a comparison between these two types of VPMM is conducted. It is concluded that the open-slot VPMM has an advantage over the split-pole VPMM considering the torque density, torque ripple, flux-weakening ability and the power losses. In [B11], by placing stator windings on both sides of the rotor as shown in Fig. 2.6(c), a dual-excitation VPMM is proposed to improve the torque density. Outer rotor VPMMs have been

used for in-wheel propulsion of EVs and direct-drive wind power generation [B12], [B14]. As shown in Fig. 2.6(d), a recent research presented a dual-stator topology whose inner stator has a half tooth displacement relative to the outer stator, and the spoke-array of PMs is used to produce flux focusing effect. It is claimed that the power factor of this machine can reach 0.9 [B15].
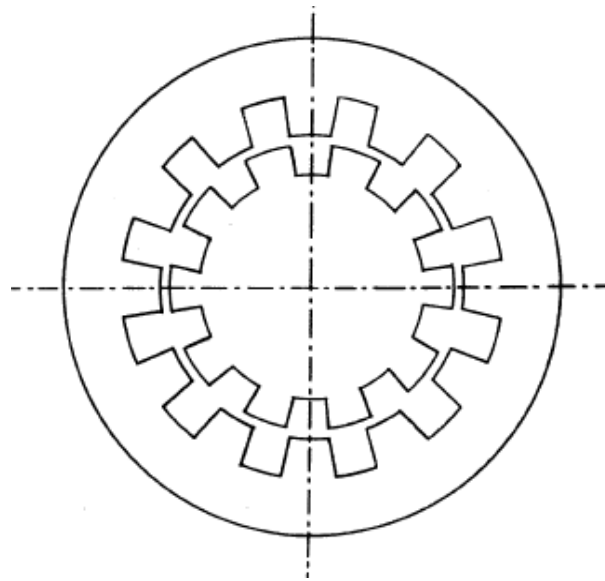
(a)
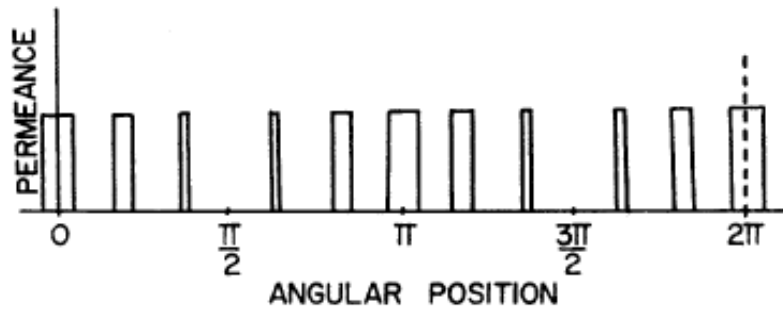
(b)
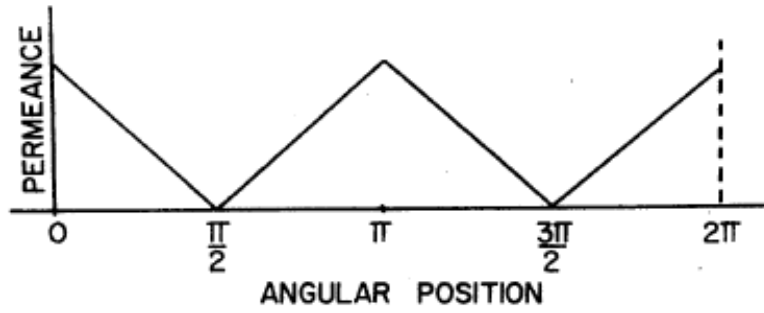
(c)

Fig. 2.5. (a) A vernier reluctance motor. (b) The airgap permeance distribution. (c) The equivalent airgap permeance distribution [B10].
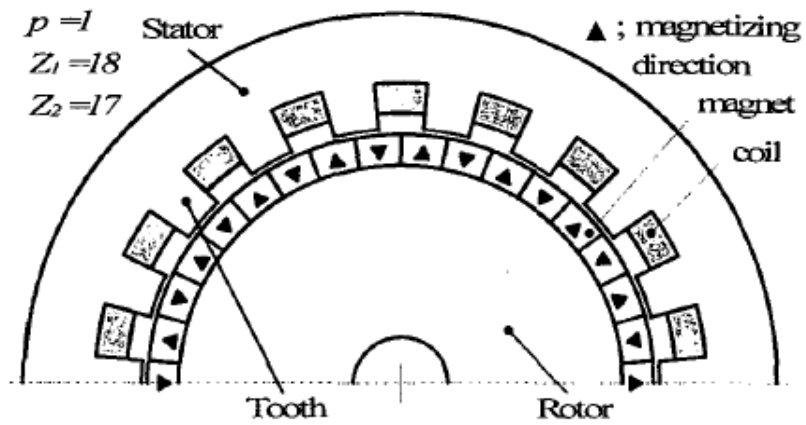
(a) Open-slot type [B11]
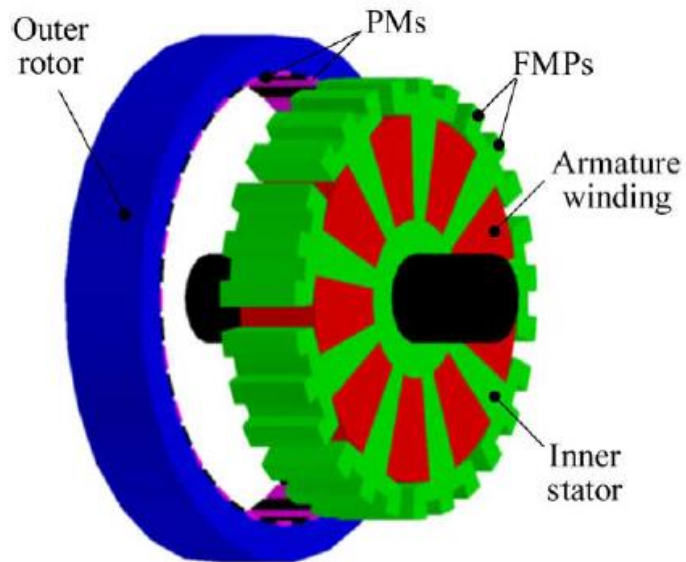
(b) Split-pole type [B12]
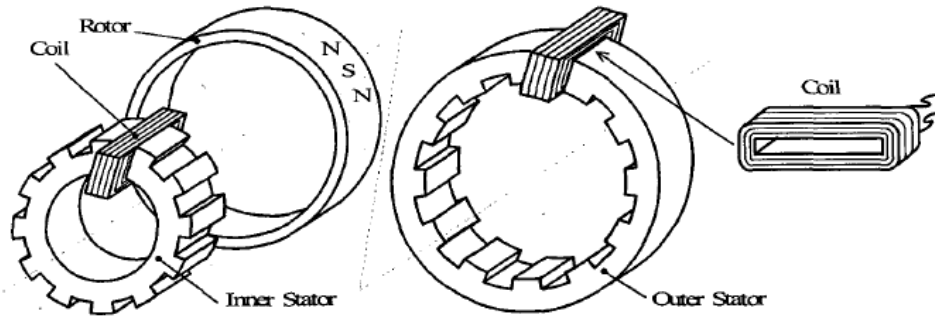
(c) Dual-excited VPMM [B11]
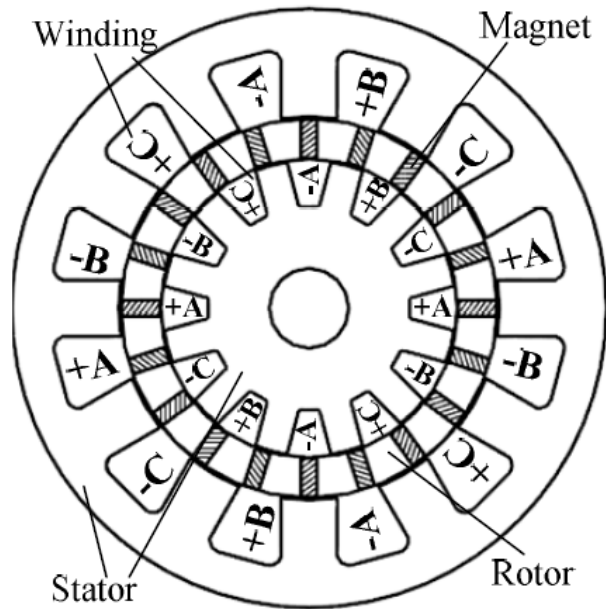
(d) Dual-stator spoke-array VPMM [B15]

Fig. 2.6. Different VPMMs.

2.3.2 Dual-excitation PM machines

Like other PM machines, a dual-excitation PM machine (DEPM) has a set of three-phase windings on its stator. Unlike conventional rotor-PM

motors and stator-PM motors, the DEPMM has PMs on both rotor and stator. The idea of DEPMM machine originally comes from vernier machines [B16]. As shown in Fig. 2.7, by placing unipolar PMs in both the stator slots and the rotor slots, equivalently sinusoidal airgap flux density can be generated. With a small rotor displacement of one rotor pole pitch, the airgap flux changes 90 degrees, which is quite similar to what happens in the vernier reluctance machine except that the permeance variation is replaced by PM flux variation.

In [B17], a DEPMM which does not require the same PM number and teeth number is proposed as shown in Fig. 2.8(a). Although this machine has a more flexible pole-pair combination, it is significantly more complex to manufacture and the robustness is reduced. Fig. 2.8(b) shows a DEPMM with flux concentrating rotor structure which is proposed in [B18]. By virtue of the improved flux density, this DEPMM is claimed to have higher torque density.
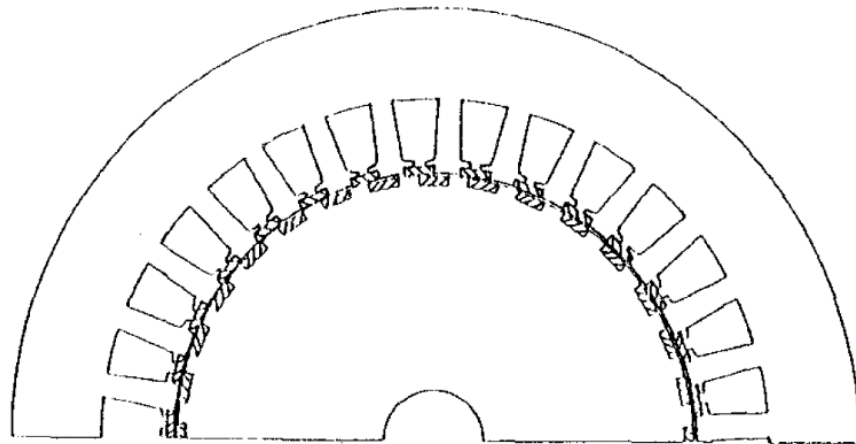
(a)
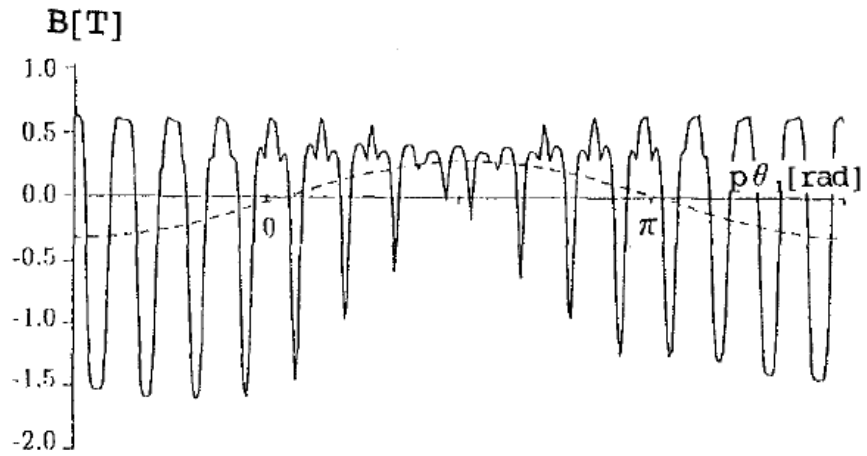
(b)

Fig. 2.7. (a) A DEPMM and (b) the airgap flux density and its equivalent sinusoidal wave [B16].
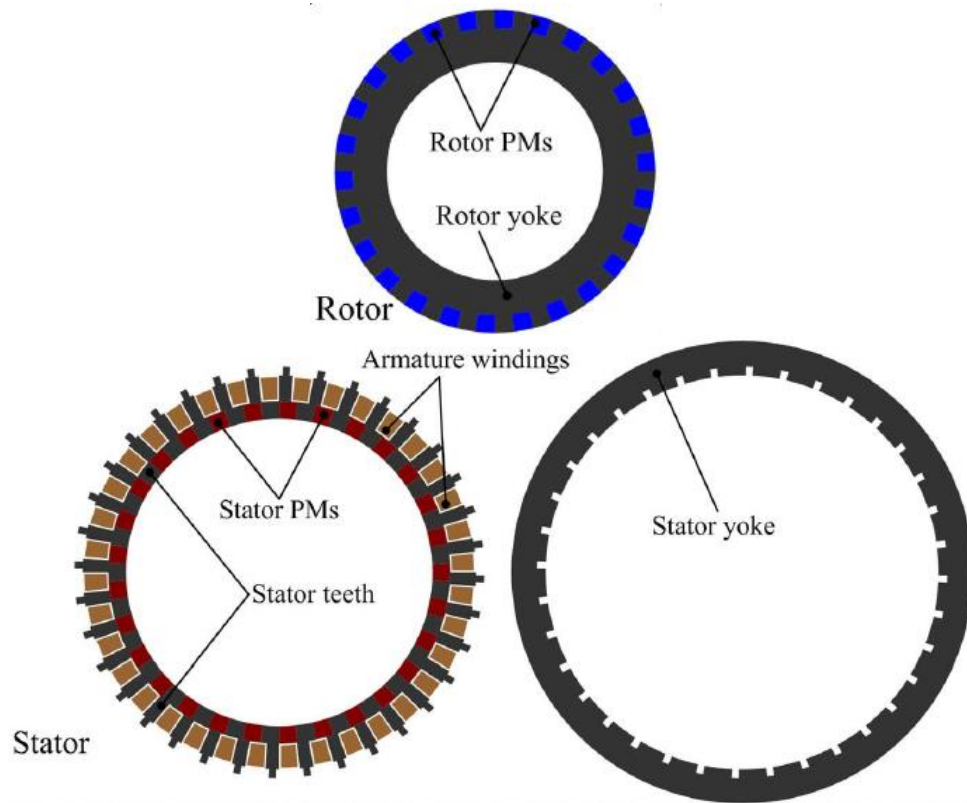
(a)
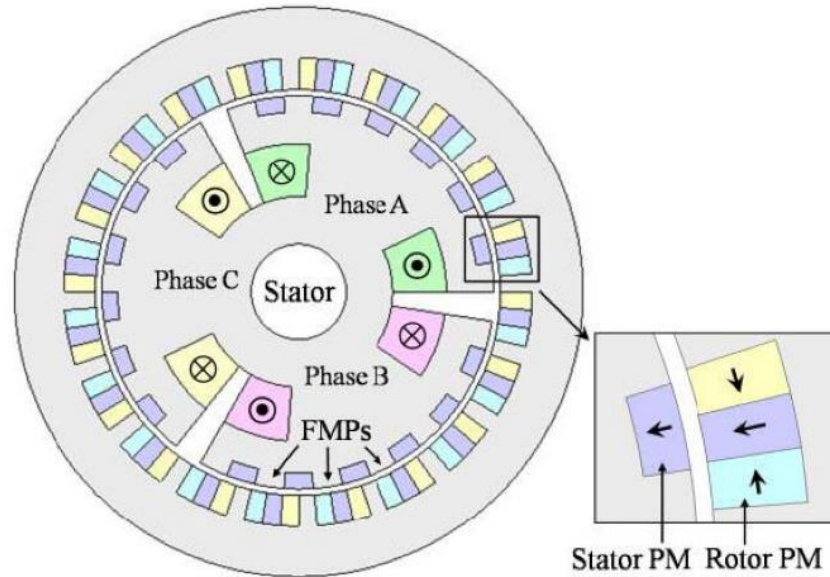
(b)

Fig. 2.8. (a) A DEPMM [B17]. (b) A DEPMM with flux concentrating rotor structure [B18].

2.3.3 Doubly-fed reluctance machines

The DFRM is a re-emerging concept which can be traced back to the early 1970's [B19]. As shown in Fig. 2.9, the DFRM consists of a reluctance rotor and two sets of windings which can be housed either in one or two stators [B19], [B20]. The DFRM can be either operated in asynchronous mode like an induction motor with one set of winding short-circuited or operated in synchronous mode with both sets of windings fed with current [B21]. The DFRM is drawing attention again because of its potential application in clean energy harvesting such as wind power generation. Connected with a partial-scale converter, the DFRM can generate constant-frequency voltage while the rotor speed can be changing.

Compared with the mostly used doubly-fed induction generator, the DFRM needs no slip ring or brushes and hence the reliability is improved and the maintenance is reduced. When compared with a conventional PM machine with a full-scale convertor for variable speed control, the doubly-fed machine only needs a partial-scale convertor, which significantly reduces the overall cost.

Fig. 2.9(c) shows a DFRM with axial laminated rotor which is proposed and compared with the counterpart with simple salient rotor in [B22]. The laminations are interleaved with non-magnetic material. The comparison result shows that the laminated rotor has an advantage over the simple salient rotor considering the torque capability and the mutual coupling between the stator windings. In [B23], the DFRM is compared with a synchronous reluctance motor (SRM) and it is concluded that the DFRM has lower torque production for the same copper losses but it requires smaller inverter for the same output power.
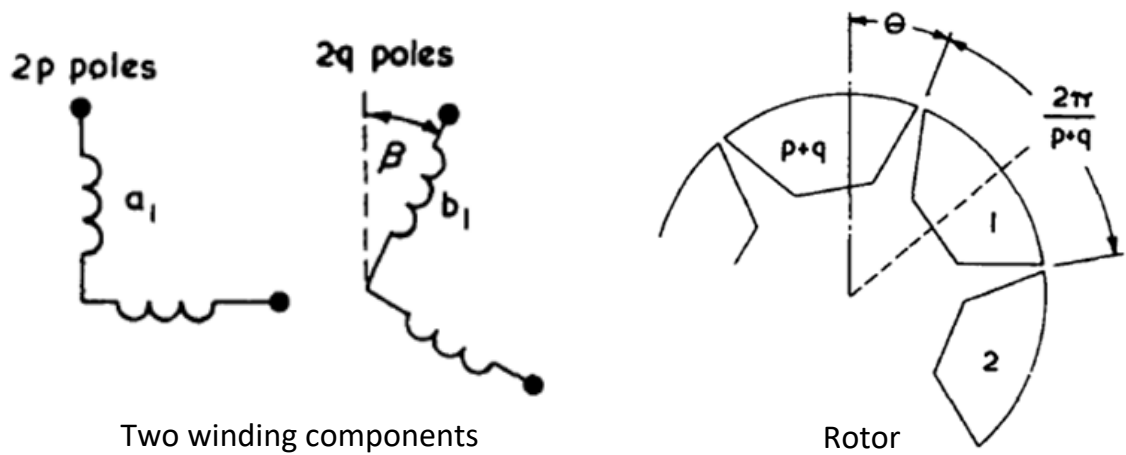
(a)
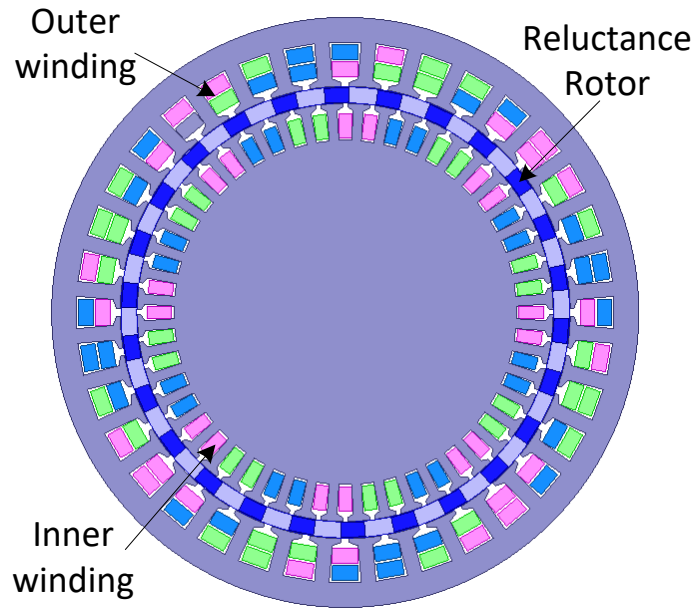
(b)
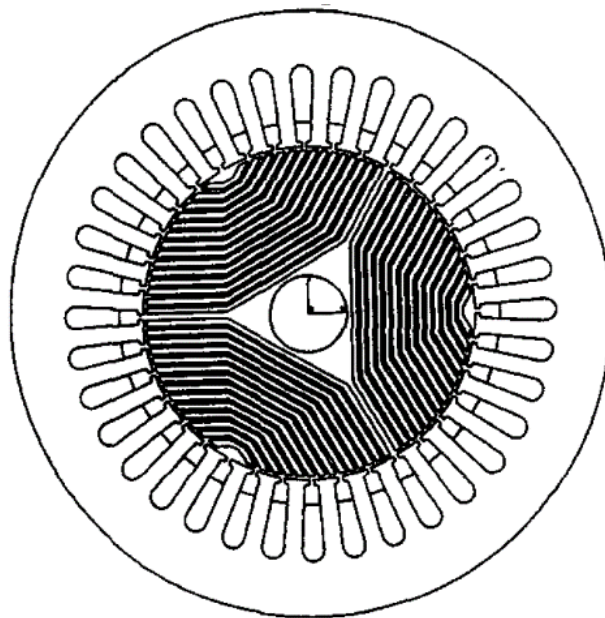
(c)

Fig. 2.9. Doubly-fed magnetic reluctance machines. (a) Components of a DFRM [B19]. (b) A DFRM with dual stator [B20]. (c) A DFRM with axial laminated rotor [B22].

2.4 Conclusion

In this Chapter, several types of newly emerged or re-emerged electric machine concepts have been reviewed. The historical development and working principles of these machines are briefly introduced. Although the working principles are explained in different ways in literature, a common feature among them is the difference in pole numbers of the stator and rotor. In this thesis, they are all classified as FM machines and further study on them is made in the following chapters.

References – part B

[B1]   K. Atallah, and D. Howe, "A novel high-performance magnetic gear," *IEEE Trans. Magn.*, pp. 2844–2846, 2001.

[B2]   K. Atallah, S. D. Calverley, and D. Howe, "Design, analysis and realization of a high-performance magnetic gear," *Inst. Electr. Eng. Proc. Electr. Power Appl.*, vol. 151, pp. 135–143, Mar. 2004.

[B3]   K. T. Chau, Z. Dong, J. Z. Jiang, L. Chunhua, and Z. Yuejin, "Design of a magnetic-geared outer-rotor permanent-magnet brushless motor for electric vehicles," *IEEE Trans. Magn.*, vol. 43, no. 6, pp. 2504–2506, Jun. 2007.

[B4]   K. Atallah, J. Rens, S. Mezani, and D. Howe, "A novel "pseudo" direct-drive brushless permanent magnet machine," *IEEE Trans. Magn.*, vol. 44, no. 11, pp. 4349–4352, Nov. 2008.

[B5]   Jian, L., G. Xu, G. Yu, J. Song, J. Liang, and M. Chang, "Electro-magnetic design and analysis of a novel magnetic-gear-integrated wind power generator using time-stepping finite element method," *Progress In Electromagnetics Research*, vol. 113, pp. 351-367, 2011.

[B6]   L. L. Wang, J. X. Shen, Y. Wang and K. Wang, "A novel magnetic-geared outer-rotor permanent-magnet brushless motor", *4*th *IET Conf. Power Electronics, Machines and Drives*, pp. 33 -36, 2008 .

[B7]   Y. Fan, L. Gu, Y. Luo, X. Han, and M. Cheng, "Investigation of a New Flux-Modulated Permanent Magnet Brushless Motor for Evs," *The Scientific World Journal*, vol. 2014, Article ID 540797, Apr. 2014.

[B8]   S. L. Ho, Shuangxia Niu, and W. N. Fu, "Design and analysis of a novel axial-flux machine," *IEEE Trans. Magn.*, vol. 47, no. 10, pp. 4368-4371, Oct. 2011.

[B9]   Longnv Li, W. N. Fu, Shuangxia Niu, S. L. Ho, and Yan Li, "A quantitative comparison study of power electronic driven flux-modulated machines using magnetic field and thermal field co-simulation," *IEEE Trans. Industrial Electronics*, vol. 99, accepted.

[B10]   C. H. Lee, "Vernier motor and its design," *IEEE Trans. Power Apparatus*, vol. 82, pp. 343 -349, Jun. 1963.

[B11]   A. Toba and T. A. Lipo, "Novel dual-excitation permanent magnet vernier machine," *Proc. Conf. Rec. IEEE IAS Annu. Meeting*, pp. 2539–2544, 1999.

[B12]   J. Li, K. T. Chau, J. Z. Jiang, C. Liu, and W. Li, "A new efficient permanent magnet vernier machine for wind power generation," *IEEE Trans. Magn.*, vol. 46, no. 6, pp. 1475–1478, Jun. 2010.

[B13]   G. Xu, L. Jian, W. Gong, and W. Zhao, "Quantitative comparison of flux-modulated interior permanent magnet machines with distributed windings and concentrated windings," *Progress In Electromagnetics Research*, vol. 129, pp. 109–123, 2012.

[B14]   C. Liu, "Design of a new outer-rotor flux-controllable vernier PM in-wheel motor drive for electric vehicle," *Proceeding of ICEMS*, pp. 1-6, 2011.

[B15]   Dawei Li, Ronghai Qu, and T. Lipo, "High power factor vernier permanent magnet machines," *IEEE Energy Conversion Congress and Exposition*, pp. 1534-1540, 15-19 Sept. 2013.

[B16]   A. Ishizaki, T. Tanaka, K. Takasaki, and S. Nishikata, "Theory and optimum design of PM vernier motor," *Proc. Of IEE ICEMD '95*, pp.208-2 12

[B17]   L. Jian, Y. Shi, C. Liu, G. Xu, Y. Gong, and C. C. Chan, "A novel dual permanent-magnet-excited machine for low-speed large-torque applications," *IEEE Trans. Magn.*, vol. 49, no. 5, pp. 2381–2384, May 2013.

[B18]   J. D. Kyu and C. J. Hwan "Design of a vernier machine with PM on both sides of rotor and stator", *IEEE Trans. Magn.*, vol. 50, no. 2, pp. 877-880, 2014.

[B19]   A. Broadway, "Cageless induction machines," *Proc. Inst. Elect. Eng.*, vol. 118, pp. 1593–1600, Nov. 1971.

[B20] Y. Wang, S. L. Ho, W. N. Fu, and J. X. Shen, "A novel brushless doubly fed generator for wind power generation," *IEEE Trans. Magn.*, vol. 48, no. 11, pp. 4172-4175, Nov. 2012.

[B21] S. WiIliamson, A. C. Ferreira, and A. K. Wallace, "Generalised theory of the brushless doubly-fed machine. Part I: Analysis," *IEE Proc.-Electr. Power Appl.*, vol. 144, pp. 111-122, March 1997.

[B22] L. Xu, F. Liang, and L. Ye, "Comparison study of rotor structures of doubly excited brushless reluctance machine by finite element analysis," *IEEE Trans. Energy Conversion*, vol. 9, no. 1, pp. 165-172, March, 1994.

[B23] R. E. Betz, and M. G. Jovanovic, "The brushless doubly fed reluctance machine and the synchronous reluctance machine ─ a comparison", *IEEE Trans. Industry Application*, vol. 36, no. 4, pp1103-1110, Aug. 2000.

Chapter 3

Analysis of flux-modulated machines - a unified theory

In this chapter, a unified theory of FM machines is proposed. At first, the unified theory is derived from a model of a coaxial magnetic gear. The theory is then expanded to FM machines. Different types of FM machines are derived from the MG model and their working principles are explained by the unified theory.

3.1 Basic principles for electromagnetic field and analytic calculation

A comprehensive description of the electromagnetic phenomena relies on Maxwell's equations [C1 – C3]. In differential form, Maxwell's equations are as follows

$$\nabla \times E = -\frac{\partial B}{\partial t}$$

(3.1)

$$\nabla \times H = J + \frac{\partial D}{\partial t}$$

(3.2)

$$\nabla \cdot D = \rho$$

(3.3)

$$\nabla \cdot B = 0$$

(3.4)

where; E is the electric field strength; B is the magnetic flux density; H is the magnetic field strength; J is the current density; D is the electric flux density; and ρ is the electric charge density.

Eq. 3.1 is called Faraday's induction law which describes a phenomenon that when a magnetic flux is changing, an electric field is created around it. Eq. 3.2 is called Ampere's law which describes how a magnetic field is created around a changing electric flux or a current. Eq. 3.3 is called Gauss's law for electric fields which describes that an electric flux always flows from a positive electric charge to a negative electric charge. Eq. 3.4 is called Gauss's law for magnetic fields. It describes the law that a magnetic flux is always a circulating flux without starting or end point.

In integral form, Faraday's induction law is

$$\oint_l E \cdot dl = -\frac{d}{dt}\int_S B \cdot dS = -\frac{d\phi}{dt} \tag{3.5}$$

It means that the changing of magnetic flux through a surface S is equal to the negative integration of electric field strength along line l which is around surface S.

Ampere's law in integral form is

$$\oint_l H \cdot dl = \int_S J \cdot dS + \frac{d}{dt}\int_S D \cdot dS = i(t) + \frac{d\psi_e}{dt} \tag{3.6}$$

It states that the current and changing electric flux through a surface S is equal to the integration of the magnetic strength along line l which is around surface S. The second term at the right

$$\frac{d}{dt}\int_S D \cdot dS = \frac{d\psi_e}{dt}$$

<div align="right">(3.7)</div>

is called Maxwell's displacement current. In electric machine design, the frequency is usually low and the displacement current can be neglected. Eq. 3.6 can be then written in its static or quasi-static form

$$\oint_l H \cdot dl = \int_S J \cdot dS = i(t)$$

<div align="right">(3.8)</div>

This equation is very important for calculating the magnetic potential or current linkage in an electric machine.

In integral form, Gauss's law for electric fields is written as

$$\int_S D \cdot dS = \int_V \rho_V dV$$

<div align="right">(3.9)</div>

It states that the charge inside a volume V is equal to the electric flux through surface S which is around volume V. Inside an electric machine, there are some components in which there is no net charge. In these areas, Eq. 3.9 is

$$\int_S D \cdot dS = 0$$

<div align="right">(3.10)</div>

In integral form, Gauss's law for magnetic fields is written as

$$\int_S B \cdot dS = 0$$

<div align="right">(3.11)</div>

It indicates that the total flux entering a closed surface is always zero. This means a magnetic flux has no starting or end point and so when a

flux gets into a volume, it must get out of the volume. In an electric machine, any flux loop is closed.

To describe the relationships between the flux density or current density and the field strengths, the permittivity ε, the permeability μ, and the conductivity σ are defined as follows.

$$D = \varepsilon E$$

(3.12)

$$B = \mu H$$

(3.13)

$$J = \sigma E$$

(3.14)

However, these quantities are not necessarily constant. For example, the ferromagnetic materials usually have nonlinear permeability.

3.2 The flux modulation effect in a magnetic gear

As is shown in Fig. 3.1, the magnetic gear has three parts. The outer part is referred as Part 1 which has a large number of PMs with p_1 pole pairs, and the inner part is referred as Part 2 which has a small number of PMs with p_2 pole pairs. The middle part consists of ferromagnetic pole-pieces (FMPs) with a number of N_{Fe}.

Basically, in the airgap of electric machines, the relationship among the magnetomotive force (MMF) drop F, the magnetizing force H and the magnetic flux density B is,

$$F = \delta H = \frac{\delta}{\mu_0} B$$

(3.15)

and

28

$$B = \frac{\mu_0}{\delta} F = \lambda F$$

, (3.16)

where; δ is the airgap length; μ_0 is the permeability of free space; and λ is the permeance per unit area.

   To simplify the model, the MG is expanded in a pseudo-polar coordinate system as shown in Fig. 3.2(a) and the corresponding permeance is shown in Fig. 3.2(b). Supposing that Part 1 is rotating at a speed of ω_1, Part 2 is rotating at a speed of ω_2, and the middle part is rotating at a speed of ω_{Fe}, the fundamental component of the MMF produced by the PMs on Part 1 can be expressed as

$$F_1 = F_{1m} \cos[p_1(\theta - d_1\omega_1 t) + \varphi_1]$$

, (3.17)

where; F_{1m} is the magnitude of MMF F_1; θ is the mechanical angular position; $d_1=1$ indicates that the MMF rotates in positive direction; $d_1=-1$ indicates that the MMF rotates in negative direction; φ_1 is the initial phase angle of F_1.
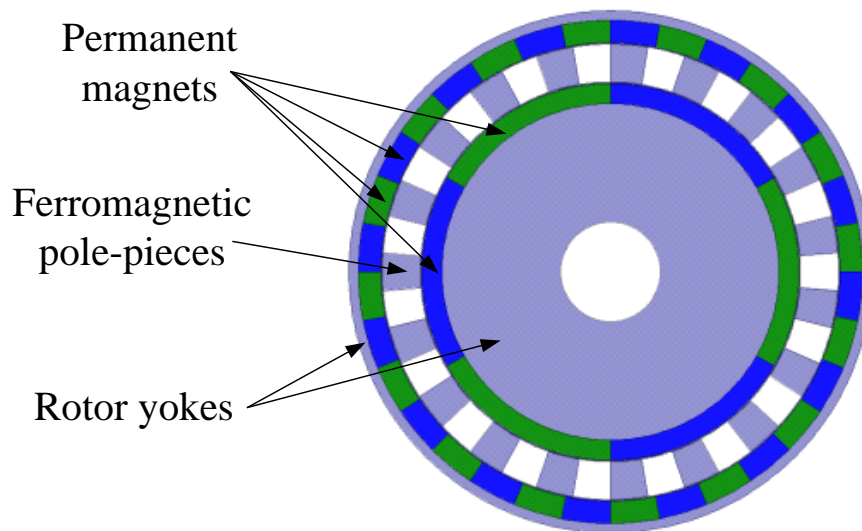
Fig. 3.1. A magnetic gear.
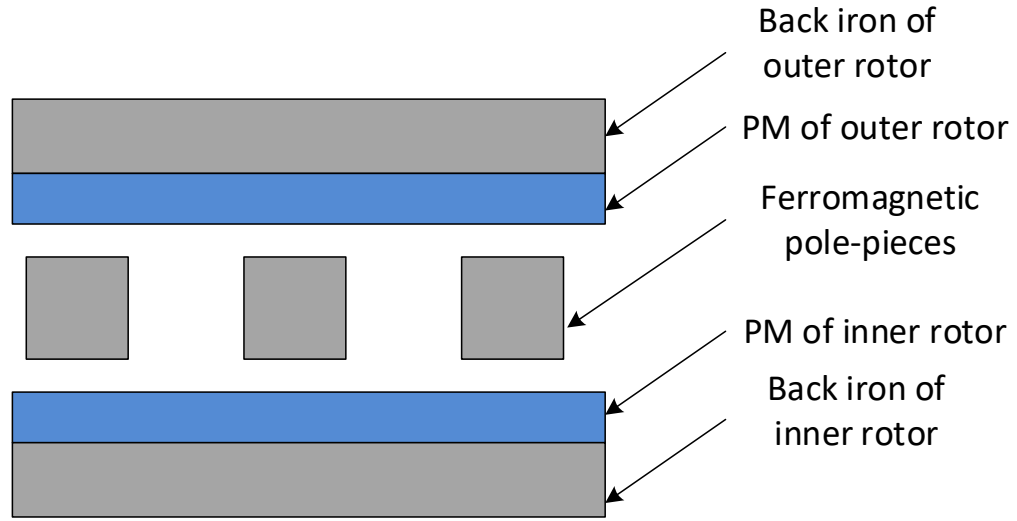
(a)
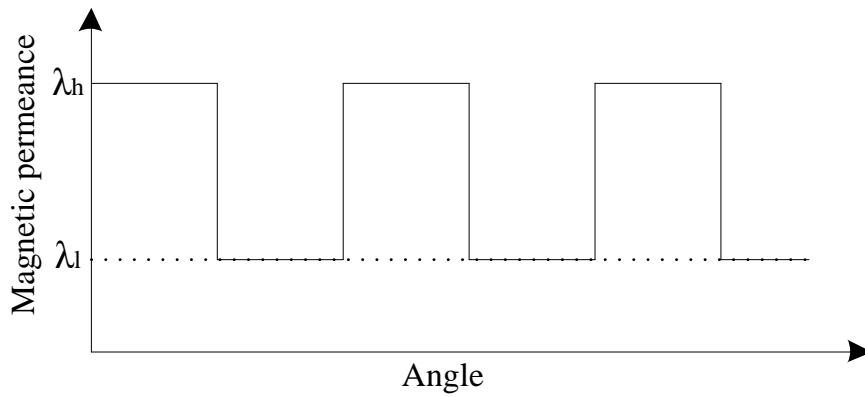
(b)

Fig. 3.2. (a) The magnetic gear in pseudo-polar coordinates; (b) the corresponding magnetic permeance.

Similarly, the fundamental component of the MMF produced by the PMs on Part 2 can be expressed as

$$F_2 = F_{2m} \cos[p_2(\theta - d_2\omega_2 t) + \varphi_2],$$ (3.18)

where; F_{2m} is the magnitude of MMF F_2; θ is the mechanical angular position; $d_2=1$ indicates that the MMF rotates in positive direction; $d_2=-1$

indicates that the MMF rotates in negative direction; φ_2 is the initial phase angle of F_2.

As shown in Fig. 3.2(b), when the middle part with N_{Fe} pieces of the iron segments is rotating at the speed of ω_{Fe}, the permeance per length of the air gap can be expressed as:

$$\lambda = \lambda_{av} + \lambda_m \cos[N_{Fe}(\theta - d_{Fe}\omega_{Fe}t) + \varphi_{Fe}],$$ (3.19)

where; λ_{av} is the average of λ; λ_m is the magnitude of alternating component of λ; $d_{Fe}=1$ indicates that the FMPs rotate in positive direction; $d_{Fe}=-1$ indicates that the FMPs rotate in negative direction; φ_{Fe} is the initial phase angle of alternating component of λ. From (3.17) and (3.19), the magnetic flux density produced by Part 1 is:

$$B_1 = \lambda F_1 = \{\lambda_{av} + \lambda_m \cos[N_{Fe}(\theta - \omega_{Fe}t) + \varphi_{Fe}]\} F_{1m} \cos[p_1(\theta - d_1\omega_1 t) + \varphi_1]$$

$$= \begin{cases} \lambda_{av}F_{1m}\cos[p_1(\theta - d_1\omega_1 t) + \varphi_1] \\ +(1/2)\lambda_m F_{1m}\cos\left[(N_{Fe}-p_1)(\theta - \dfrac{d_{Fe}N_{Fe}\omega_{Fe}-d_1 p_1\omega_1}{N_{Fe}-p_1}t) + (\varphi_{Fe}-\varphi_1)\right] \\ +(1/2)\lambda_m F_{1m}\cos\left[(N_{Fe}+p_1)(\theta - \dfrac{d_{Fe}N_{Fe}\omega_{Fe}+d_1 p_1\omega_1}{N_{Fe}+p_1}t) + (\varphi_{Fe}+\varphi_1)\right] \end{cases}$$

$$= B_{11} + B_{12} + B_{13},$$ (3.20)

where;

$$B_{11} = \lambda_{av}F_{1m}\cos[p_1(\theta - d_1\omega_1 t) + \varphi_1],$$ (3.21)

$$B_{12} = (1/2)\lambda_m F_{1m} \cos\left[(N_{Fe} - p_1)(\theta - \frac{d_{Fe}N_{Fe}\omega_{Fe} - d_1 p_1 \omega_1}{N_{Fe} - p_1}t) + (\varphi_{Fe} - \varphi_1)\right] \tag{3.22}$$

$$B_{13} = (1/2)\lambda_m F_{1m} \cos\left[(N_{Fe} + p_1)(\theta - \frac{d_{Fe}N_{Fe}\omega_{Fe} + d_1 p_1 \omega_1}{N_{Fe} + p_1}t) + (\varphi_{Fe} + \varphi_1)\right] \tag{3.23}$$

Similarly, the magnetic flux density produced by Part 2 is:

$$B_2 = B_{21} + B_{22} + B_{23} \tag{3.24}$$

where;

$$B_{21} = \lambda_{av} F_{2m} \cos[p_2(\theta - d_2\omega_2 t) + \varphi_2] \tag{3.25}$$

$$B_{22} = (1/2)\lambda_m F_{2m} \cos\left[(N_{Fe} - p_2)(\theta - \frac{d_{Fe}N_{Fe}\omega_{Fe} - d_2 p_2 \omega_2}{N_{Fe} - p_2}t) + (\varphi_{Fe} - \varphi_2)\right] \tag{3.26}$$

$$B_{23} = (1/2)\lambda_m F_{2m} \cos\left[(N_{Fe} + p_2)(\theta - \frac{d_{Fe}N_{Fe}\omega_{Fe} + d_2 p_2 \omega_2}{N_{Fe} + p_2}t) + (\varphi_{Fe} + \varphi_2)\right] \tag{3.27}$$

To achieve stable torque transmission, there must be at least one component of B_1 which can interact with one component of B_2. The two field components must have the same pole-pair number, the same rotating speed and the same rotating direction. In detail, the following cases can be studied.

(a) If B_{11} interacts with B_{22} and produces constant torque, it requires

$$p_1 = N_{Fe} - p_2 \tag{3.28}$$

and

$$\omega_{B11} = \omega_{B22} .$$
(3.29)

Considering

$$\omega_{B11} = d_1 \omega_1 ,$$
(3.30)

and

$$\omega_{B22} = \frac{d_{Fe} N_{Fe} \omega_{Fe} - d_2 p_2 \omega_2}{N_{Fe} - p_2} ,$$
(3.31)

one can deduce that

$$d_{Fe} N_{Fe} \omega_{Fe} = d_1 p_1 \omega_1 + d_2 p_2 \omega_2 .$$
(3.32)

It can be simply verified that when B_{11} interacts with B_{22}, B_{12} also interacts with B_{21} to produce constant torque.

(b) If B_{11} interacts with B_{23} to produce constant torque, it requires

$$p_1 = N_{Fe} + p_2 ,$$
(3.33)

and

$$\omega_{B11} = \omega_{B23} .$$
(3.34)

Considering

$$\omega_{B23} = \frac{d_{Fe} N_{Fe} \omega_{Fe} + d_2 p_2 \omega_2}{N_{Fe} + p_2} ,$$
(3.35)

one can deduce that

33

$$d_{Fe}N_{Fe}\omega_{Fe}=d_1p_1\omega_1-d_2p_2\omega_2 \tag{3.36}$$

It can be simply verified that when B_{11} interacts with B_{23}, B_{13} also interacts with B_{21} to produce constant torque.

(c) According to the symmetry of Part 1 and Part 2, another possible design is

$$p_2 = N_{Fe} + p_1 \tag{3.37}$$

and similarly, one can deduce that

$$d_{Fe}N_{Fe}\omega_{Fe}=-d_1p_1\omega_1+d_2p_2\omega_2 \tag{3.38}$$

Overall, the pole-pair number combination and the rotational speeds of the three parts should meet:

$$\begin{cases} N_{Fe} = p_1 + p_2 \\ d_{Fe}N_{Fe}\omega_{Fe} = d_1p_1\omega_1 + d_2p_2\omega_2 \end{cases} \tag{3.39}$$

or

$$\begin{cases} N_{Fe} = p_1 - p_2 \\ d_{Fe}N_{Fe}\omega_{Fe} = d_1p_1\omega_1 - d_2p_2\omega_2 \end{cases} \tag{3.40}$$

or

$$\begin{cases} N_{Fe} = -p_1 + p_2 \\ d_{Fe}N_{Fe}\omega_{Fe} = -d_1p_1\omega_1 + d_2p_2\omega_2 \end{cases} \tag{3.41}$$

3.3 Derivation of FM machines

In the MG, when the part with PMs rotates, it will produce a rotating magnetic field. It is well known that a three-phase winding system excited with symmetrical ac currents can also produce a rotating magnetic field. Therefore, if one or two parts with PMs are replaced by three-phase windings, different types of electric machines can be derived.

3.3.1 Basic Flux-modulated Machine
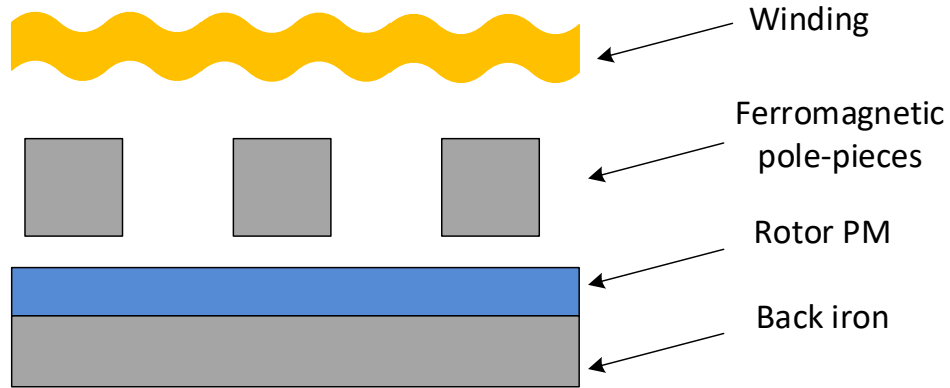
Fig. 3.3. A simplified BFMM model in pseudo-polar coordinates.

If the outer part of the MG model is replaced by a three-phase winding, a BFMM can be derived whose simplified model is shown in Fig. 3.3. Assuming that the winding has a pole-pair number of $p_{Winding}$ and it is excited by electric current whose frequency is f. The rotor has p_{Rotor} pole pairs with the rotating speed ω_{Rotor}. According to (3.39),

$$N_{Fe} = p_{Winding} + p_{Rotor} \qquad (3.42)$$

The rotation speed of the fundamental magnetic field produced by the three-phase winding is governed by

$$\omega_{Winding} = \frac{2\pi f}{p_{Winding}}$$

(3.43)

Replacing ω_2 with $\omega_{Winding}$, and ω_1 with ω_{Rotor} in (3.39), one has

$$f = \frac{1}{2\pi}(N_{Fe}\omega_{Fe} - p_{Rotor}\omega_{Rotor})$$

(3.44)

As the iron segments are kept stationary, that is $\omega_{Fe} = 0$, one has

$$f = -\frac{p_{Rotor}\omega_{Rotor}}{2\pi}$$

(3.45)

In machine design, a large pole-pair number is usually required by machines with low operation speed [C4]. However, in conventional machines, the large pole-pair number makes it hard to design the slots and windings. From (3.45), it can be seen that the frequency of the winding is related to p_{Rotor} instead of the small $p_{Winding}$. Hence, the motor has an equivalent pole-pair number of p_{Rotor}. Hence, considering its small real winding pole-pair number and large equivalent pole-pair number, BFMM is expected to be especially suitable for low-speed operations. For example, it can be used as a motor for direct drive in low speed electric vehicles, or as a wind power PM synchronous generator.

3.3.2 Vernier PM Machine
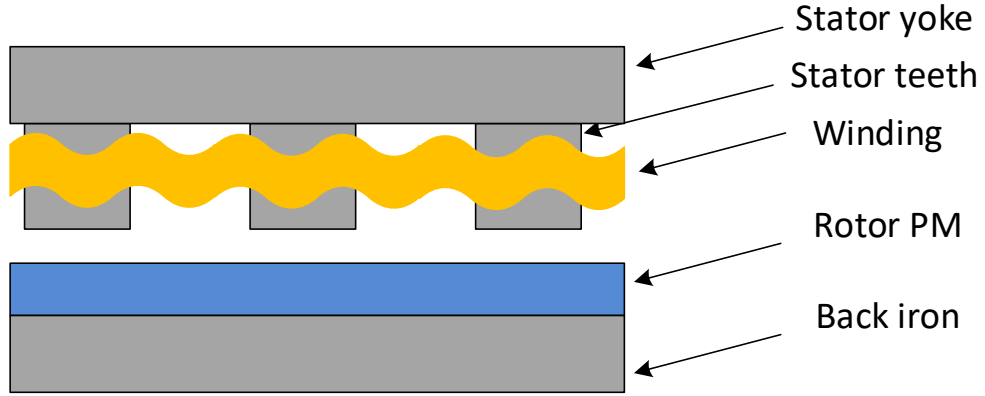
Fig. 3.4. A simplified VPMM model in pseudo-polar coordinates.

From the perspective of our proposed theory, the VPMM has no difference to a BFMM except that the FMPs are replaced by the stator teeth as is shown in Fig. 3.4. One can also consider that the machine has special pole-pair/slot combination, and the airgap between the FMPs and the stator is removed. The difference gives advantages to the VPMM because it is easier to manufacture and more compact without the FMPs distributed in the airgap. But due to the limited pole-pair/slot combination, the pole-pair numbers and slots cannot be chosen as flexibly as in BFMM.

So similarly to those of the BFMM, substituting N_{Fe} with N_{Teeth} in (3.42), the basic principle of the pole-pair/slot combination for the vernier machine should be,

$$N_{Teeth} = p_{Winding} + p_{Rotor} \tag{3.46}$$

$$f = -\frac{p_{Rotor}\omega_{Rotor}}{2\pi} \tag{3.47}$$

where; N_{Teeth} is the number of stator teeth; $p_{Winding}$ is the pole-pair number of the stator winding; p_{Rotor} is the pole-pair number of the PMs; f is the frequency of the winding current; and ω_{Rotor} is the rotor speed in RPM.

37

3.3.3 Dual-excitation PM Machine
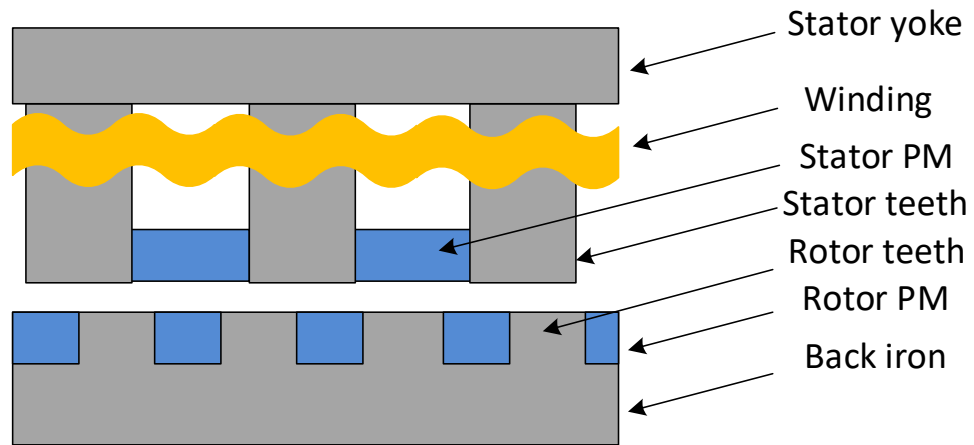
Fig. 3.5. A simplified DEPMM model in pseudo-polar coordinates.

A simplified model of a DEPMM in pseudo-polar coordinates is shown in Fig. 3.5. The DEPMM can be viewed as the combination of two separate machines. The first part is a VPMM as shown in Fig. 3.6. The second part is a special BFMM with its PM position and FMP position exchanged as is shown in Fig. 3.7. According to our analysis in Section 3.2, this positon change does not affect the basic working principle. The winding is shared by these two parts.
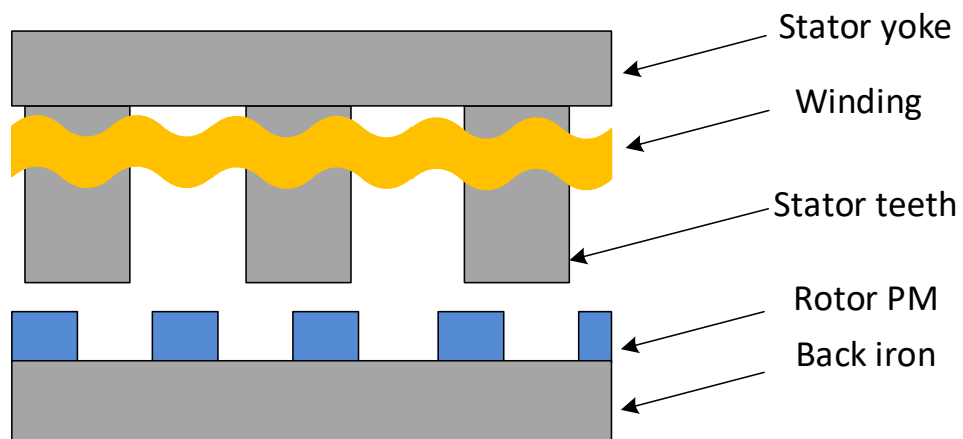
Fig. 3.6. The VPMM part of the DEPMM in pseudo-polar coordinates.
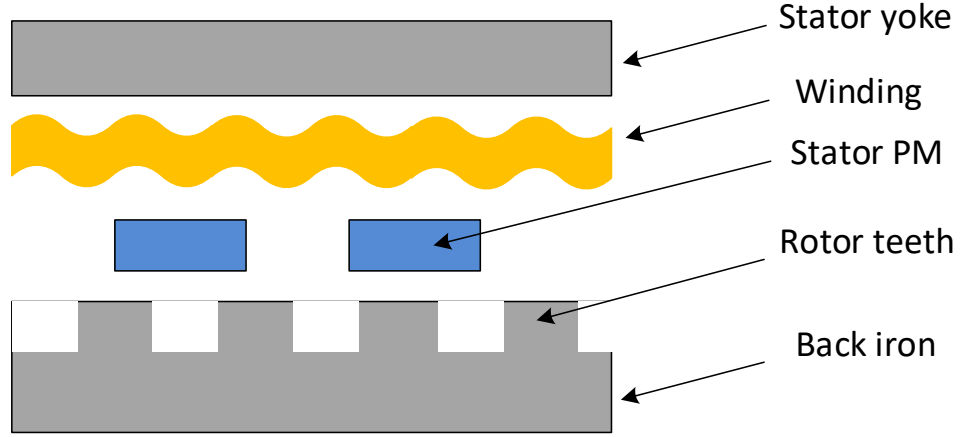
Fig. 3.7. The special BFMM part of the DEPMM in pseudo-polar coordinates.

First, a VPMM is constructed of the stator armature winding with $p_{Winding}$ pole pairs, the PMs on the rotor with p_{Rotor} pole pairs, and the N_{Stator} teeth which serve as modulation teeth in the stator. Their pole pairs and stator teeth should meet the condition of

$$N_{Stator} = p_{Rotor} - p_{Winding} \tag{3.48}$$

$$p_{Rotor}\omega = 2\pi f_{Winding} \tag{3.49}$$

where ω is the rotor speed, and $f_{Winding}$ is the winding frequency.

Second, a special BFMM is constructed of the stator armature winding with $p_{Winding}$ pole pairs, the p_{Stator} PMs on the stator, and the N_{Rotor} teeth which serve as FMPs in the rotor. Compared with the BFMM in Section 3.3.1, this special BFMM has its PMs and winding on the same side of the FMPs. The pole number combination should meet the condition of

$$N_{Rotor} = p_{Stator} + p_{Winding} \tag{3.50}$$

$$N_{Rotor}\omega = 2\pi f_{Winding}$$

(3.51)

In the design, we intentionally let

$$p_{Rotor} = N_{Rtator}$$

(3.52)

and

$$p_{Stator} = N_{Stator}$$

(3.53)

which means that both the rotor and the stator have consequent-pole PMs in the slots. Therefore, Eqs. 3.48 and 3.50 are actually the same, and Eqs. 3.49 and 3.51 are also the same. From the working principle analysis of the VPMM and the BFMM, it can be easily found out that when the working principle of the VPMM part is satisfied, the working principle of the BFMM part is also satisfied. Vice versa, when the BFMM part works, the VPMM part also works. This means that these two sets of machines can all work simultaneously.

In this machine, the flux modulation effect is achieved in two ways. Both the rotor PMs and stator PMs can interact with the windings via the stator teeth and rotor teeth, respectively. Compared with the rotor-PM machine and the stator-PM machine, the DEPMM is expected to have improved torque density because of its dual PM excitation. However, as the number of rotor PMs equals the number of rotor teeth, and the number of stator PMs equals the number of stator teeth, the pole-pair number combination for DEPMM is also less flexible than that of the BFMM, which may result in larger torque ripple [C5], [C6].

3.3.4 Doubly-fed Reluctance Machine
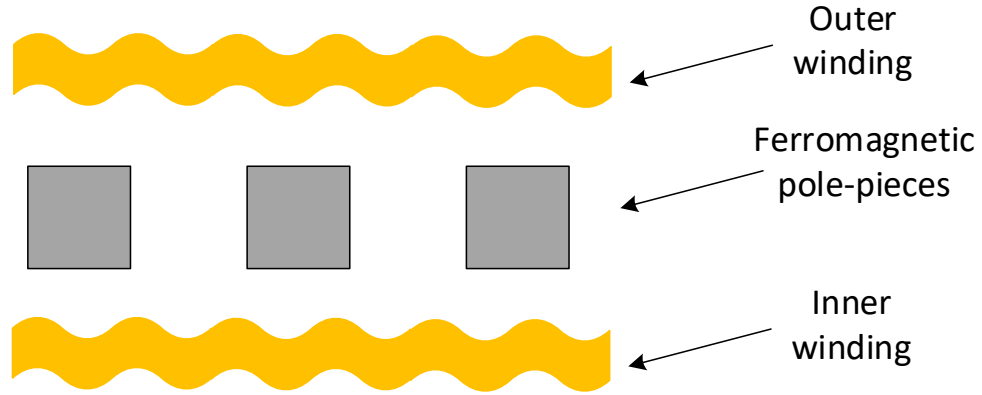
Fig. 3.8. A simplified DFRM model in pseudo-polar coordinates.

In the MG model, if the PMs of both Part 1 and Part 2 are replaced by three-phase windings, a doubly-fed magnetic reluctance motor with dual stators is generated. The part of FMPs is used as the rotor. From Eq. 3.39, the pole number combination needs to satisfy,

$$N_{FMP} = p_1 + p_2$$

(3.54)

where; N_{FMP} is the number of FMPs; p_1 and p_2 are the pole-pair numbers of the outer winding and the inner winding, respectively. The relationship among the winding frequencies and the rotor speed is,

$$N_{FMP}\omega = 2\pi d_1 f_1 + 2\pi d_2 f_2$$

(3.55)

where; ω is the rotor speed; f_1 and f_2 are the frequencies of the outer winding and the inner winding, respectively. d_1 and d_2 indicate the rotation directions of the magnetic fields produced by the outer winding and the inner winding, respectively.

According to Eq. 3.55, it can be easily understood that if the machine is used as a motor, it has a wide speed range [C7].

When the inner winding is fed with dc current, the DFRM can operate as a simple electric-excited synchronous machine with a pole-pair number of N_{FMP}. Its advantage is that no brushes and slip rings are required.

When the inner winding is fed with ac current whose frequency is adjusted according to the rotor speed,

$$f_2 = \pm(\frac{N_{FMP}\omega}{2\pi} - f_C)$$

(3.56)

the outer winding can output a voltage with constant frequency f_C. In this way, the DFRM can be used for variable-speed constant-frequency wind power generation.

Compared with the mostly used doubly-fed induction generator, the DFRM needs no slip ring or brushes and hence the reliability is improved and the maintenance is reduced. When compared with a conventional PM machine with a full-scale convertor for variable speed control, the doubly-fed machine only needs a partial-scale convertor, which significantly reduces the overall cost.

3.4 Conclusion

In this chapter, starting from a magnetic gear model, a comprehensive insight into the flux modulation effect is made. The basic rules for flux modulation are explained by analyzing the magnetic gear. Using this theory, different FM machines are derived and their working principles are explained in a unified way.

References – part C

[C1]   D. J. Griffiths, *Introduction to electrodynamics*, Prentice Hall, 1999.

[C2]   B. J. Hunt, *The Maxwellians*, Cornell University Press, 1991.

[C3]   J. D. Jackson, *Classical Electrodynamics*, Wiley, 1998.

[C4]   A. Rezzoug, M. El-Hadi Zaim, *Non-conventional Electrical Machines*, Wiley-ISTE, 2011.

[C5]   K. T. Chau, Z. Dong, J. Z. Jiang, L. Chunhua, and Z. Yuejin, "Design of a magnetic-geared outer-rotor permanent-magnet brushless motor for electric vehicles," *IEEE Trans. Magn.*, vol. 43, no. 6, pp. 2504–2506, Jun. 2007.

[C6]   Z. Q. Zhu and D. Howe, "Influence of design parameters on cogging torque in permanent magnet machines," *IEEE Trans. Energy Convers.*, vol. 15, no. 5, pp. 407–412, May 2000.

[C7]   S. WiIliamson, A. C. Ferreira, and A. K. Wallace, "Generalised theory of the brushless doubly-fed machine. Part I: Analysis," *IEE Proc.-Electr. Power Appl.*, vol. 144, pp. 111-122, March 1997.

Chapter 4

Design of flux-modulated machines

Basically, the FM machines belong to the category of synchronous machines. Many methods or procedures for the design of synchronous machines have been presented in a number of references [D1, D2]. In this section, the basic principles for designing a FM machine are presented.

4.1 General design principles

An important point for the design of an electric machine is the quantitative determination of the magnetic flux. As is introduced in Section 3.1, Faraday's induction law and Ampere's law are extremely important for the design of an electric machine. To be more specific, Ampere's law is the basis to design the magnetic circuit and the required current linkage. So the dimensional parameters of different parts of the electric machine can be decided accordingly. Faraday's law is the basis for determining the induced voltage in the windings.

From Ampere's law, the line integration of magnetic field strength H along the magnetic circuit is equal to the current linkage penetrating through the circuit.

However, in an electric machine, the magnetic flux is usually uneven in different components. A practical way is to divide the magnetic circuit into different parts and in each part, the flux is assumed to be distributed evenly. This strategy to solve a magnetic field is sometimes called

equivalent magnetic circuit method. In this way, Ampere's law is written as

$$U_{m,tot} = \sum U_{m,i} = \oint_l H \cdot dl = \int_S J \cdot dS = \sum i = \Theta$$

(4.1)

where; $U_{m,tot}$ is the total magnetic voltage; $U_{m,i}$ is the magnetic voltage of part i; and Θ is the current linkage. Since the flux in each part is assumed to be evenly distributed, the magnetic voltage across each part is

$$U_{m,ab} = \int_a^b Hdl = Hl$$

(4.2)

If the electric machine is excited with PM, an apparent current linkage is defined as

$$\Theta_{PM} = H_c' h_{PM}$$

(4.3)

where $H_{c'}$ is the coercive force and h_{PM} is the thickness of the PM.

When a magnetic flux is assumed, the flux density and then the magnetic field strength in different parts can be determined. The required magnetizing current can be decided accordingly. Also, as the magnetic flux is assumed, the induced voltage in the windings can be calculated by Faraday's induction law. By selecting different magnetic flux, the no-load curve of the machine, which shows the relationship between the magnetizing current and the induced voltage, can be plotted.

4.2 Windings

In an electric machine, the basic working principle exists in the interaction between the magnetic field and the current in the windings.

The winding configurations and the current or voltage fed into the windings decide the electric machine type. Based on the functions of the windings, there can be several types of windings in a synchronous electric machine, such as armature windings, field windings, and damper windings [D3]. Generally, the armature windings are the place where actual energy conversion is performed; the field windings are for the creation of magnetic fields; the damper windings are for the prevention of oscillations and opposite rotary direction of fields and they do not work under normal operation.

For FM machines, it is sometimes required that the pole number should be relatively high. It is well known that integral slot windings are not suitable for high pole numbers because of the large slot number required. To address the problem, fractional slot windings are used in many FM machines.

The three phase armatures windings are usually spatially distributed in the stator slots. The basic aim is to make the current linkage along the periphery as sinusoidal as possible so that a sinusoidal magnetic field can be created. In Fig. 4.1, the division of airgap periphery into phase zones in a three phase electric machine with four poles is shown. The pole pitch τ, which corresponds to a pole arc of 180 electrical degrees, can be expressed as

$$\tau = \frac{\pi D}{2p}$$

(4.4)

where D is the diameter of the airgap and p is the pole-pair number. Starting from the phase zone positive phase U, the first zone of positive phase V should be 120 electrical degrees from it, since it is a three phase machine. Similarly, the first zone of positive phase W should be 120

electrical degrees from the zone of positive phase *V*. The negative phase zones should be 180 electrical degrees from the corresponding positive phase zones.

The number of slots for each phase zone, which is also known as the number of slots per pole and phase, can be expressed as,

$$q = \frac{Q}{2pm}$$

(4.5)

where *Q* is the total number of slots. The term q determines the type of the winding, namely, when *q* is an integer, it is called an integer slot winding; and when *q* is a fraction, it is called a fractional slot winding [D4].

Compared with integer slot windings, fractional slot windings enjoy more flexible pole slot combination. In other words, if the slot number has been determined, the fractional slot winding has more choices for pole number. Also, certain pole slot combination can reduce some specific harmonics hence the induced voltage waveform can be improved [D5]. However, the main drawback of fractional slot windings is the subharmonics, the frequencies of which are lower than the fundamental.
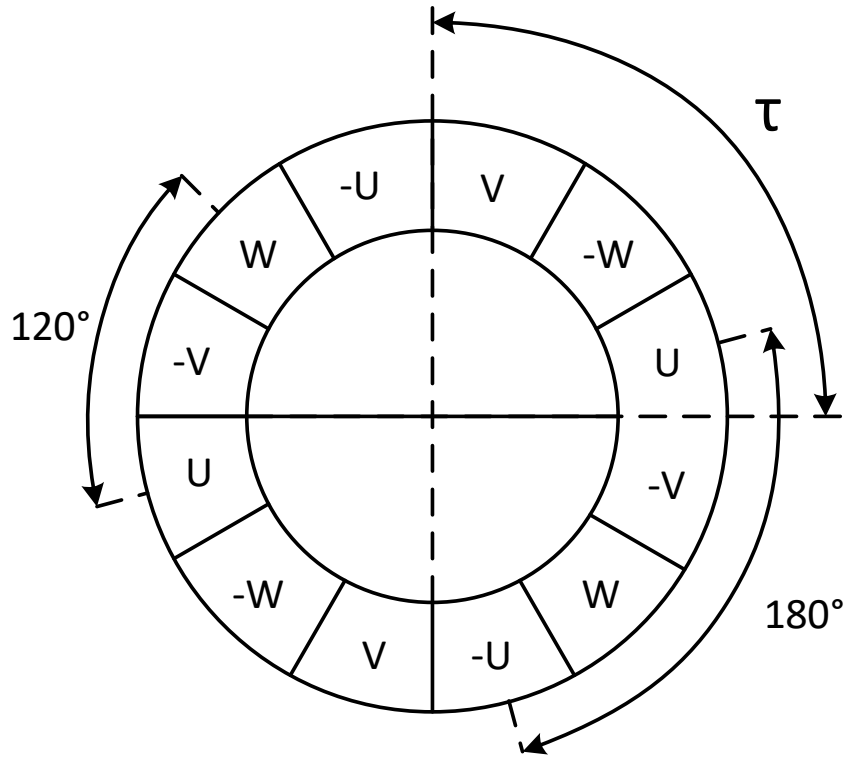
Fig. 4.1. Division of airgap periphery into phase zones in a three phase electric machine.

4.3 Permanent magnets

As most FM machines use PM for field excitation, it is of great importance to determine proper PM dimensional parameters. The basic characteristics of PMs can be chiefly described by the hysteresis curve as shown in Fig. 4.2 [D6]. When a magnetic field is applied to a magnet material, the flux density of the magnet will increase with the field strength as curve 0-1 which is called the initial magnetization curve. Point 1 is called the saturation point. Further increase of field strength after point 1 will cause marginal increase or, in other word, increase at a rate of around the permeability of vacuum, of flux density. If the field strength decreases from point 1, the flux density will decrease along curve 1-2.

The flux density at point 2 is called the remanence or remanent flux density. An external field in the opposite direction will cause further decrease in the magnet flux density along curve 2-3 which is called the normal demagnetization curve. The field strength at which the flux density reaches zero is called the coercivity or coersive force. Further increase of the reverse field will cause magnetization of the magnet in the opposite direction along curve 3-4.
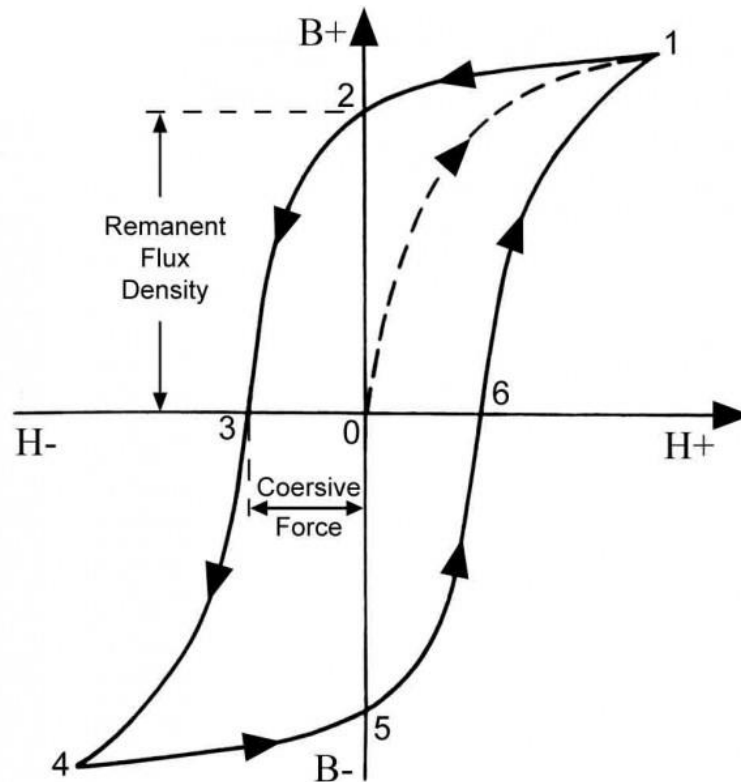
Fig. 4.2. Hysteresis curve of PM [D6].

The flux density in magnet material can be divided into two components. One is the part like in vacuum $\mu_0 H$ and the other part is due to the properties of the magnet B_i. It can be expressed by,

$$B_i = B - \mu_0 H$$

(4.6)

The curves between B_i and H is called the intrinsic hysteresis loop.

Considering a loop of permanent magnet and air gap, from Ampere's law, we have

$$\oint Hdl = H_{pm}l_{pm} + H_{\delta}\delta = 0 \tag{4.7}$$

where; H_{pm} and H_{δ} are the field strengths in the magnet and the airgap, respectively; l_{pm} and δ are the lengths of the magnet and the airgap, respectively. In an electric machine, however, the magnetic field loop usually has an additional part of steel. The effect of steel is usually considered by a reluctance factor K_r as

$$H_{pm}l_{pm} = K_r H_{\delta}\delta \tag{4.8}$$

The relationship between the magnet flux and the airgap flux is,

$$B_{pm}S_{pm} = K_l B_{\delta}S_{\delta} \tag{4.9}$$

where; B stands for flux density and S stands for area; K_l is a factor for consideration of leakage.

If the working point is known, the dimensions of the magnet can be decided using the above equations together with the hysteresis loop. Vice versa, if the magnet and airgap dimensions are known, the working point of the magnet can be determined similarly. Assume the working point to be ($-H_m$, B_m), the volume of the magnet can be decided by [D7],

$$S_{pm}l_{pm} = \frac{K_l K_r B_{\delta}^2 S_{\delta}\delta}{\mu_0 B_m H_m} \tag{4.10}$$

The term B_mH_m is called the energy product which represents the energy in the magnet. It can be seen that, the higher the energy product is, the smaller the volume of magnet is required.

4.4 Flux modulation poles

The FMPs are important for the FM machine design since they are the key for achieving the flux modulation effect. The determination of the number of FMPs in a FM machine has been introduced in Chapter 3. The FMPs can be isolated steel segments distributed in the airgap like in BFMM and DFRM, or they can be integrated into the stator like in VPMM. In DEPMM, as it has two types of flux modulation, FMPs are integrated with both the stator and the rotor.

The shape of FMP affects the airgap permeance distribution. In Eq. 3.19, the coefficients λ_{av} and λ_m are partially determined by the height and width of FMPs which need to be designed from case to case so that the effective flux density component is the highest. To ensure the accuracy, a good choice to design the FMPs is using the finite element method (FEM).

The ratio of the FMP width to pole pitch has been investigated in [D8]. According to the study, in most cases, the flux modulation effect is good when the ratio is roughly 0.5~0.6.

References – part D

[D1]   T. A. Lipo, *Introduction to AC Machine Design*, Wisconsin Power Electron. Res. Center, Univ. of Wisconsin, 1996.

[D2] D. Hanselman, *Brushless Permanent-Magnet Motor Design*, 1994, McGraw-Hill.

[D3] H. Pyrhonen, etc, *Design of rotating electrical machines*, Wiley, UK, 2008.

[D4] N. Bianchi , S. Bolognani and G. Grezzani, "Design considerations for fractional-slot winding configurations of synchronous machines ", *IEEE Trans. Ind. Appl.*, vol. 42, no. 4, pp. 997-1006, 2006.

[D5] L. J. Wu , Z. Q. Zhu , J. T. Chen and Z. P. Xia, "An analytical model of unbalancedmagnetic force in fractional-slot surface-mounted permanent magnet machines", *IEEE Trans. Magn.*, vol. 46, no. 7, pp. 2686-2700, 2010.

[D6] A. E. Fitzgerald , D. E. Higginbotham, and A. Grabel, *Basic Electrical Engineering*, pp. 568-623, 1975, McGraw-Hill.

[D7] J. F. Gieras and M. Wing, *Permanent Magnet Motor Technology*, 2002, Marcel Dekker.

[D8] B. Kim and T. A. Lipo, "Operation and Design Principles of a PM Vernier Motors", *IEEE Trans. Industry Applications*, vol. 50, No. 6, 2014, pp. 3656-3663.

Chapter 5

Optimization and performance comparison of flux-modulated machines

5.1 Introduction

In this chapter, a quantitative comparison among different types of FM machines and a CPMSM is presented. The aim is to evaluate the performance of these FM machines and classify their potential applications. Before comparison, it is of vital importance to make sure that all machines are optimal designs under the predetermined criteria.

The optimization algorithms used for electric machines can be classified into two categories, namely the classical gradient-based algorithms and the modern intelligent algorithms. The popular intelligent algorithms include genetic algorithm (GA), ant colony optimization (ACO), and particle swarm optimization (PSO) [E1].

To analyze the electromagnetic performance of the electric machine design, several methods can be used, including the analytical method, magnetic circuit method, and the FEM. For the former two methods, as they reveal physical working principles, a model needs to be constructed for a specific machine. FEM is a numerical method. It is a more universal method which is widely applicable to the analysis of various

electromagnetic devices [E2]. However, FEM also consumes much more computation time than the other two methods. Nowadays, with the development of computer technology, FEM is becoming more and more popular.

5.2 Genetic algorithm

As is indicated by its name, the idea of evolutionary algorithm comes from the natural evolutionary. The process of natural evolutionary is in a sense to optimize the fitness of species to the environment. Applying this idea to optimization problems generates the evolutionary algorithms.

In evolutionary algorithms, each solution is called an individual. The parameters of an individual are called its code or genes and the performance evaluation is called its fitness value. Usually, a group of individuals are used in evolutionary algorithms so that the optimization process is conducted in parallel. This individual group is called a population. The individuals need to take a number of variations in their codes in the process of optimization.

Various EAs have been proposed since the 1960s. A timeline of the development of EA is depicted in Fig. 5.1 [E1].

As an example, the process of a classical EA, namely GA, is briefly introduced as follows [E3].

1) Initialization. Set the basic parameters for GA, including the population size, the maximum generation, and the possibilities for crossover and mutation. Then, generate the initial population and evaluate the fitness values of every individual.

2) Main loop. Choose two random individuals to crossover with the predetermined probability. In the crossover operation, random genes are exchanged between the individuals to generate the individual for next generation, namely the offspring. Still, every gene has a chance to mutate in the generation of the offspring, which is called the mutation operator. Repeat these operations to generate the whole population to replace the former population.

3) Repeat the replacement of population until the convergence condition is satisfied or the maximum generation. The final generation of population is the GA result.
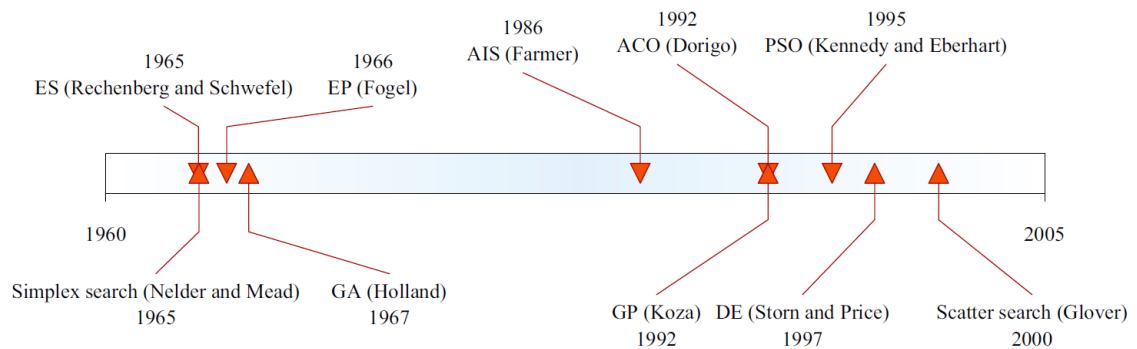
Fig. 5.1. Timeline of the development of EA [E1].

5.3 FEM in electric machine analysis

The basic design for an electrical machine can be performed using analytical equations. However, to know the accurate performance of the machine, numerical methods are usually needed. These numerical methods make it possible to accurately model the machine's behavior and assess the dynamic performance of the machine. The most widely used numerical method for the analysis of electric machines is the FEM. The

55

mathematical analysis and detailed implementation of FEM have been introduced in a number of references [E4] – [E7]. In this thesis, all FE analysis is performed using commercial software Maxwell of Ansys Inc.

5.4 Optimization of flux-modulated machines

5.4.1 Optimization objective and criteria

The optimization of different machines is performed using GA and FEM in this thesis. The objective is to achieve the highest output torque within the constraints. The detailed criteria are as follows.

(a) All machines have the same outer diameter and axial length. The same types of PM material and silicon steel are used.

(b) All machines have the same number of rotor poles and their rated rotor speeds are the same.

(c) The slot fillet is 50% and the maximum current density in the winding conductors is 4A/mm^2.

 The optimization is conducted with the following considerations: a population of 30 elements; the maximum generation number of 20; crossover probability of 0.8; mutation probability of 0.1.

Ignoring the mechanical losses in the comparison of electromagnetic performance of different types of FM machines, the losses are taken as the sum of the core loss P_{Fe} which is calculated using FEM [E8], [E9] and the copper loss which is calculated by,

$$P_{Cu} = 3I^2 \times \frac{1}{3} N_{slot} N_{conductor}^2 \frac{\rho(L + L_{end})}{S_{slot}} = I^2 N_{slot}^2 N_{conductor}^2 \frac{\rho(L + L_{end})}{S_{tot\_slot}}$$

(5.1)

where; I is the rms value of phase current; N_{slot} is the number of slots, $N_{conductor}$ is the number of conductors per slot; S_{slot} is the cross-sectional area of one slot; S_{tot_slot} is the cross-sectional area of all the slots; ρ is the resistivity of conductor; L is the axial length of the machine; and L_{end} is the end winding length.

The efficiency of the motor is calculated by,

$$\eta = \frac{T\omega}{T\omega + P_{Cu} + P_{Fe}} \times 100\%$$

(5.2)

where; T is the output torque; and ω is the rotor speed in rad/s.

5.4.2 Performance of the BFMM

The optimized BFMM with an outer rotor configuration is shown in Fig. 5.2 with its key design data listed in Table 5.1. Using FEM, the flux distribution as well as the output torque, the no-load back-EMF and the core loss under full-load operation are computed and shown in Figs. 5.3 - 5.6. The output torque ripple is small and the back-EMF is generally sinusoidal.
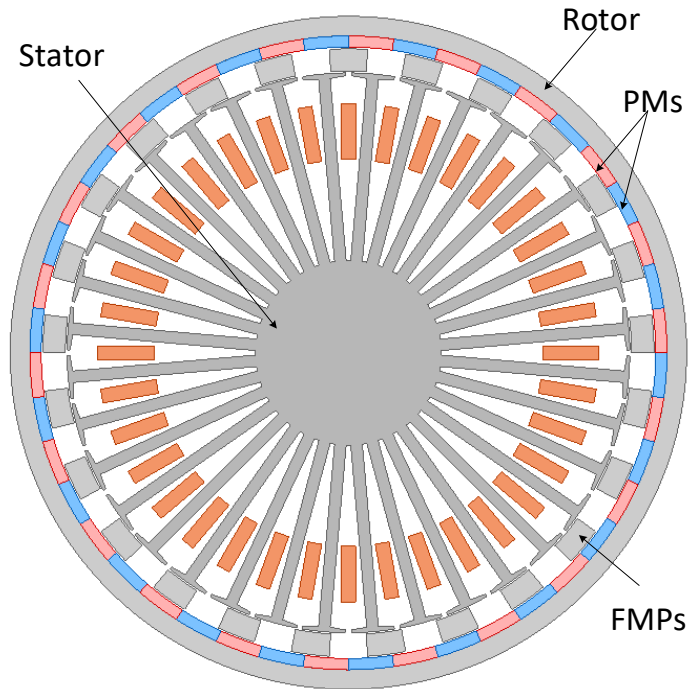
Fig. 5.2. The designed BFMM.

Table 5.1. Key design data of the BFMM

Frequency	220 Hz
Axial length	100 mm
Outside radius of outer rotor	120 mm
Thickness of rotor yoke	6.8 mm
Thickness of rotor PM	3.9 mm
Thickness of FMPs	7.7 mm
Airgap	0.6 mm
Stator tooth width	4.2 mm
Stator tooth height	65.3 mm
Number of outer rotor pole pairs	22
Number of stationary iron pieces	25

| Number of stator pole pairs | 3 |
| Number of stator slots | 36 |
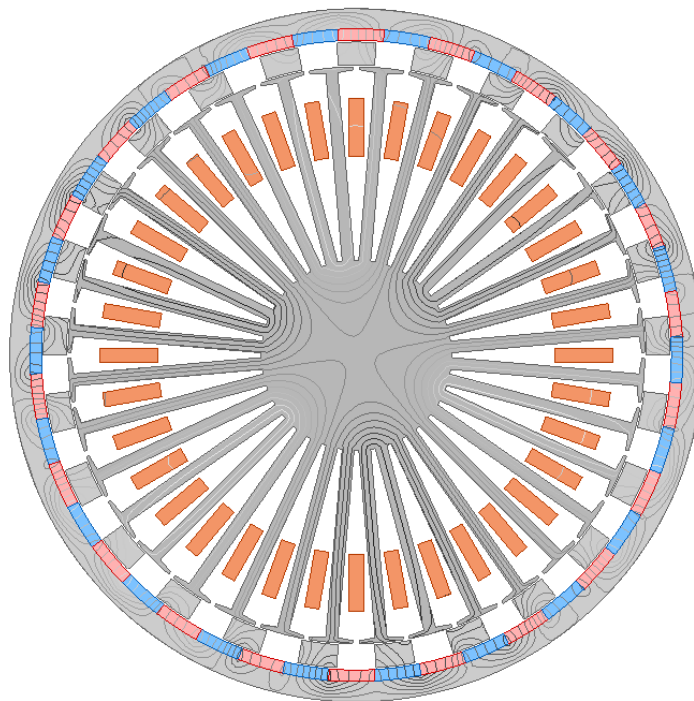
Fig. 5.3. The flux distribution of BFMM.
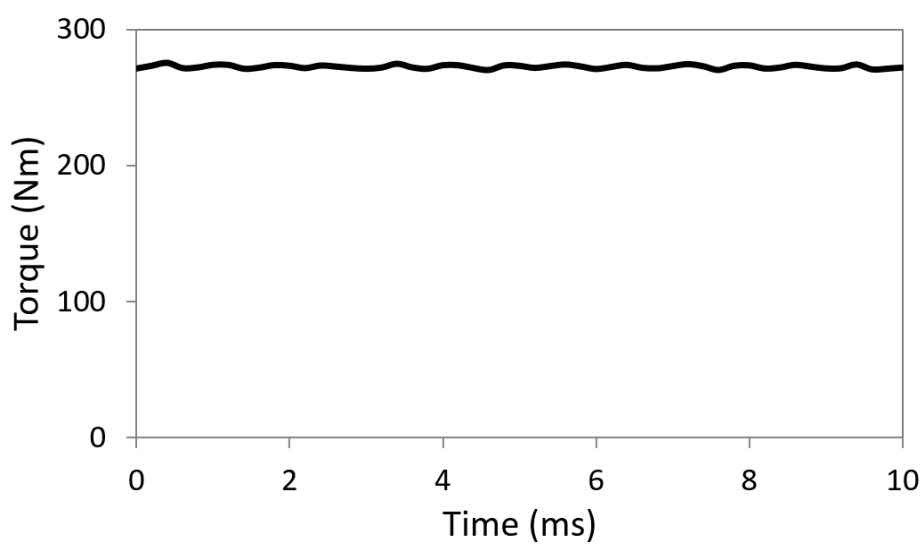
Fig. 5.4. The full-load torque of BFMM.
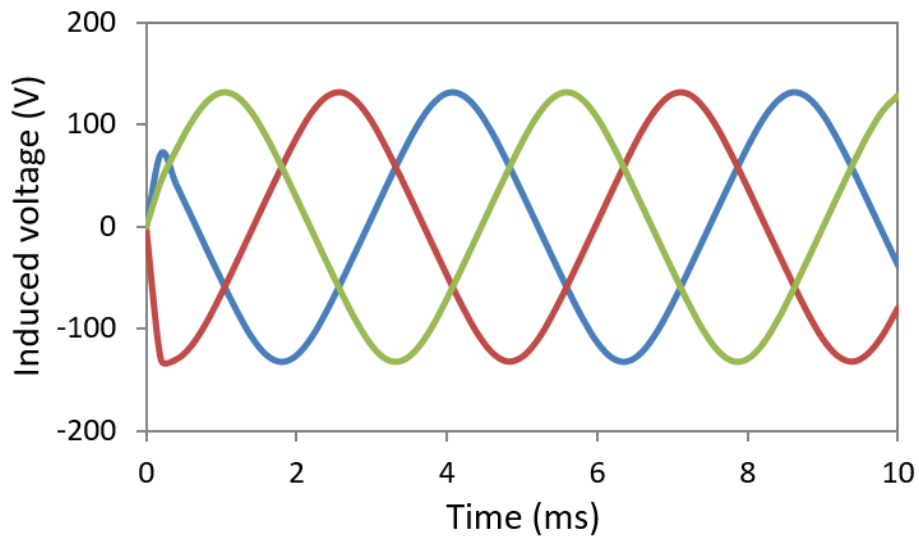
Fig. 5.5. The no-load back-EMF of BFMM.
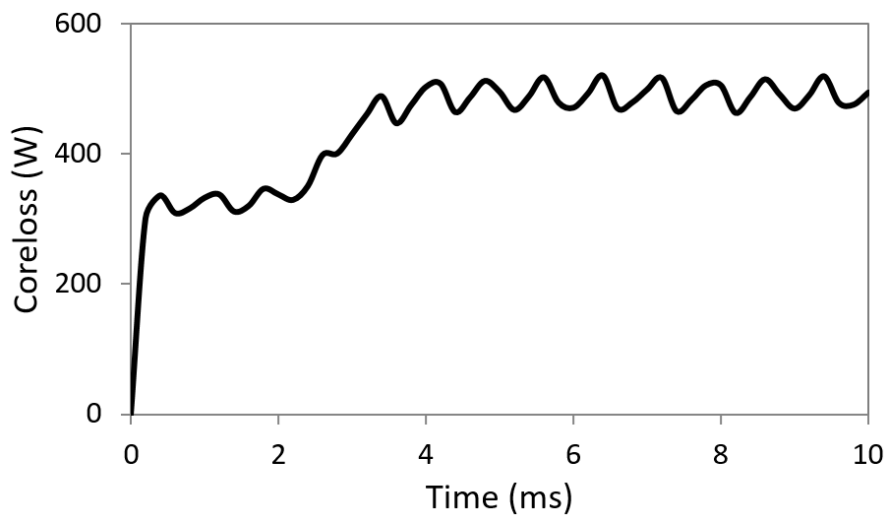
Fig 5.6. The full-load coreloss of BFMM.

5.4.3 Performance of the VPMM

A typical open-slot type VPMM is designed and optimized as shown in Fig. 5.7. The main parameters are listed in Table 5.2. The results of FEM

analysis are shown in Figs. 5.8 – 5.11. The torque ripple is small considering the high average torque and it is quite acceptable for common drive use. The back-EMF is very sinusoidal.
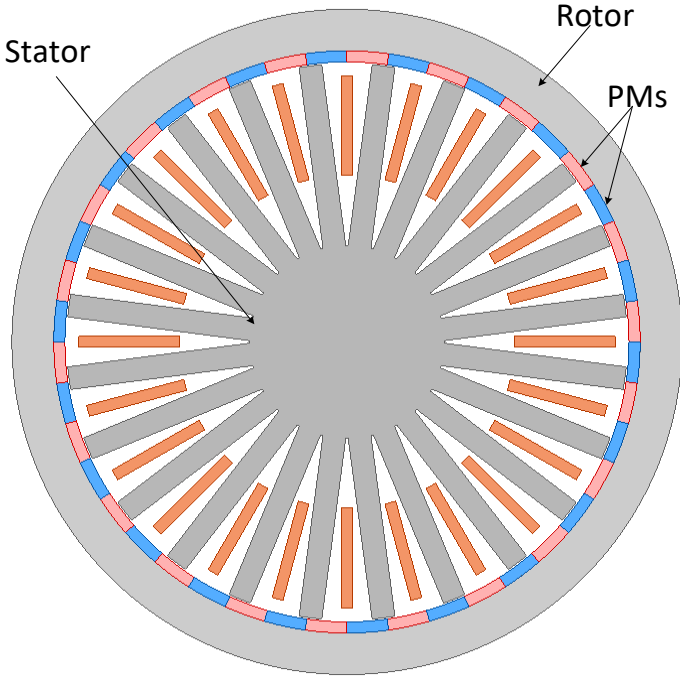
Fig. 5.7. The designed VPMM.

Table 5.2. Key design data of VPMM

Frequency	220 Hz
Axial length	100 mm
Outside radius of outer rotor	120 mm
Thickness of rotor yoke	15.2 mm
Thickness of rotor PM	3.9 mm
Airgap	0.6 mm
Stator tooth width	8.1 mm

Stator tooth height	65.9 mm
Number of outer rotor pole pairs	22
Number of stator pole pairs	2
Number of stator slots	24
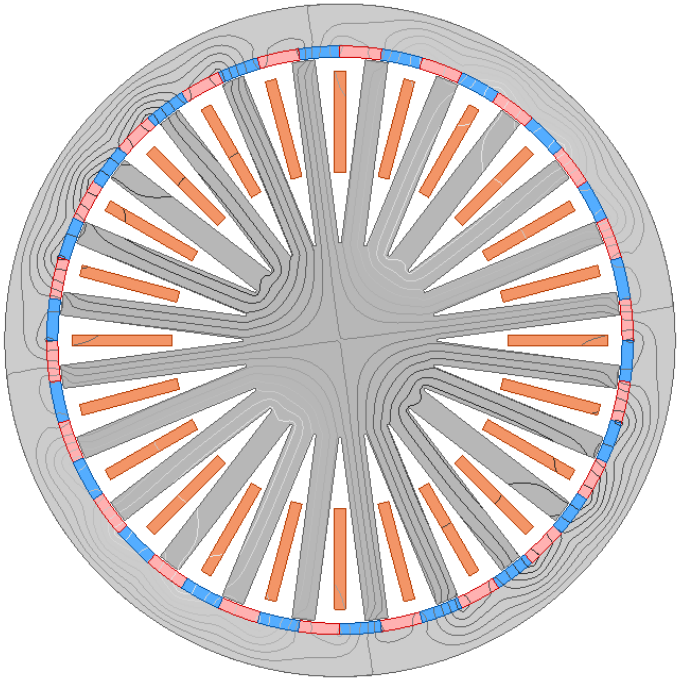
Fig. 5.8. The flux distribution of the VPMM.
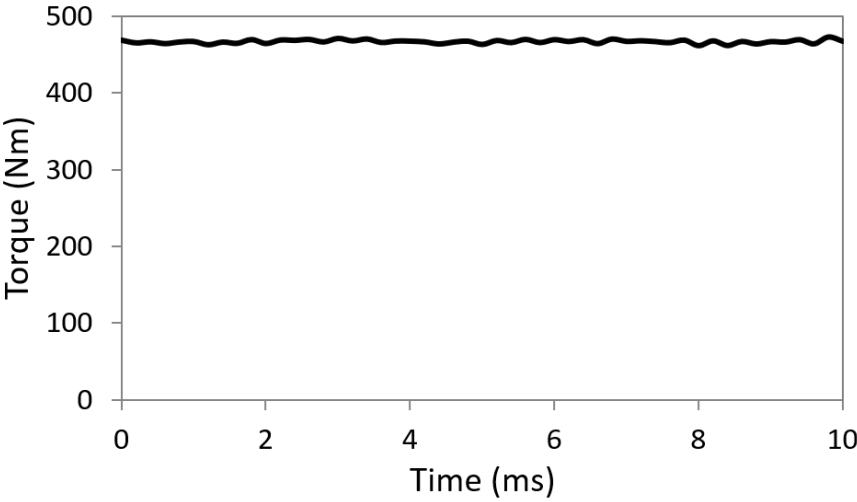
Fig. 5.9. The full-load torque of the VPMM.
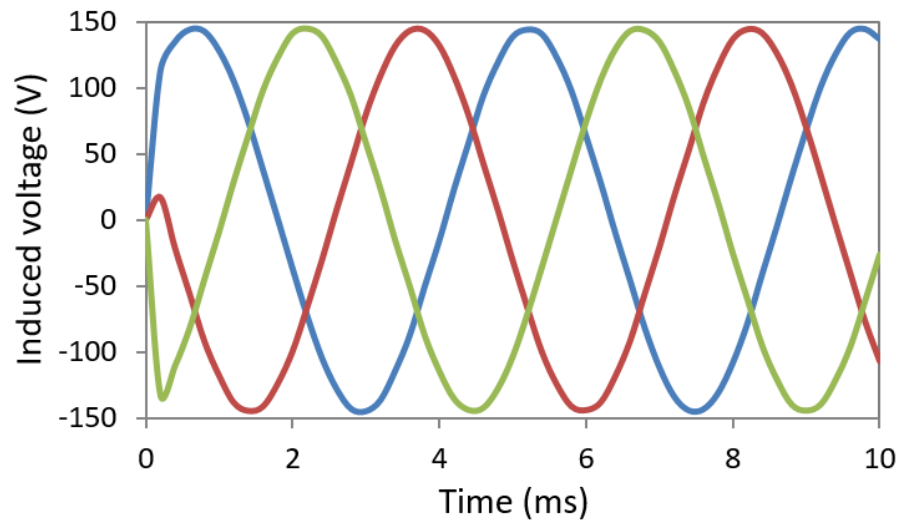
Fig. 5.10. The no-load back-EMF of VPMM.
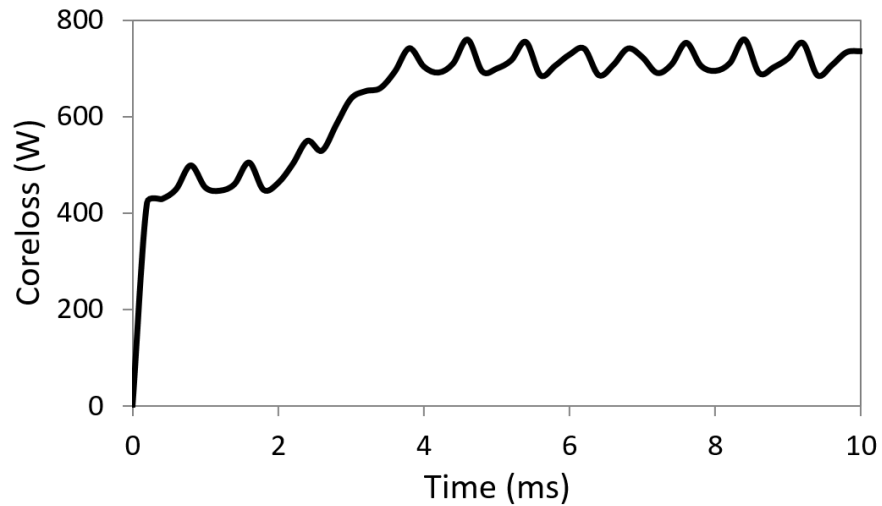
Fig. 5.11. The full-load coreloss of VPMM.

5.4.4 Performance of the DEPMM

An outer rotor DEPMM is designed as shown in Fig. 5.12. The stator PMs are placed at the slot openings. All the PMs in the DEPMM are

magnetized radial outwards. The main parameters of the DEPMM are listed in Table 5.3. The results of FEM analysis are shown in Figs. 5.13 – 5.16. Benefiting from the dual-PM excitation, the DEPMM has a high torque density. Although the torque ripple is obvious, it is still acceptable for common drive applications. The coreloss counts for a relatively large part of the total loss because of its strong PM excitation field.
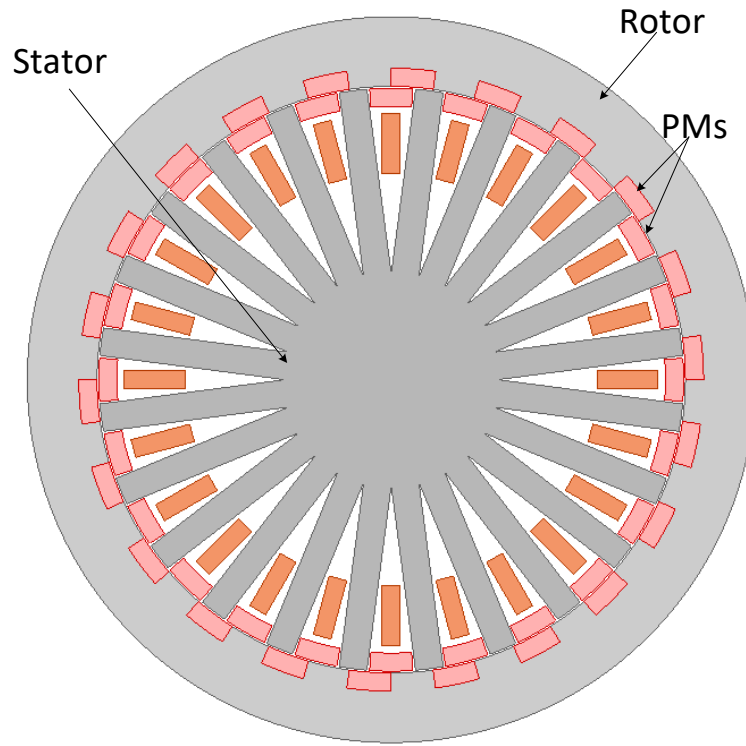
Fig. 5.12. The designed DEPMM.

Table 5.3. Key design data of DPM

Frequency	220 Hz
Axial length	100 mm
Outside radius of outer rotor	120 mm
Thickness of rotor yoke	7.1 mm
Thickness of rotor PM	3.7 mm

Airgap	0.6 mm
Stator tooth width	10.8 mm
Stator tooth height	51.1 mm
Thickness of Stator PM	3.8 mm
Number of outer rotor teeth	22
Number of stator winding pole pairs	2
Number of stator slots	24
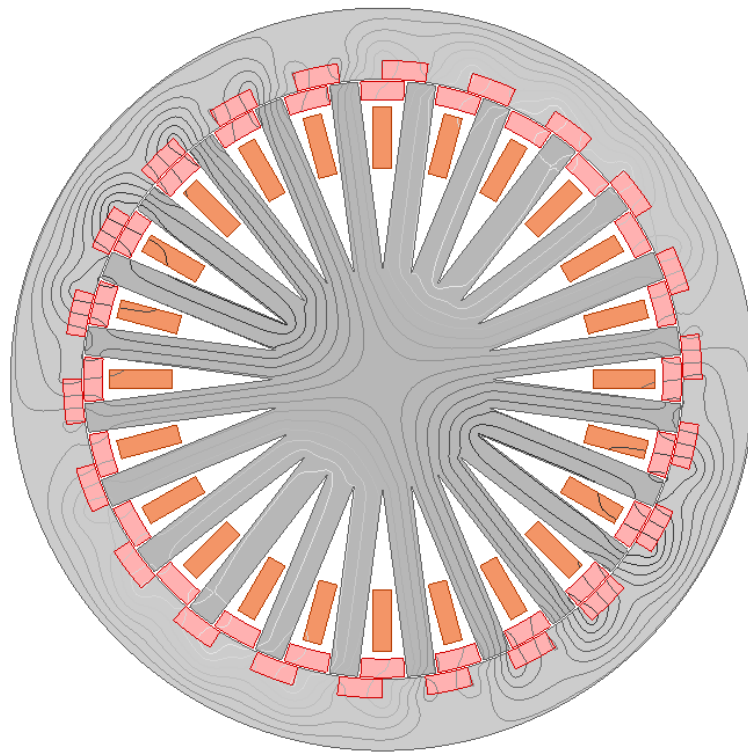
Fig. 5.13. The flux distribution of the DEPMM.
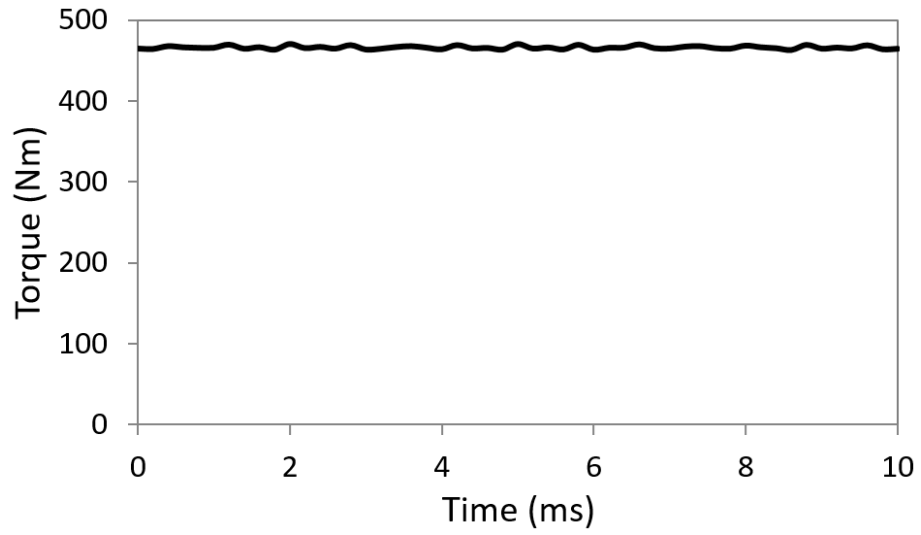
Fig. 5.14. The full-load torque of the DEPMM.
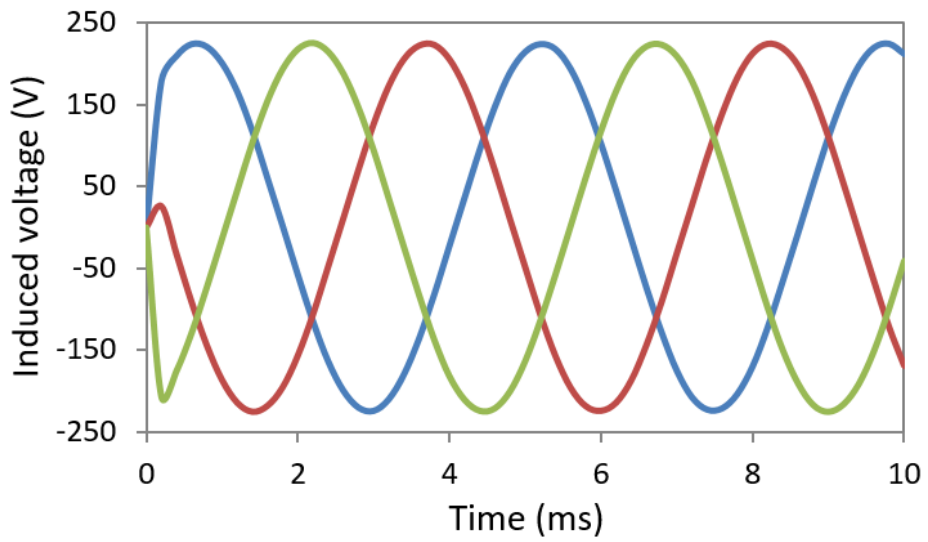
Fig. 5.15. The no-load back-EMF of the DEPMM.
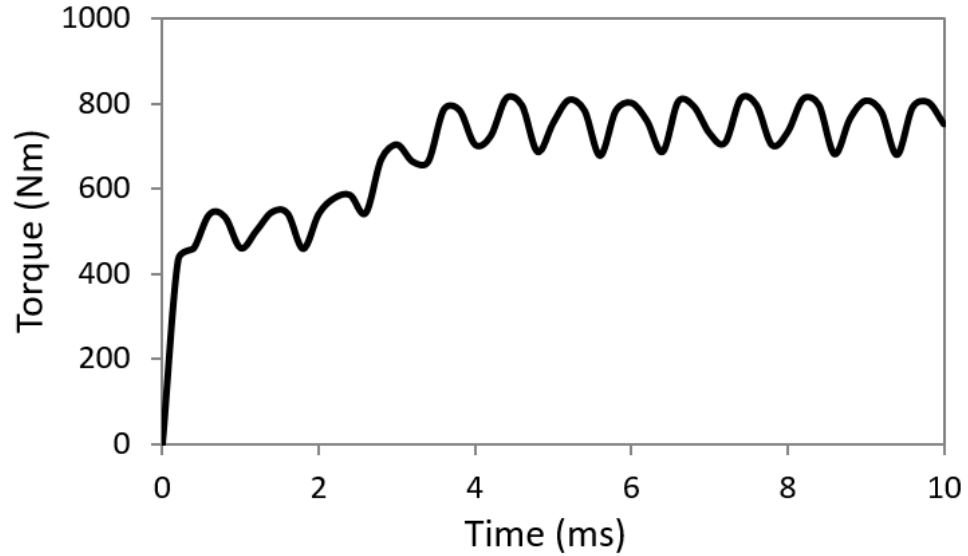
Fig. 5.16. The full-load coreloss of the DEPMM.

5.4.5 Performance of the DFRM

A DFRM is designed and optimized as shown in Fig. 5.17. The main parameters of the DFRM are shown Table 5.4. The teeth widths are much smaller than those of the previous FM machines. The reason is that the DFRM is electrically excited instead of PM excited, which causes the copper loss to be large. To balance the copper loss and coreloss, the slot area is designed to be relatively large. The results of FEM analysis are shown in Figs. 5.18 – 5.21. During the FEM analysis, the outer stator winding is fed with dc current and the inner stator winding is fed with ac current.

Clearly, as no PM is used for field excitation, the torque density of the DFRM is not comparable to that of the PM machines. The flux density in the airgap is low, which largely limits the torque performance of the DFRM. Considering the low average output torque, the torque ripple is

quite big. As the excitation field is weak, the flux leakage is significant, which makes the no-load back-EMF not so sinusoidal.
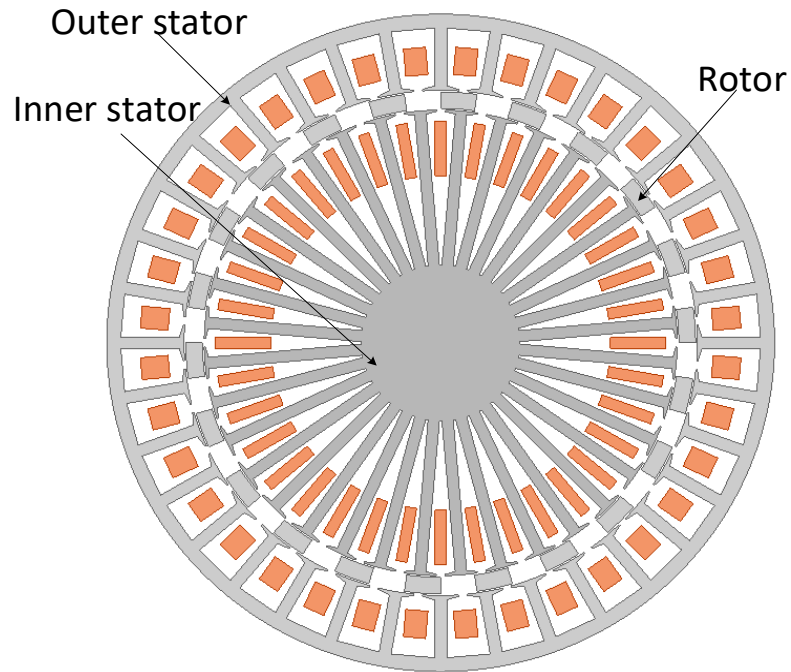
Fig. 5.17. The designed DFRM.

Table 5.4. Key design data of DFRM

Frequency	220 Hz
Axial length	100 mm
Outside radius of outer stator	120 mm
Inside radius of outer stator	92.2 mm
Teeth width of outer stator	4.3 mm
Teeth height of outer stator	22.1 mm
Airgaps	0.6 mm
Thickness of FMPs	6.0 mm

Teeth width of inner stator	3.1 mm
Teeth height of inner stator	56.7 mm
Number of outer stator pole pairs	19
Number of FMPs	22
Number of inner stator pole pairs	3
Number of outer stator slots	36
Number of inner stator slots	36
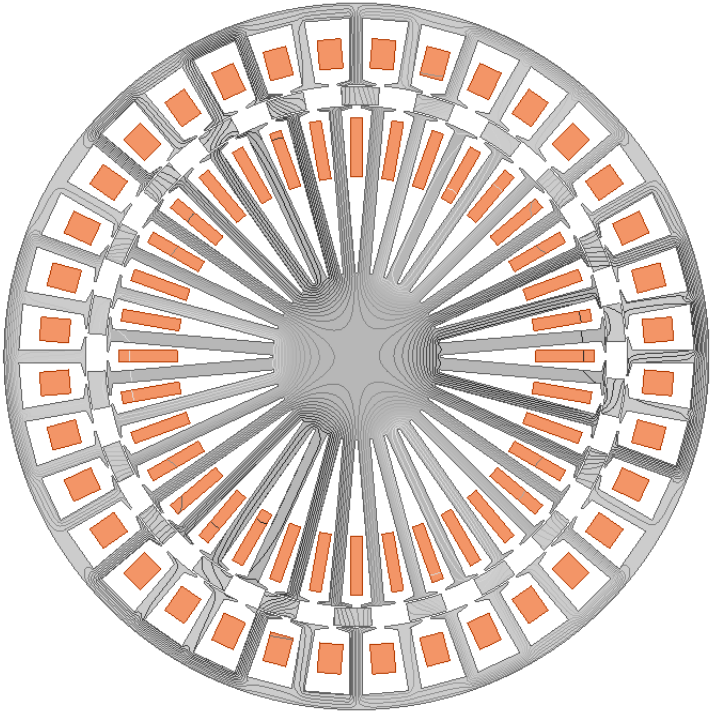
Fig. 5.18. The flux distribution of the DFRM.
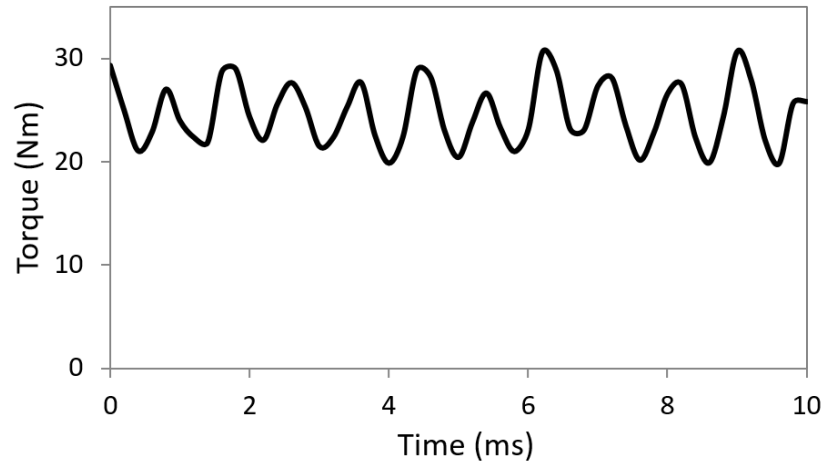
Fig. 5.19. The full-load torque of the DFRM.
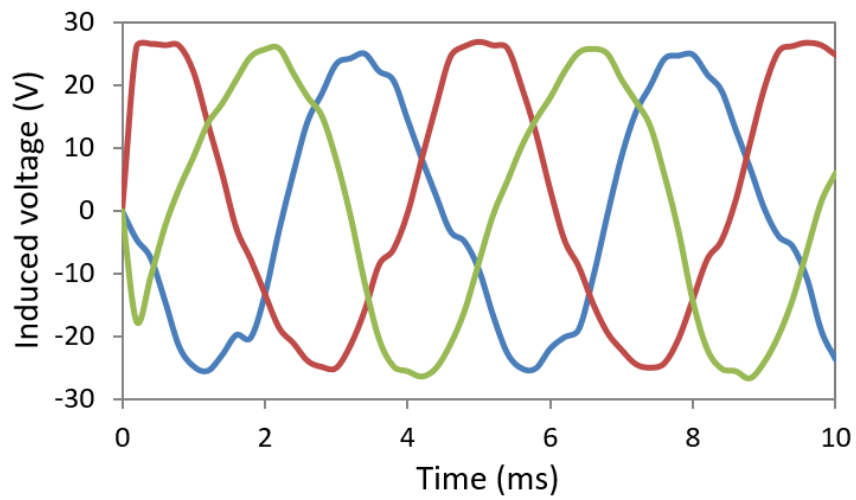
Fig. 5.20. The no-load back-EMF of the DFRM.
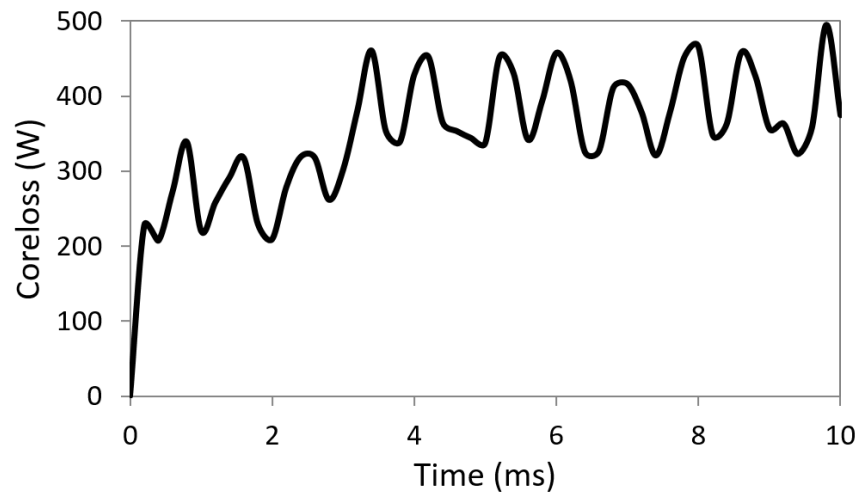
Fig. 5.21. The full-load coreloss of the DFRM.

5.4.6 Performance of the CPMSM

A CPMSM with radial flux outer-rotor configuration is designed and optimized for comparison as shown in Fig. 5.22. As 22 is a relatively large pole-pair number for a machine of this size, fractional slot concentrated winding is used to reduce the slot number. The main parameters of the CPMSM are shown Table 5.5. As the fundamental component of the flux has 22 pole-pairs, the stator yoke is significantly thinner than the PM FM machines. The results of FEM analysis are shown in Figs. 5.23 – 5.26.
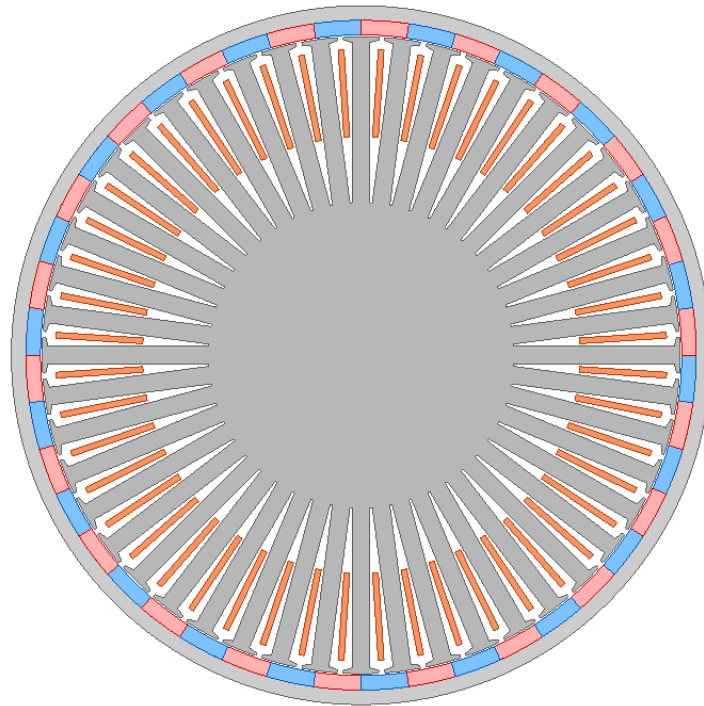
Fig. 5.22. The designed CPMSM.

Table 5.5. Key design data of the CPMSM

Frequency	220 Hz
Axial length	100 mm

Outside radius of the rotor	120 mm
Yoke height	4.5 mm
Teeth width of the stator	6.0 mm
Teeth height of the stator	55.3 mm
Airgap	0.6 mm
Number of rotor pole pairs	22
Number of stator pole pairs	22
Number of stator slots	48
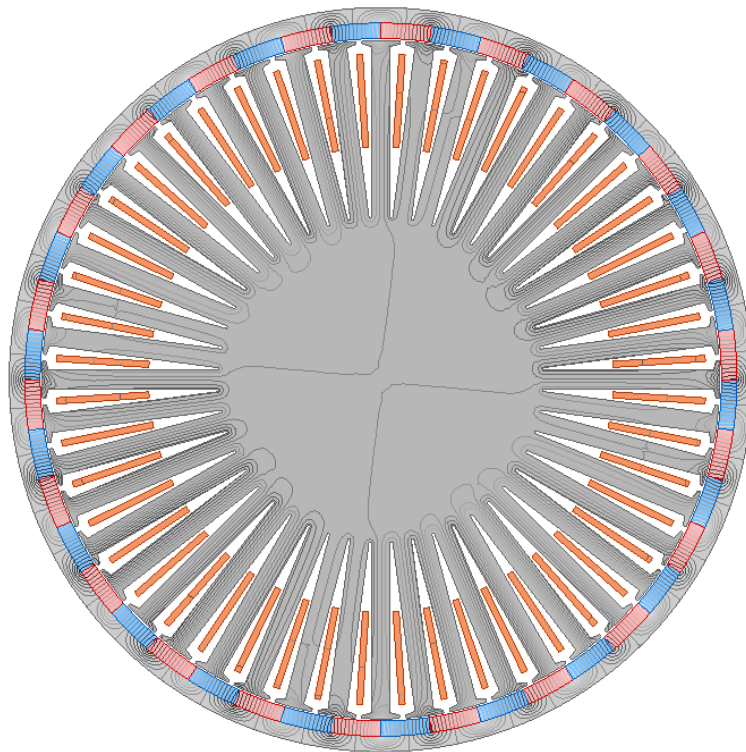
Fig. 5.23. The flux distribution of the CPMSM.
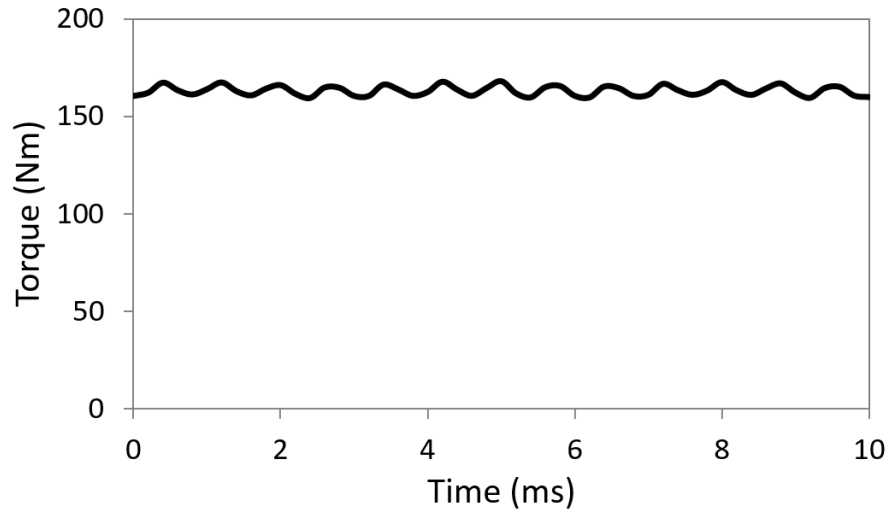
Fig. 5.24. The full-load torque of the CPMSM.
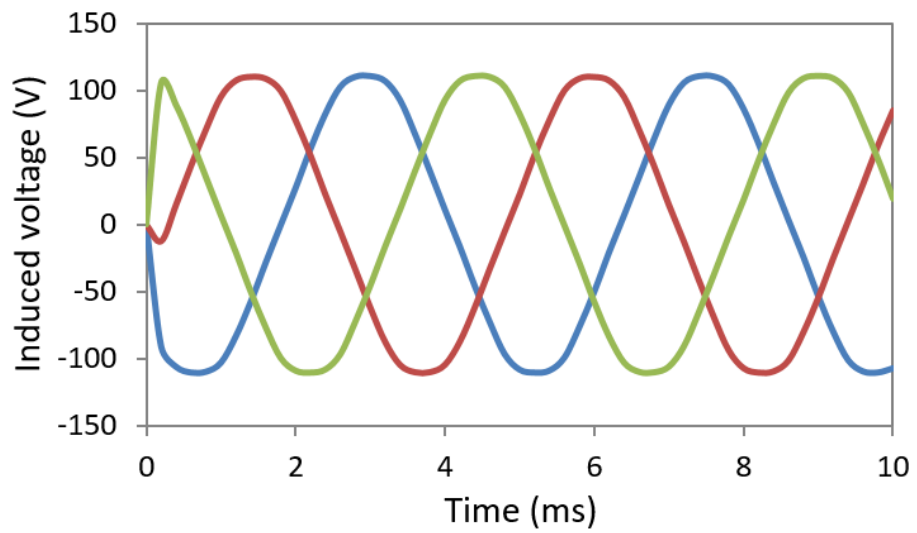
Fig. 5.25. The no-load back-EMF of the CPMSM.
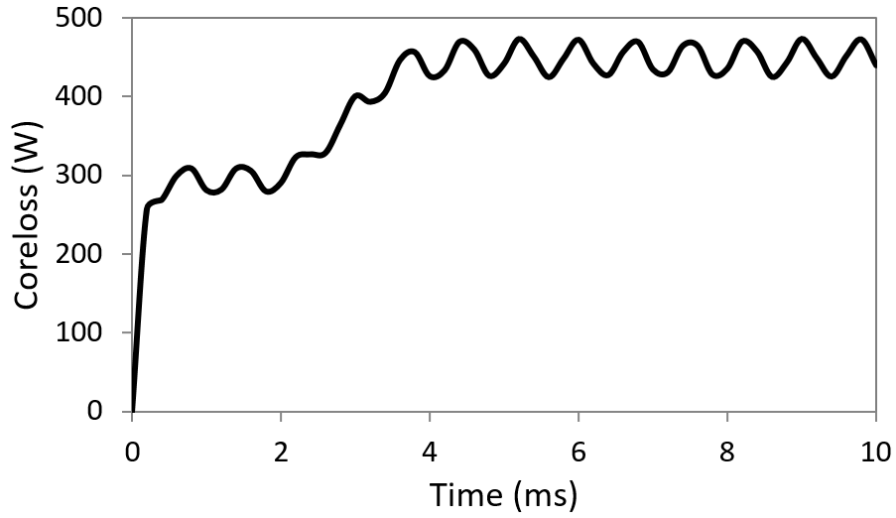
Fig. 5.26. The full-load coreloss of the CPMSM.

5.5 Comparison results

Table 5.6. Performance comparison of FM machines

Motor type	BFMM	VPMM	DEPMM	DFRM	CPMSM
Pull-out torque (Nm)	273	467	466	25	163
No-load back-EMF (V)	125	145	227	26	125
Copper loss (W)	476	568	383	527	213
Core loss (W)	492	721	749	393	440
Efficiency (%)	94.7	95.8	96.3	63.1	94.0
Power factor	0.51	0.50	0.68	0.20	0.97
Torque ripple (%)	1.8	2.6	1.9	39.8	5.5

To make the comparison clear, the main parameters of the above five FM motors are depicted in Table 5.6. The following conclusions are drawn from the results.

(1) Compared with the CPMSM, higher torque densities can be achieved by the PM FM machines, namely the BFMM, the VPMM, and the DEPMM. The reason is that, when a big pole-pair number is required, the slot number is large for a CPMSM even with concentrated winding. The large slot number limits the radial depth of the slots, which limits the total slot area accordingly. Hence, the electric load of the CPMSM is small and its torque density is relatively low. On the contrary, the winding pole-pair number in a PM FM machine can be small even though the rotor pole-pair number is large, so its torque density is not limited by the large rotor pole-pair number.

The VPMM and the DEPMM have higher torque densities than BFMM because they each have only one airgap, which reduces the reluctance of the magnetic circuit. Although the DEPMM has larger volume of PM, the stator PM compresses the room of the windings and the electric load is reduced accordingly. Hence, the torque densities of the VPMM and the DEPMM are quite close.

Note that although the torque densities of the PM FM machines are higher than that of the CPMSM, their losses are also higher, which means that they need better thermal dissipation.

 (2) The torque ripples of the PM FM machines are quite acceptable compared with that of the CPMSM, particularly when the ratio to the average torque is considered. According to [E10], [E11], the cogging torque is decided by the cogging torque factor which is the greatest common divisor between the number of stator poles and the number of

FMPs. In this comparison, all FM machines are designed with a small cogging torque factor of 1 or 2.

(3) The efficiencies of the PM FM machines are even slightly higher than that of the CPMSM. The main reason is that these PM FM machines have a better utilization of the ferromagnetic material. From Fig. 5. 23, it can be seen that a large room at the center of the stator has very small flux. The DEPMM machine has the highest efficiency because it uses the most PM material among these machines, but its coreloss is also the highest.

(4) The power factors of the FM machines are generally low compared with that of the CPMSM. According to the analysis in Chapter 3, the FM machines work on the flux harmonics. However, the airgap flux has many significant harmonic components but only a part of them contribute to the energy conversion, which somewhat reduces the effective airgap flux. The leakage inductance is hence large and the power factor is limited. The power factor of the DEPMM is the highest among these FM machines because it uses the most PM and its field excitation is stronger.

(5) Overall, the PM FM machines have a good potential to be used for general purpose drive or power generation, particularly when the pole-pair number needs to be high and an outer-rotor configuration is needed. For example, in EV in-wheel drive and wind power generation, the torque density of the electric machine needs to be high and an outer-rotor configuration is preferred for simpler mechanical design. The PM FM machines are expected to be suitable for these applications.

(6) The performance of the DFRM is not comparable to the other machines. As no PM is used, the excitation field set up by the field winding is much weaker, which largely limits its torque density and power factor. Moreover, the copper loss is significantly increased by the

excitation winding, which further reduces its efficiency. However, the doubly-fed feature makes it possible to be used in wind power generation. The DFRM also has a robust structure as it has a reluctance rotor and its cost is low. Moreover, the DFRM can be operated in different modes as it has two sets of windings. In this comparison, the field winding is fed with direct current, but it can also be fed with alternating current so that energy conversion can happen in both windings. The operating range of the DFRM can be hence expanded and its performance may also be different. The possibility of using DFRM for in-wheel electric vehicle propulsion has been studied and it will be introduced in Chapter 6.

5.6 Conclusion

In this chapter, the optimization of electric machines is simply introduced at first. Using GA and FEM, several typical FM machines are designed and optimized for a quantitative performance comparison. Based on the comparison results, the pros and cons of these FM machines are concluded and their potential applications are identified accordingly.

References – part E

[E1]   X. Yu, and M. Gen, *Introduction to evolutionary algorithms*, Springer, 2010.

[E2]   G. Lei, J. Zhu, and Y. Guo, *Multidisciplinary design optimization methods for electrical machines and drive systems*, Springer, 2016.

[E3]   R. L. Haupt, and D. H. Werner, *Genetic Algorithms in electromagnetics*, John Wiley & Sons, Inc., Hoboken, New Jersey, 2007.

[E4]   J. N. Reddy, *An introduction to the finite element method*, McGraw-Hill, 2006.

[E5]   O. C. Zienkiewicz, R. L. Taylor, and J. Z. Zhu, *The finite element method: its basis and fundamentals*, Butterworth-Heinemann, 2005.

[E6]   K. J. Bathe, *Finite element procedures*, Klaus-Jurgen Bathe, Cambridge, MA, 2006.

[E7]   P. P. Silvester, and R. L. Ferrari, *Finite Elements for Electrical Engineers*, Cambridge Press, 1990.

[E8]   D. Lin, P. Zhou, W. N. Fu, Z. Badics and Z. J. Cendes, "A dynamic core loss model for soft ferromagnetic and power ferrite materials in transient finite element analysis," *IEEE Trans. Magn.*, vol. 40, no. 2, pp. 1318-1321, March 2004.

[E9]   S. L. Ho, W. N. Fu and H. C. Wong, "Estimation of stray losses of skewed induction motors using coupled 2-D and 3-D time stepping finite element methods," *IEEE Trans. Magn.*, vol. 34, no. 5, pp. 3102-3105, September, 1998.

[E10] K. Atallah, S. D. Calverley, and D. Howe, "Design, analysis and realization of a high-performance magnetic gear," *IEE Proc.—Electric Power Appl.*, vol. 151, no. 2, Mar. 2004, pp. 135–143.

[E11] Z. Q. Zhu and D. Howe, "Influence of design parameters on cogging torque in permanent magnet machines," *IEEE Trans. Magn.*, vol. 15, no. 5, May 2000, pp. 407–412.

Chapter 6

A doubly-fed reluctance machine for in-wheel electric vehicle propulsion

6.1 Introduction

The exhaustion of fossil fuel as well as environmental issues gives a compelling impetus to develop sustainable, efficient and clean alternative vehicles. Electric and hybrid electric vehicles (HEVs) are among the most popular solutions. Several studies on the applications of FM machines in HEV are presented in [F1 – F3]. Compared with the internal combustion engine (ICE) driven vehicles, electric vehicles are clean and efficient and they can even regenerate electrical energy during unurgent braking [F4]. However, EV is not a new concept. The history of EV can be traced back to the early 19th century following the invention of DC motors. The early EVs are proposed to replace the steam powered transportation, but due to the limitations in motor and battery technologies, the early EVs are later overtaken by gasoline powered vehicles [F5].

As a key of the propulsion system, the electric motor decides the performance of the EV in a significant sense. It is of great importance to design suitable motors which satisfy the needs of electric vehicle propulsion. In this chapter, a DFRM is designed for in-wheel electric vehicle propulsion. The design aims and design process are introduced. A prototype is made and the experiment results are compared with FEM simulation results to validate its performance.

6.2 Preliminary design considerations

To have a knowledge of the required performance parameters of the motor, the weight and performance specifications of the vehicle need to be determined. In this thesis, an electric vehicle which has a similar size to a passenger car Nissan Leaf is decided to be the target application. The specifications of the car are listed in Table 6.1.

Generally, the traction force needs to overcome the aerodynamic drag and provide the needed acceleration. When the vehicle is in hill climbing, the traction force is,

$$F_t = F_d + F_i + F_a$$

$$(6.1)$$

where; F_d is aerodynamic drag; F_i is hill climbing force; and F_a is acceleration force. The aerodynamic drag force can be calculated by [F6],

$$F_d = \frac{1}{2} \cdot C_D \cdot A \cdot u^2$$

$$(6.2)$$

where; C_D is the aerodynamic drag coefficient; A is the cross sectional area; u is the velocity.

A simple force analysis model of the car during hill climbing is shown in Fig. 6.1.
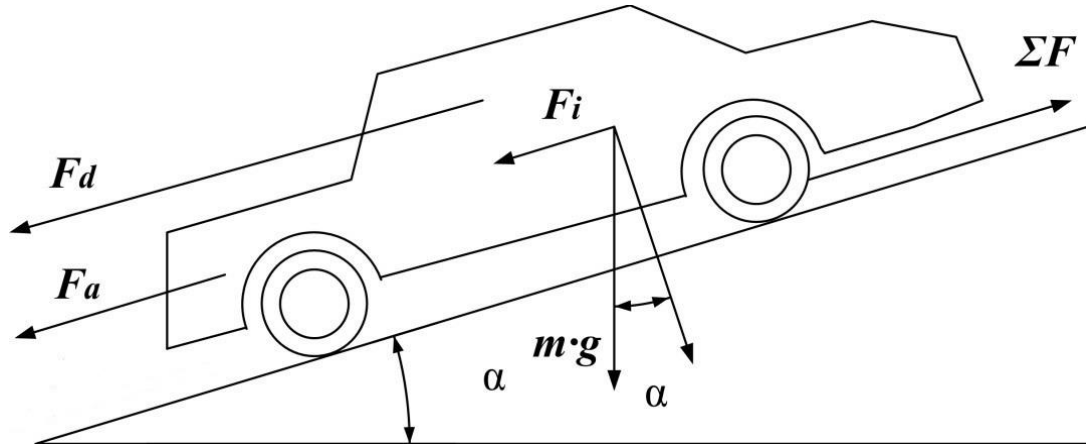
Fig. 6.1. Force analysis of a car.

Considering the vehicle running at 100 km/h (rotor at 924 rpm), the output power of one in-wheel motor is,

$$\frac{1}{4} P_N \bigg|_{ua=100} = \frac{1}{3600 \cdot \eta} \cdot (m \cdot g \cdot f + \frac{C_D \cdot A \cdot u_a^2}{21.15}) = 4.5 \text{kW}$$

(6.3)

And the rated torque is,

$$T\big|_{n=924} = \frac{9550 \cdot P_N}{n} = 47 \text{Nm}$$

(6.4)

TABLE 6.1
SPECIFICATIONS OF THE CAR

Parameters	Symbol	Value
Length (mm)	L	4100
Width (mm)	W	1700
Height (mm)	H	1500
Cross sectional area (m^2)	A	2

Curb weight (kg)	*m*	1300
Aerodynamic drag coefficient	C_D	0.33
Rolling friction coefficient	f_0	0.014
Wheel radius (m)	*r*	0.285

The structure of the proposed motor is shown in Fig. 6.2. The DFRM has two parts of stator and one rotor of ferromagnetic segments. Each part of the stator has a set of windings housed in it. The working principle of the brushless doubly fed FM machine has been introduced in Section 3.3.4. The main parameters of the DFRM are listed in Table 6.1.

(a)

(b)
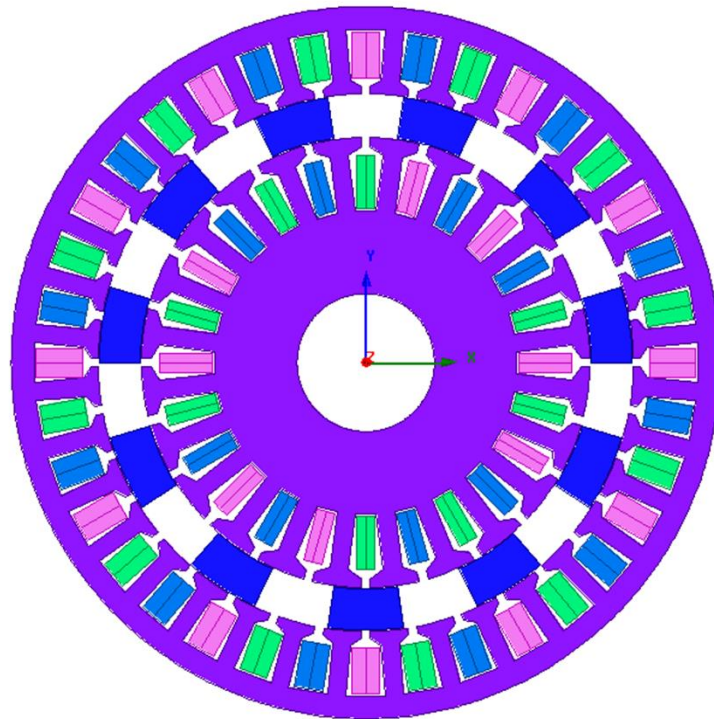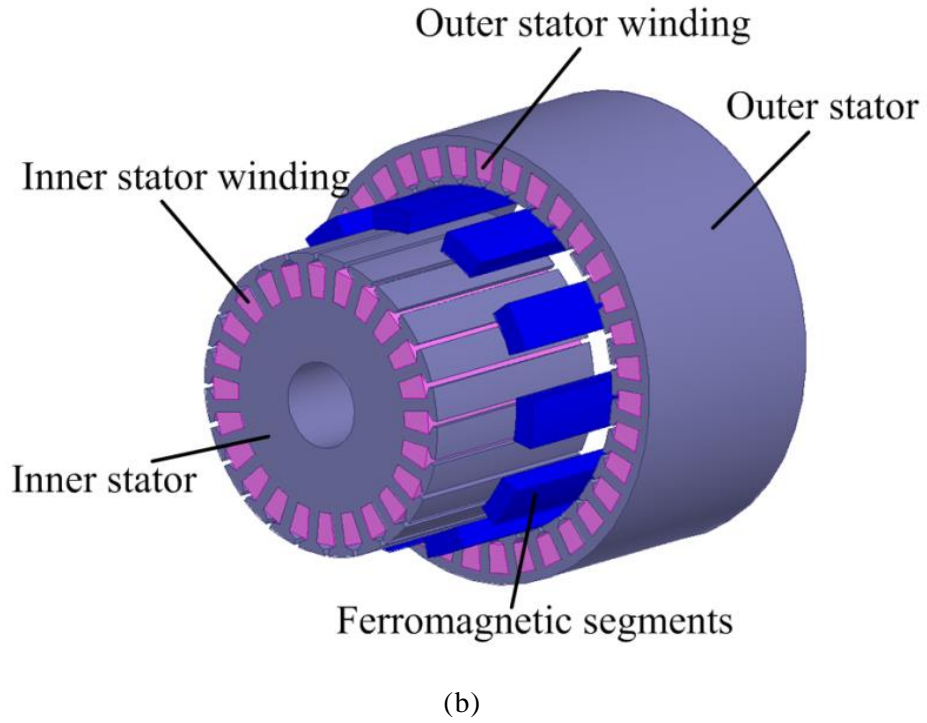
Fig. 6.2. Configuration of the DFRM (a) radial cross section (b) full view.

Table 6.2. Key design data of DFRM

Rated speed	924 rpm
Axial length	160 mm
Outside radius of outer stator	155 mm
Inside radius of inner stator	30 mm
Airgaps	0.6 mm
Number of outer stator pole pairs	6
Number of FMPs	11
Number of inner stator pole pairs	5
Number of outer stator slots	36
Number of inner stator slots	24

6.3 Optimal design

For the optimal design, a parameterized model is constructed as is shown in Fig. 6.3. The following criteria are considered for the design.

1) The outer and inner diameters and the axial length of the DFRM are fixed.
2) The minimum output torque is 47 Nm as discussed in Section 6.2.
3) The maximum current density is 5 A/mm^2 to ensure a safe temperature rise of the winding conductors.

The optimization is conducted using GA and FEM. The objective is to maximize the efficiency of the DFRM. The efficiency is calculated by Eq. 5.2. Note that for the copper loss calculation, both the outer and inner windings need to be considered. The coreloss is calculated using time-stepping FEM with the windings excited at the same frequency [F7], [F8]. The GA optimization is conducted with the following considerations: a population of 100 elements; a maximum generation number of 20; a crossover probability of 0.8; a mutation probability of 0.1.

The optimal parameters of the DFRM are listed in Table 6.3.

(a)

(b)

(c)
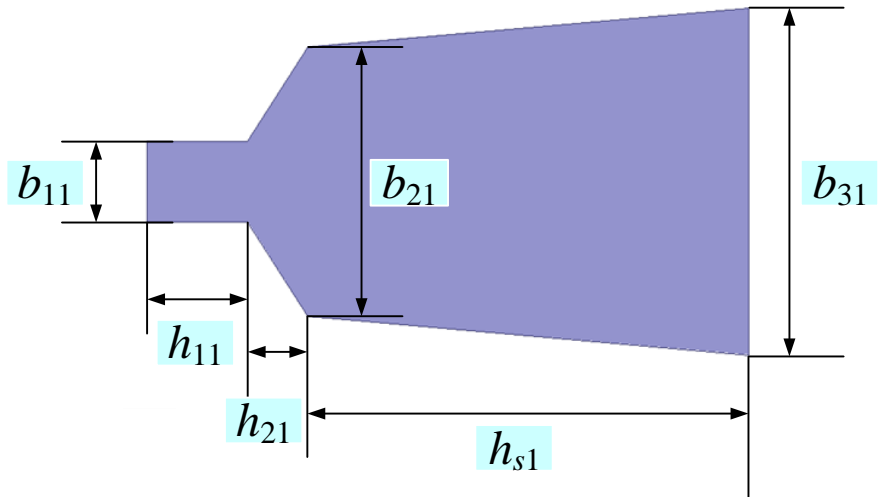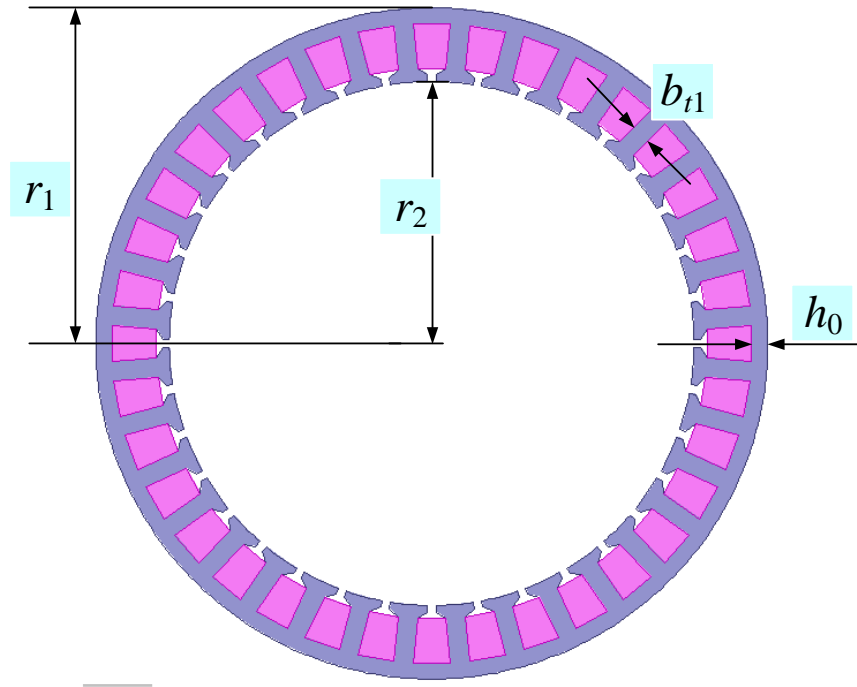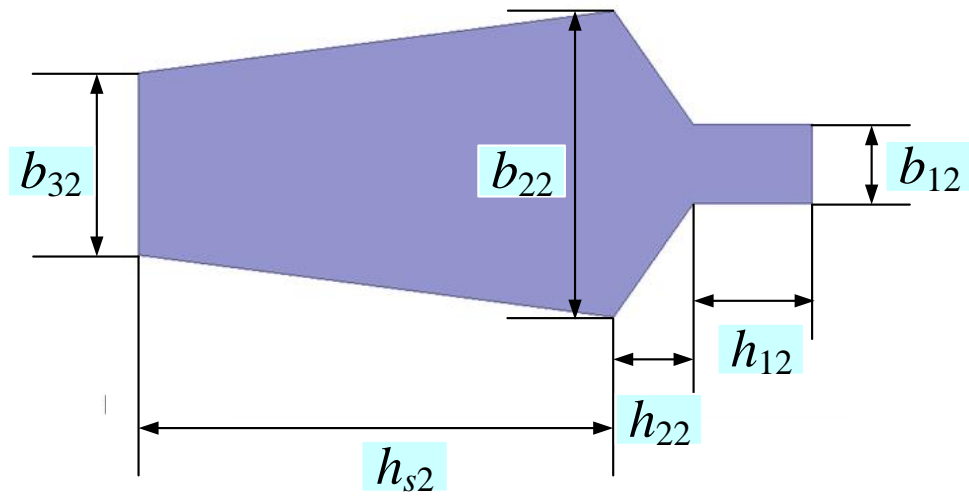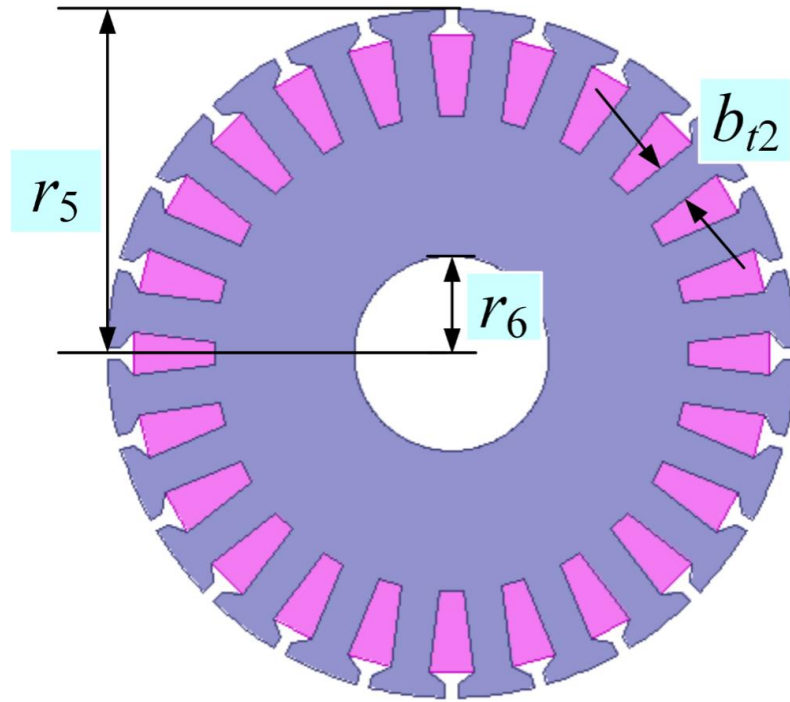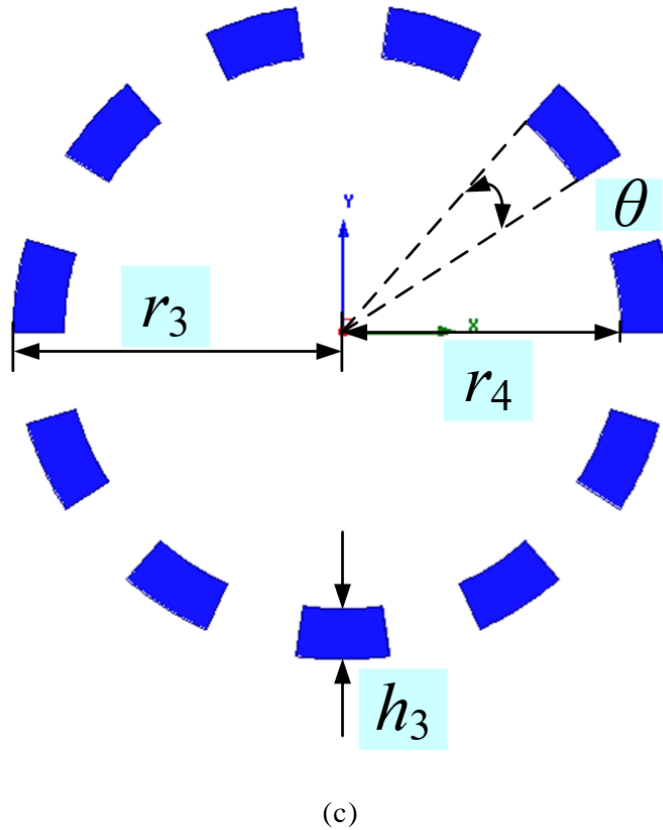
Fig. 6.3. Parameterized model of the DFRM. (a) The outer stator, (b) the inner stator, and (c) the rotor.

TABLE 6.3
THE OPTIMAL PARAMETERS OF THE DFRM

Parameter	Value	Parameter	Value
r_1 (mm)	155.0	r_4 (mm)	107.8
r_2 (mm)	121.4	h_3 (mm)	13.5
b_{t1} (mm)	9.1	θ (deg)	16.4
h_0 (mm)	7.2	r_5 (mm)	107.2

r_3 (mm)	120.8	r_6 (mm)	30.0
h_{11} (mm)	3.0	b_{t2} (mm)	12.1
h_{21} (mm)	2.8	h_{12} (mm)	4.2
h_{s1} (mm)	20.4	h_{22} (mm)	3.7
b_{11} (mm)	3.9	h_{s2} (mm)	24.9
g (mm)	0.6	b_{12} (mm)	4.1

6.4 Control strategy

Due to the special configuration with two sets of windings, the DFRM can work in various modes. Either of the two windings can be used for field excitation when the other one can be controlled to drive the rotor. Still, for field excitation, both DC and AC can be used. As is introduced in Section 3.3.4, the relationship between the rotor speed and winding frequencies is,

$$n_r = 60\left(f_p + f_s\right)\big/p_r$$

(6.5)

The relationship between the rotor and the winding field position changes is,

$$\theta_r = \theta_p + \theta_s$$

(6.6)

where the subscript "r", "p", and "s" represent rotor, primary winding and secondary winding, respectively.

When the primary winding is fed with DC for field excitation, and the secondary winding is used as the control winding, the control block diagram is depicted in Fig. 6.4. In this operation mode, the position of the primary winding field is fixed, which means $\theta_p = 0$.

When the field is set up by AC excitation, the control block diagram is shown in Fig. 6.5. In this control mode, the position of the primary winding field is needed for the determination of the control current.
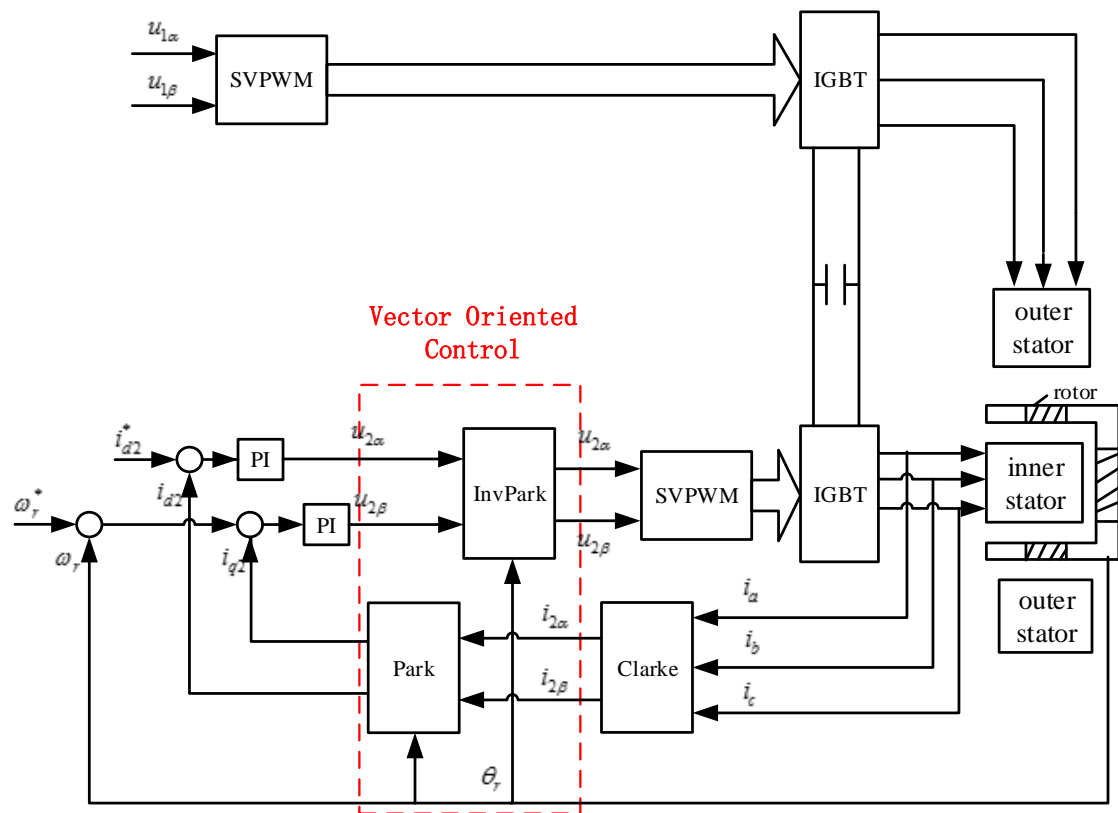
Fig. 6.4. Control block diagram with dc for field excitation.
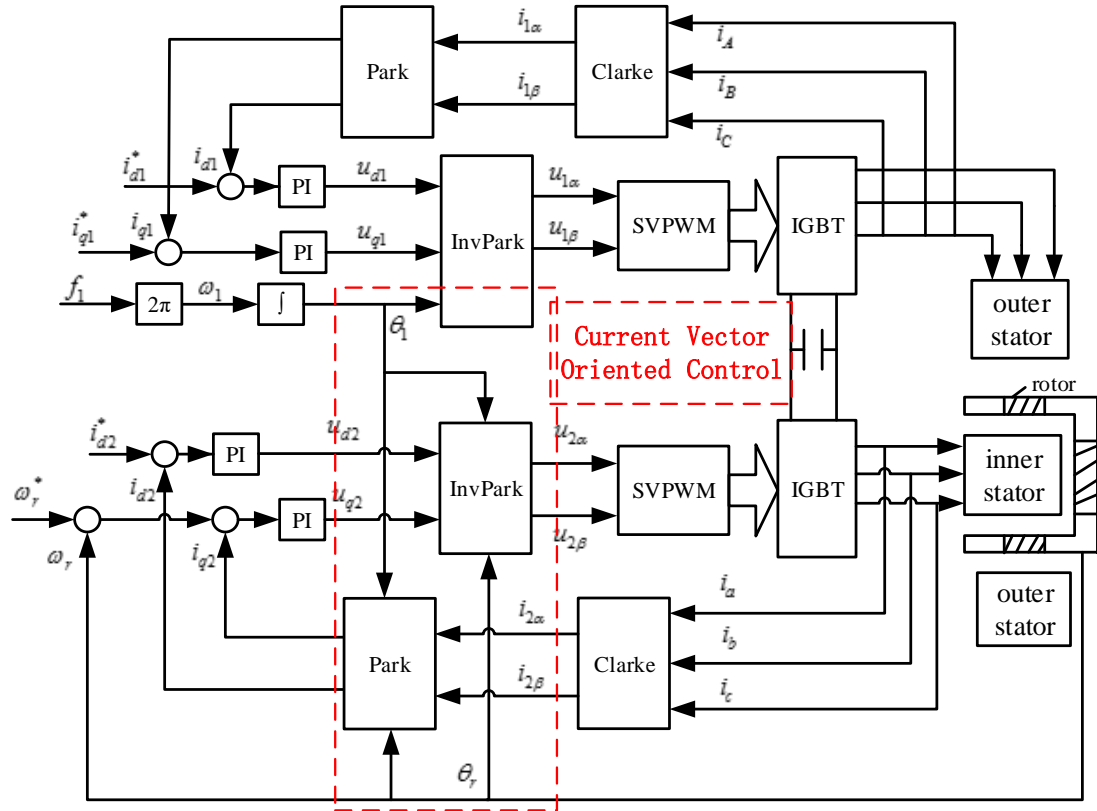
Fig. 6.5. Control block diagram with ac for field excitation.

6.5 Performance analysis

A prototype of the designed DFRM is made as shown in Fig. 6.6. The test bed is shown in Fig. 6.7. In this section, the back-EMF, torque, and efficiency performance of the prototype are tested. The test results are compared with the FEM result for validation.

Fig. 6.6. Prototype of the DFRM.
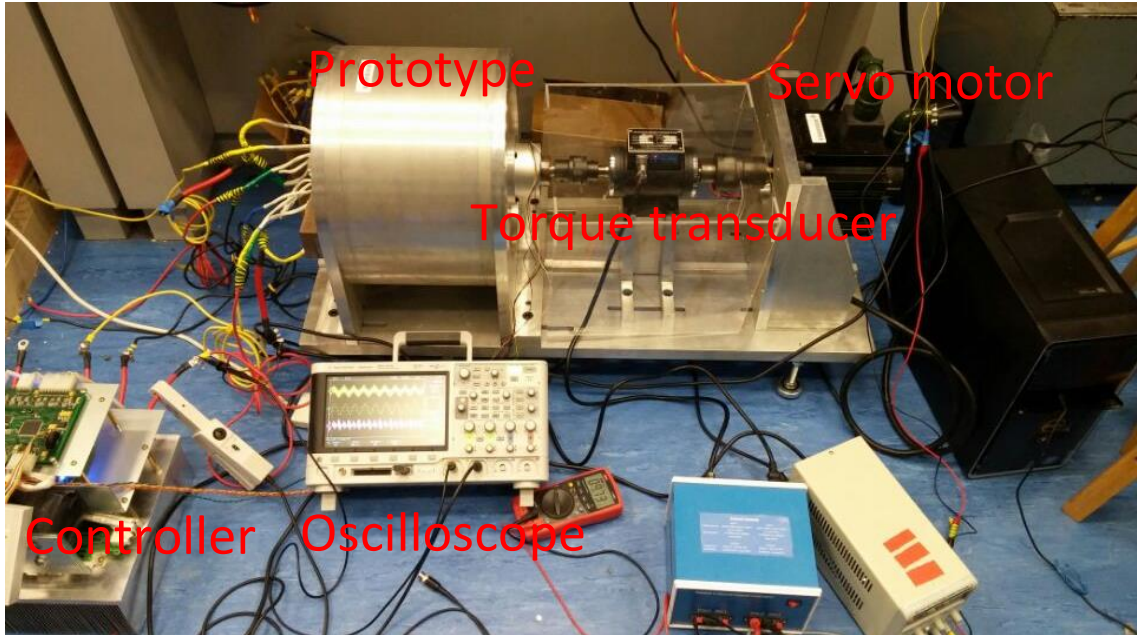
Fig. 6.7. The test bed.

6.5.1 Back-EMF test

For the back-EMF test, a DC of 15A is applied to phase B and phase C of the outer winding for field excitation and the rotor is driven by the servo motor at 924 rpm. Both the test result and the FEM simulation result of the induced voltage in the inner winding are shown in Fig. 6.8. Similarly, when the same DC is applied to the inner winding, the induced voltage in the outer winding is shown in Fig. 6.9. It can be seen that the test results correspond well with the FEM results. The relationship between the rotor speed and winding frequency agree with the analysis.
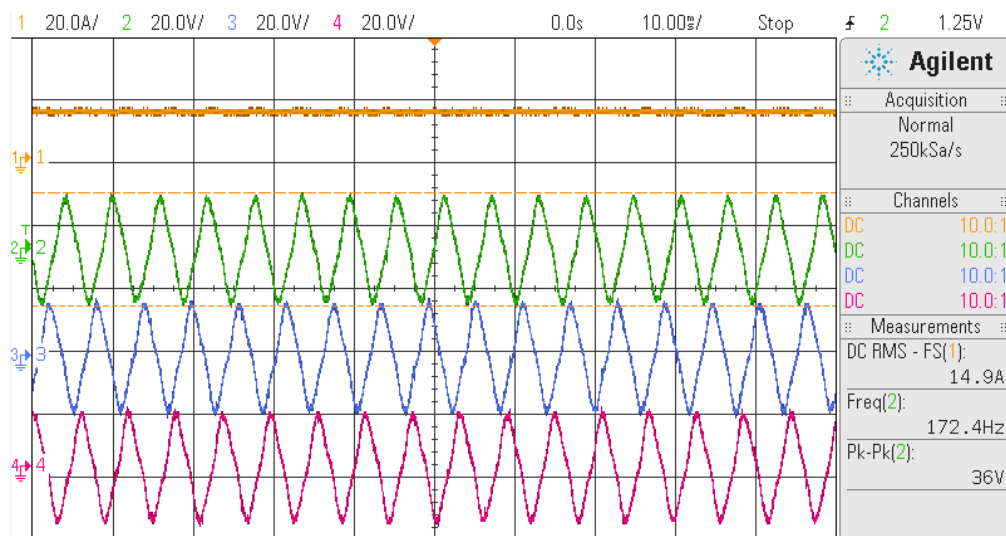
(a)
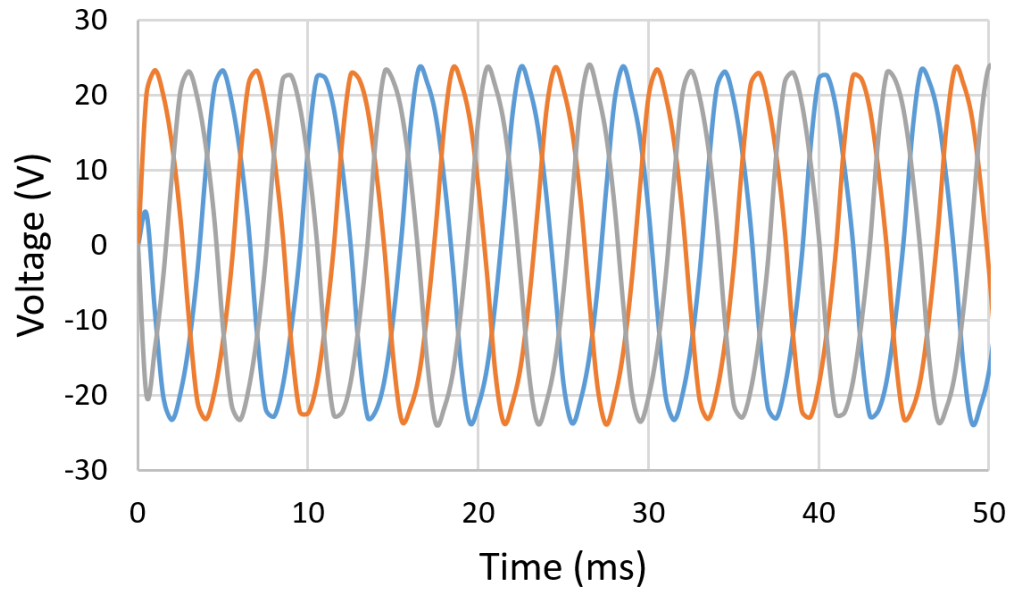
(b)

Fig. 6.8. Back-EMF of the inner winding. (a) The test result. (b) The FEM result.
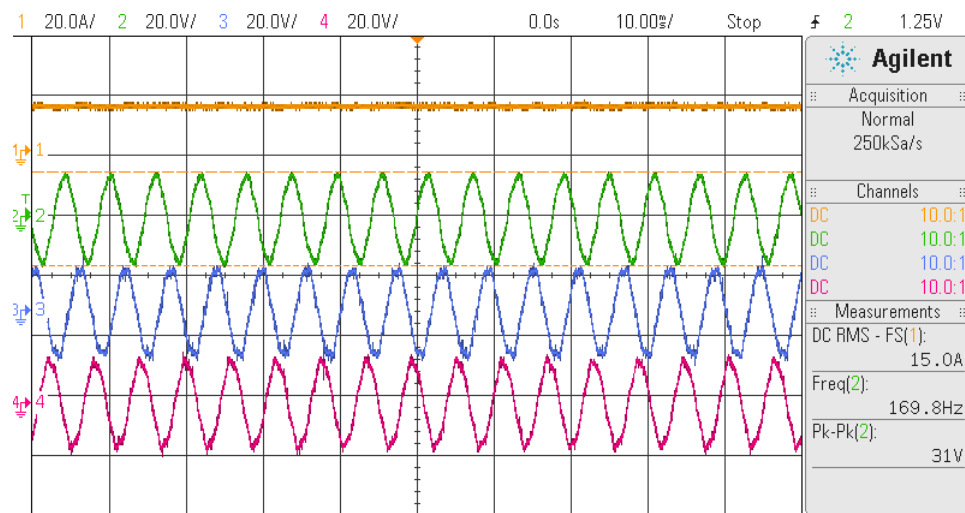
(a)
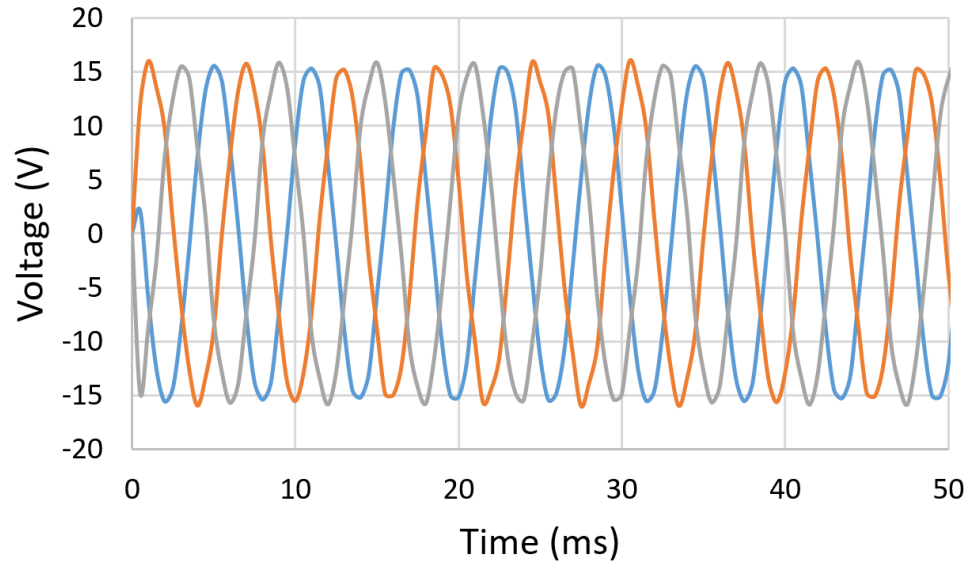
(b)

Fig. 6.9. Back-EMF of the outer winding. (a) The test result. (b) The FEM result.

6.5.2 Operation under load condition

Under different rotor speed and output torque, the losses and efficiency of the motor are tested. During this test, both the frequencies and amplitudes of the two windings are kept close to each other. The servo motor is used as the load. The input power is calculated by adding the output power with the mechanical loss, the coreloss, and the copper loss which are shown in Figs. 6.10 – 6.12. The efficiency map is plotted in Fig. 6.13.
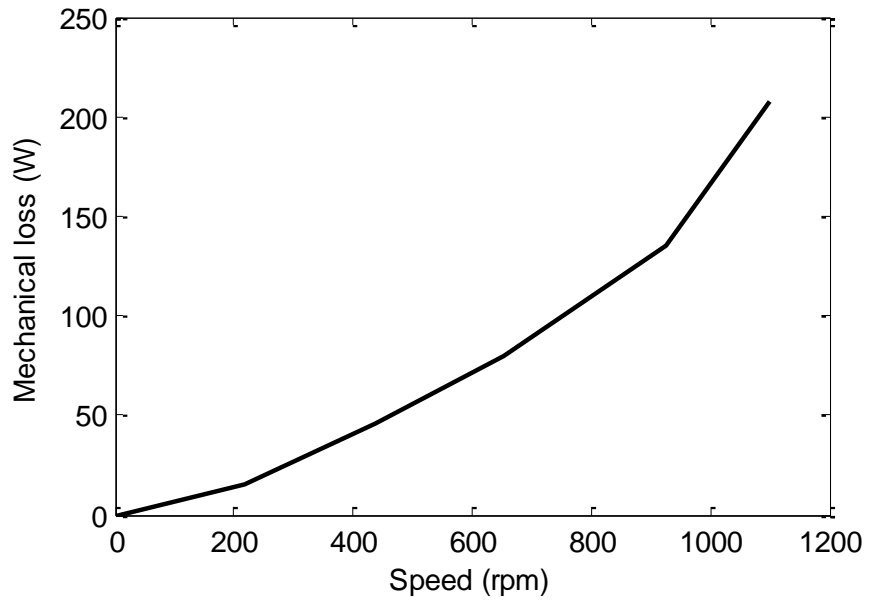
Fig. 6.10. The mechanical loss under different rotor speeds.
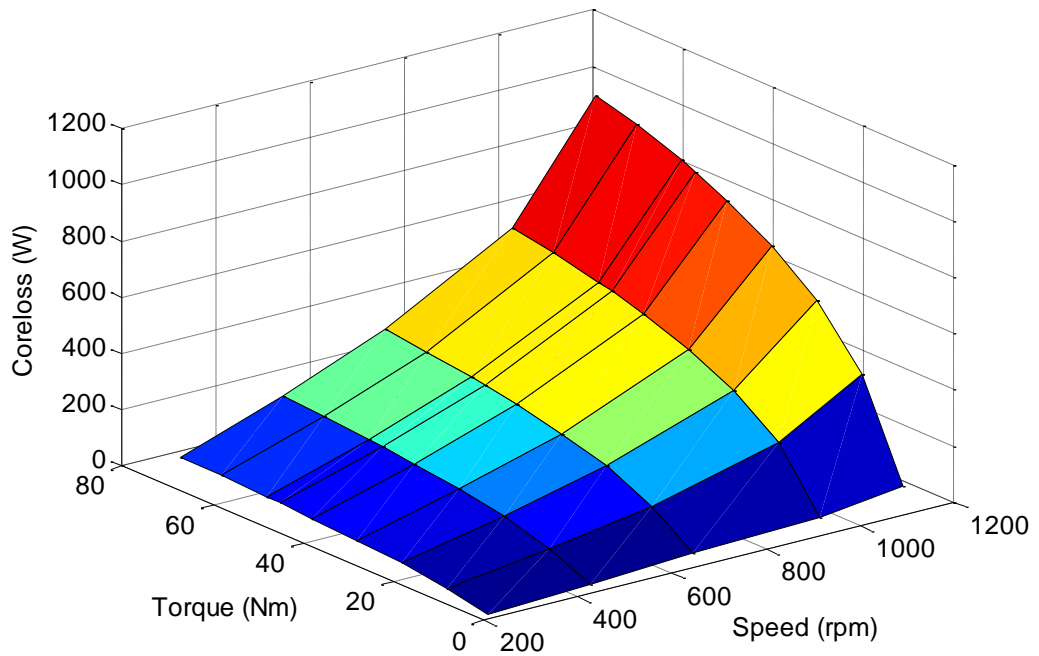
Fig. 6.11. The coreloss under different rotor speeds and torque.
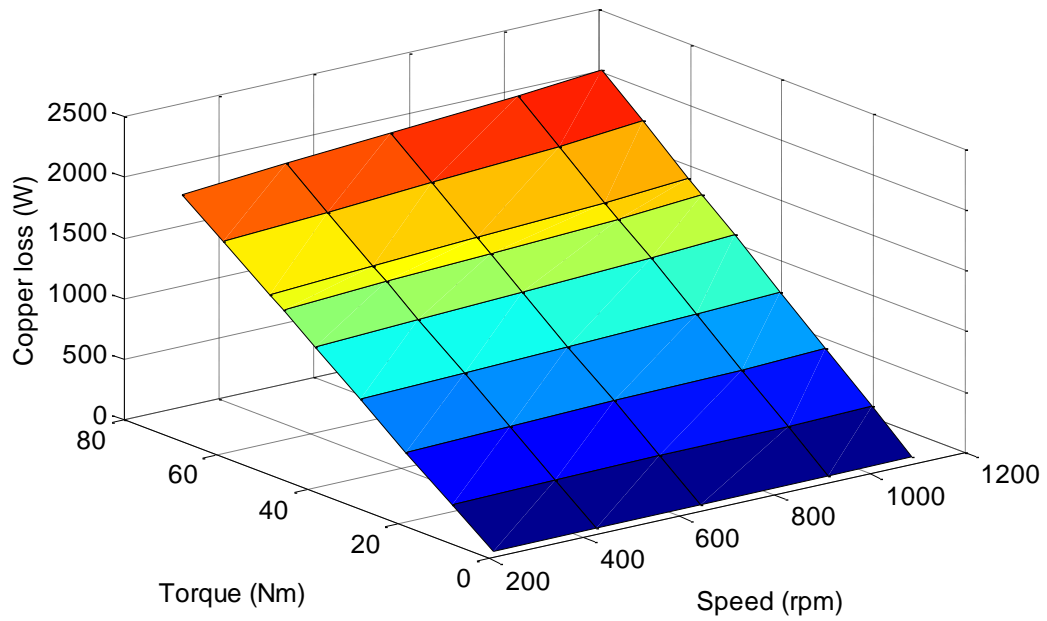
Fig. 6.12. The copper loss under different rotor speeds and torque.
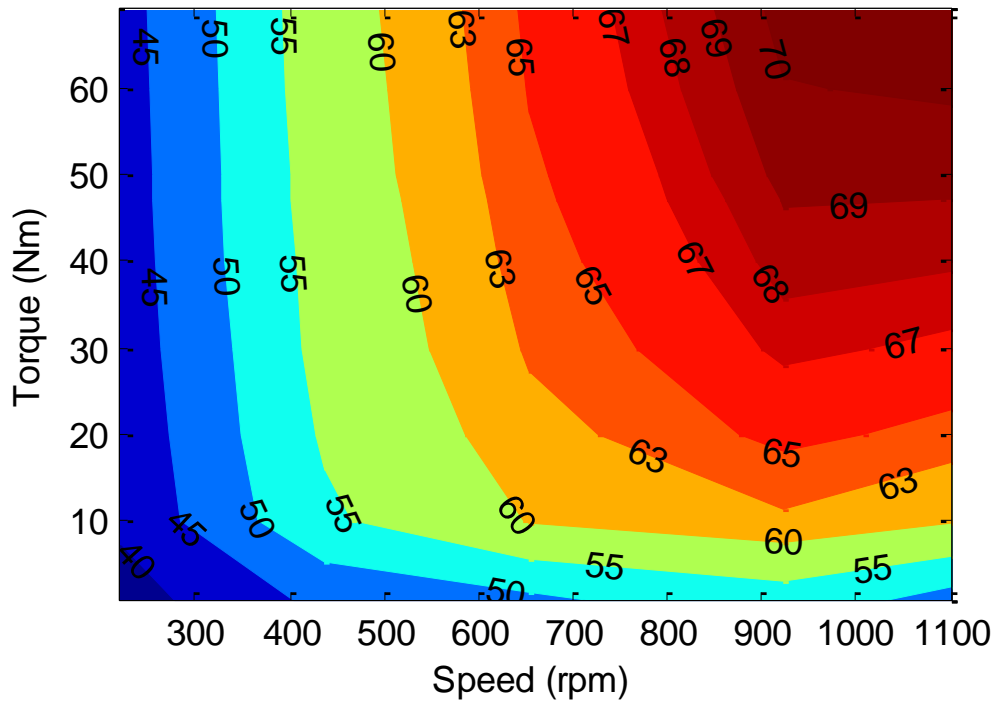
Fig. 6.13. The efficiency map of the DFRM.

It can be seen that the DFRM does have a wide speed range as the frequency variations in both windings result in the speed change. However, as the DFRM is by nature an electric-excited machine, the copper loss is relatively high, and the low power factor of the DFRM even amplifies this effect, which significantly limits the efficiency performance.

Besides a wide speed range, the main advantages of the DFRM are its low cost and robust structure since no PM is used. In conclusion, the DFRM can be used for EV propulsion when the above factors are the key considerations. However, when the efficiency, the power factor, or the torque density is more important, the DFRM is not as good as a PM machine.

6.6 Conclusion

In this chapter, a DFRM for in-wheel EV propulsion is designed, optimized, prototyped, and tested. The working principles and performance of the DFRM are validated. The pros and cons of the DFRM are concluded. Although the DFRM is not always a good choice for in-wheel EV propulsion, it does have some particular features meeting certain requirements on speed range, cost, and robustness.

References - part F

[F1]   Y. Liu, S. L. Ho, and W. N. Fu, "Novel electrical continuously variable transmission system and its numerical model," *IEEE Trans. Magn*, vol. 50, no. 2, Feb. 2014.

[F2]   Yulong Liu, Shuangxia Niu, S. L. Ho, and W. N. Fu, "A New Hybrid-Excited Electric Continuous Variable Transmission System," *IEEE Trans. Magn.,* vol. 50, no. 11, Nov. 2014.

[F3]   Yulong Liu, S. L. Ho, W. N. Fu and Xiu Zhang, "Design Optimization of a Novel Doubly Fed Dual-Rotor Flux-Modulated Machine for Hybrid Electric Vehicles," *IEEE Trans. Magn.,* vol. 51, no. 3, Mar. 2015.

[F4]   M. Terashima , T. Ashikaga , T. Mizuno , K. Natori , N. Fujiwara and M. Yada, "Novel motors and controllers for high-performance electric vehicle with four in-wheel motors", *IEEE Trans. Ind. Electron.*, vol. 44, no. 1, pp. 28-38, 1997.

[F5]   D. A. Kirsch, *The electric vehicle and the burden of history*, Rutgers University Press, USA, 2000.

[F6]   J. D. Jr. Anderson, *Introduction to flight*, McGraw Hill Higher Education, Boston, Massachusetts, USA, 2015.

[F7]   D. Lin, P. Zhou, W. N. Fu, Z. Badics and Z. J. Cendes, "A dynamic core loss model for soft ferromagnetic and power ferrite materials in transient finite element analysis," *IEEE Trans. Magn.*, vol. 40, no. 2, pp. 1318-1321, March 2004.

[F8]   S. L. Ho, W. N. Fu and H. C. Wong, "Estimation of stray losses of skewed induction motors using coupled 2-D and 3-D time stepping finite element methods," *IEEE Trans. Magn.*, vol. 34, no. 5, pp. 3102-3105, September, 1998.

Chapter 7

A doubly-fed dual-rotor flux-modulated machine for wind power generation

7.1 Introduction

As an environmentally clean, renewable and cost-effective energy source, wind power has a great significance for addressing the rising electric power consumption and the global warming problem. According to the Global wind 2014 report, since the late 20th century, the global wind energy capacity has been increasing rapidly as is shown in Fig. 7.1 [G1]. Many countries around the world published government policies or decisions to provide help to the development of wind energy. The increasing contribution of wind power generation has motivated development of new wind turbine systems.

Basically, the most important objective for wind turbines is to minimize the cost of the generated electricity energy. To fulfil this objective, the following aspects of the generator system need to be considered.

The capital expenditures, which include cost of manufacturing, transportation and installation, need to be noted. Usually, the use of rare-earth permanent magnet material increases the manufacturing cost. A generator with higher power density (power capacity per unit volume)

usually makes the transportation and installation simpler and hence lowers the cost.

The system efficiency is another important factor. To offer the same electric power, the needed wind farm area is smaller when the system efficiency is higher. Generally, the permanent magnet machines have higher efficiencies than the electric-excited machines or induction machines.

The maintenance is also an important part of the cost. For offshore wind farms, the maintenance may count for about 30% of the cost. For this consideration, a low maintenance generator system is favorable. Usually, the use of gearboxes, especially the multi-stage gearboxes, will increase the maintenance.
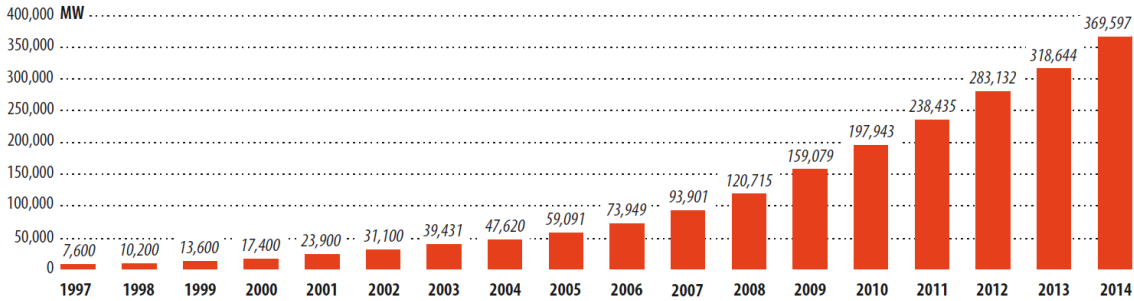
Fig. 7.1. Global cumulative installed wind capacity [G1].

7.2 Overview of wind turbine concepts

The development of wind turbines has been well reviewed in literature [G2]-[G4]. Generally, modern grid-connected wind turbines can be classified into the constant speed constant frequency (CSCF) concept and the variable speed constant frequency (VSCF) concept. The VSCF

concept can be further classified into the semi-variable speed type and the full-variable speed type. Generally, the VSCF system has higher power conversion efficiency than CSCF system as it allows the turbine speed to vary and match the wind speed. As the key component to perform the mechanical to electrical energy conversion, the generators play an important role in wind energy conversion systems, which urges engineers to design new generators suitable for wind turbines.

Considering the use of gearboxes, the wind turbine generators can be classified into geared types and direct drive types. A number of comparisons between geared and direct drive systems have been conducted. Generally, the geared systems have an advantage in terms of the cost and the size or weight. The direct drive systems, however, usually have an advantage in terms of the efficiency, the system reliability and maintenance. Currently, the geared systems have a larger share in the market, but the direct drive systems are drawing more and more attention.

For the VSCF concept, two solutions are popular, namely the doubly-fed induction generator (DFIG) system and the direct-drive permanent magnet synchronous generator (PMSG) system as shown in Figs. 7.2(a) and 7.2(b). The main merit of the DFIG system is its low cost as no permanent magnet (PM) is used and it needs only a partial-scale converter which is around 30 percent of the generator power level [G5]. But the additional mechanical gearbox design reduces the reliability of DFIG system. In contrast, the direct-drive PMSG system has high torque density and it does not need gearboxes or carbon brushes which cause mechanical problems. But the cost of the direct-drive PMSG system is much higher because of the PM material and full-scale converter. It has also been investigated to realize the variable speed operation using a mechanical torque/speed converter as shown in Fig. 7.2(c) [G6], [G7]. Hence a

synchronous generator (SG) can be used for power generation. This type of VSCF system has a lower cost as no power electronic converter is needed but it is rarely used in industry because of issues related to the mechanical converter.
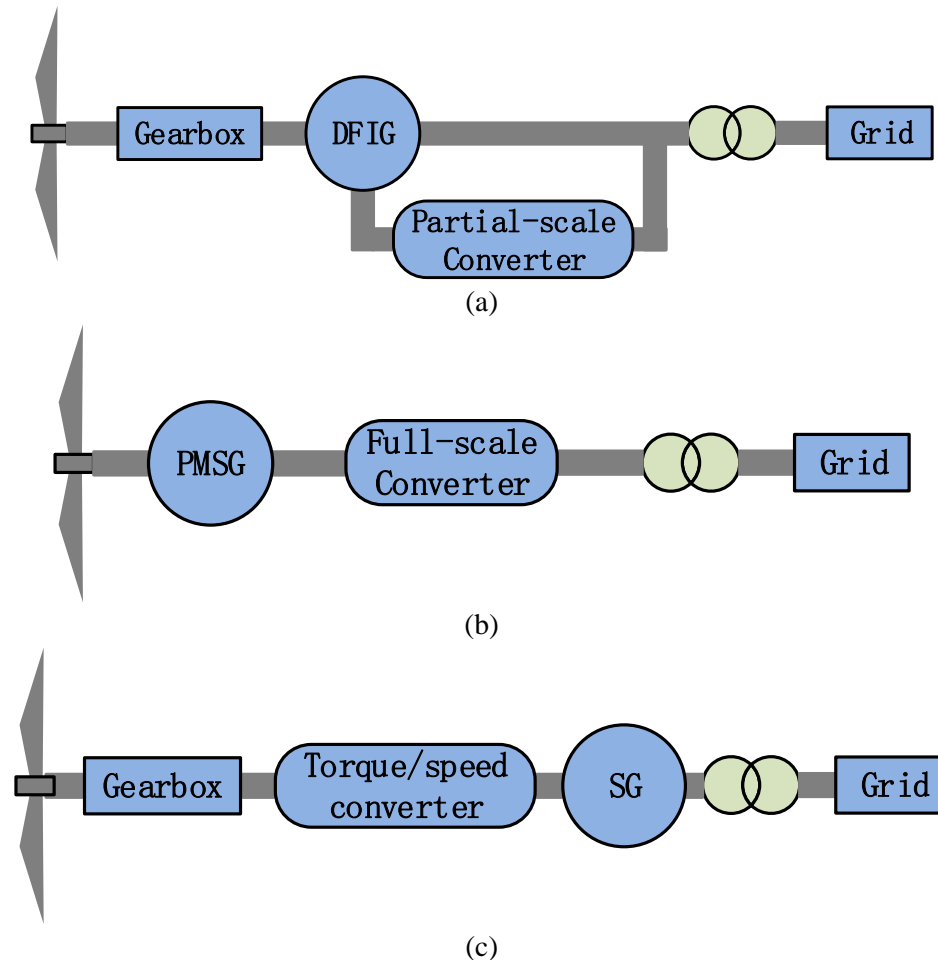
Fig. 7.2. Schematics of (a) the DFIG system, (b) the direct-drive PMSG system, and (c) the SG system with mechanical torque/speed converter.

7.3 An E-CVT based WECS

Recently, the possibility of using electrical continuously variable transmission (E-CVT) system for wind power generation has been investigated in [G8]-[G10]. In [G8], an E-CVT system based on a set of planetary gear and a drive motor is proposed and it is connected to a

generator for wind power generation. In [G9], another design is proposed by replacing the planetary gear with a magnetic gear. These designs are quite bulky due to the multiple components. In [G10], the variable-speed operation is realized by one double rotor machine, but this machine needs carbon brushes as it has windings in a rotor and it still needs an additional synchronous generator for power generation.

In this section, a novel E-CVT based wind energy conversion system (WECS) is proposed. This WECS is gearless and it needs only a partial scale converter as shown in Fig. 7.3. The most outstanding feature is that the variable speed operation and power generation are realized within one single machine, which greatly reduces the size and simplifies the whole generation system. This machine has a doubly-fed dual-rotor structure and compact construction. Inspired by the flux-modulation effect, it allows to keep the speed of the outer rotor constant under the varying speed of the inner rotor. In the meanwhile, it generates power by the electromagnetic interaction between the secondary winding and the outer rotor. As PM material is used for both the inner and outer rotor, the PM excited machine has a relatively high torque density. By virtue of the flux-modulation effect, it can be designed with high pole-pair number for direct-drive system. The gearless and brushless structure makes the machine more reliable and maintenance free. After introducing the structure and working principle of the WECS, the design and FEM based optimization of this doubly-fed dual-rotor permanent magnet machine (DFDR-PM) is presented. The DFDR-PM is also prototyped and experiments are carried out to validate its performance.
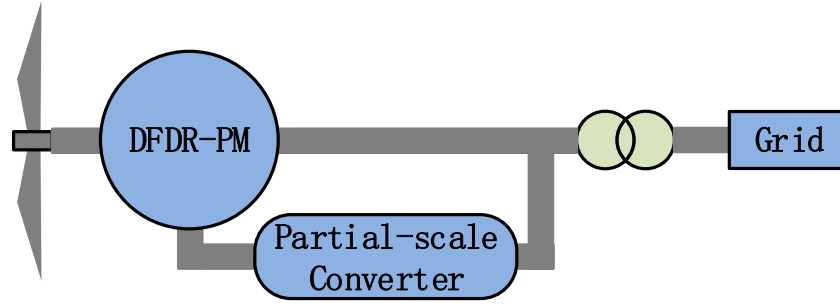
Fig. 7.3. Schematics of the proposed WECS.

7.3.1 Structure and Working Principle
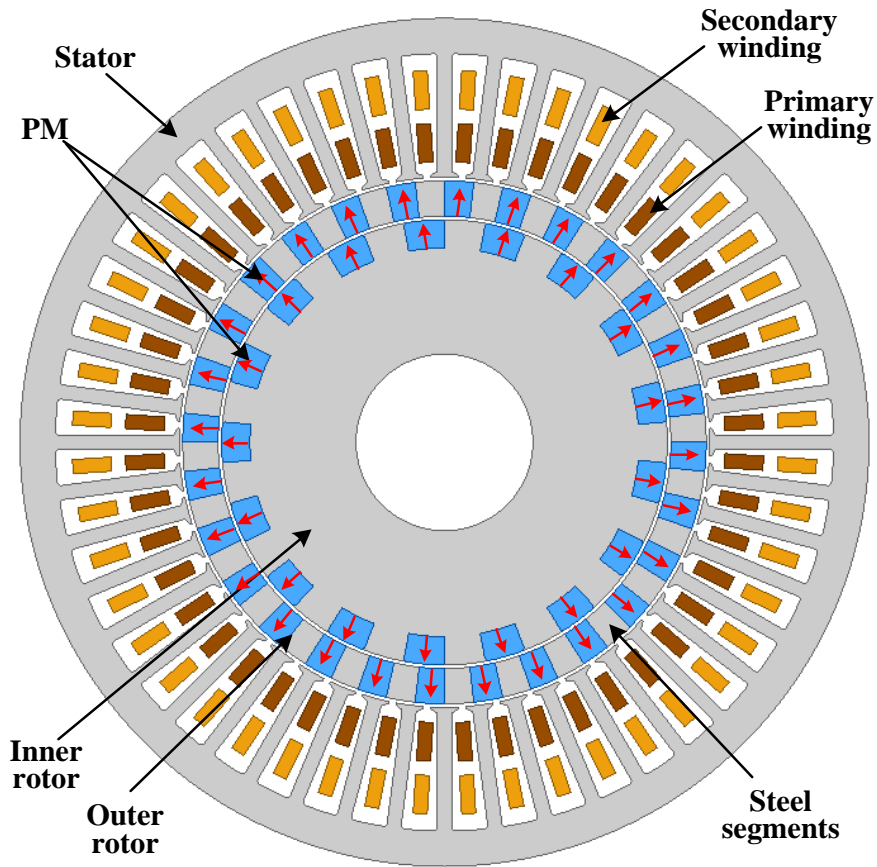
Fig. 7.4. Radial cross section of the DFDR-PM.
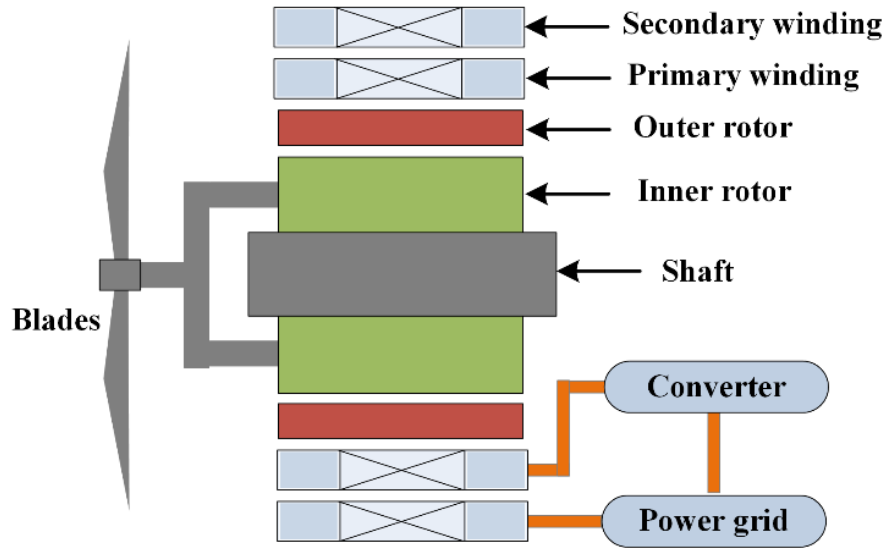
Fig. 7.5. Configuration of the proposed WECS.

A. Machine Structure and Working Principle

As the key component of the proposed WECS, the DFDR-PM machine is introduced first. A radial cross section of the DFDR-PM is shown in Fig. 7.4. It has two sets of windings which are housed in one stator, and two coaxial rotors which are installed inside the stator. The inner rotor is a consequent-pole PM rotor in which all the PMs are magnetized in radially outward direction. The outer rotor comprises interleaved PMs and steel segments. Basically, the secondary winding interacts with the outer rotor like a conventional single-rotor PM machine, and the primary winding interacts with both rotors with the flux modulation effect.

The flux modulation effect means to take advantage of the harmonic components of the magnetic field [G11]. In the proposed DFDR-PM machine, bi-direction flux modulation is employed.

Basically, in the airgap, the relationship between the magnetomotive force (MMF) drop F and the flux density B is,

$$B = \lambda F \tag{7.1}$$

where λ is the permeance per unit airgap area.

The MMF developed by the PM can be expressed as a sum of two components,

$$F \approx F_1 \cos[N_{ri}(\theta - \omega_1 t) + \phi_1] + F_2 \cos[N_{ro}(\theta - \omega_2 t) + \phi_2] \tag{7.2}$$

where; F_1 and F_2 are the magnitudes of the MMF components due to the inner rotor and the outer rotor, respectively; N_{ri} and N_{ro} are the pole-pair numbers of the inner rotor and the outer rotor; ω_1 and ω_2 are the rotation speeds of the inner rotor and the outer rotor; ϕ_1 and ϕ_2 are the initial phase angles of the two MMF components.

Similarly, the permeance can be expressed as,

$$\lambda \approx \lambda_0 + \lambda_1 \cos[N_{ri}(\theta - \omega_1 t) + \phi_3] + \lambda_2 \cos[N_{ro}(\theta - \omega_2 t) + \phi_4] \tag{7.3}$$

where; λ_0 is the average value of λ; λ_1 is the magnitude of the alternating component due to the inner rotor; λ_2 is the magnitude of the alternating component due to the outer rotor; and ϕ_3 and ϕ_4 are the initial phase angles of the two alternating components, which are $\phi_3 = \phi_1 + \pi$ and $\phi_4 = \phi_2 + \pi$, as the PMs and steel segments are arranged alternately.

By substituting F and λ in Eq. (7.1) with Eq. (7.2) and Eq. (7.3), it can be deduced that,

$$B \approx \left\{ \begin{array}{l} \lambda_0 F_1 \cos[N_{ri}(\theta - \omega_1 t) + \phi_1] + \lambda_0 F_2 \cos[N_{ro}(\theta - \omega_2 t) + \phi_2] \\[2mm] -\dfrac{1}{2}\{\lambda_1 F_1 \cos[2N_{ri}(\theta - \omega_1 t) + 2\phi_1] + \lambda_2 F_2 \cos[2N_{ro}(\theta - \omega_2 t) + 2\phi_2]\} \\[2mm] -\dfrac{1}{2}(\lambda_1 F_2 + \lambda_2 F_1) \left\{ \begin{array}{l} \cos[(N_{ro} - N_{ri})(\theta - \dfrac{N_{ro}\omega_2 - N_{ri}\omega_1}{N_{ro} - N_{ri}} t) + \phi_2 - \phi_1] \\[3mm] + \cos[(N_{ro} + N_{ri})(\theta - \dfrac{N_{ro}\omega_2 + N_{ri}\omega_1}{N_{ro} + N_{ri}} t) + \phi_2 + \phi_1] \end{array} \right\} \\[6mm] -\dfrac{1}{2}(\lambda_1 F_1 + \lambda_2 F_2) \end{array} \right\}$$

(7.4)

Obviously, the airgap flux density has six rotating components whose pole-pair numbers (PPNs) are N_{ri}, N_{ro}, $2N_{ri}$, $2N_{ro}$, N_{ro} - N_{ri}, and N_{ro} + N_{ri}, respectively. In a conventional PM machine, the N_{ro} - N_{ri} component is neglectable. But in the DFDR-PM, due to the existence of the steel segments, the N_{ro} - N_{ri} component becomes significant. By designing the PPN of the primary winding to be

$$P_{pw} = N_{ro} - N_{ri},$$

(7.5)

voltage will be induced in the primary winding with the rotors rotating. From Eq.7.5, the rotation speed of the N_{ro} - N_{ri} component is,

$$\omega_{pw} = \frac{N_{ro}\omega_2 - N_{ri}\omega_1}{N_{ro} - N_{ri}}$$

(7.6)

Accordingly, the frequency of the induced voltage in the primary winding is,

$$f_{pw} = \frac{\omega_{pw}(N_{ro} - N_{ri})}{2\pi} = \frac{N_{ro}\omega_2 - N_{ri}\omega_1}{2\pi}$$

(7.7)

The configuration of the proposed WECS is depicted in Fig. 7.5. The inner rotor is fixed on the shaft which is connected to the turbine blades.

The primary winding is linked to the power grid through a converter and the secondary winding is linked to the power grid directly. Reforming Eq. 7.7, the speed of the outer rotor is,

$$\omega_2 = \frac{N_{ri}\omega_1 + 2\pi f_{pw}}{N_{ro}}$$

(7.8)

When the blade speed ω_1 varies, by adjusting the excitation current of the primary winding, the speed of the outer rotor ω_2 can be kept constant. Hence, the frequency and amplitude of the induced voltage in the secondary winding are constant, enabling it to be directly connected to the power grid.

For the secondary winding, as it constitutes a conventional PM machine with the outer rotor, its pole-pair number is the same to that of the outer rotor.

Fractional slot design is adopted to reduce the slot number for both windings. Concentrated winding is used by the secondary winding to reduce the copper loss. The pole-slot combination for fractional slot concentrated winding has been investigated in [G12], [G13].

B. Energy Conversion

During stable operation, the mechanical torque from the turbine is balanced by the electromagnetic torque on the inner rotor T_{ri}. For the outer rotor, its torque T_{ro} comprises two electromagnetic components, namely the part due to the primary winding T_{ro1} and the part due to the secondary winding T_{ro2}. As the outer rotor is a floating rotor, the two

torque components need to cancel each other, which means $T_{ro} = T_{ro1} + T_{ro2} = 0$. The torque relationship between the rotors in a FM machine has been introduced in [G14], which in this machine is

$$\frac{T_{ro1}}{N_{ro}} = \frac{T_{ri}}{N_{ri}}$$

(7.9)

When the losses in the system are not considered, the input power of the converter is,

$$P_{con} = P_{rated} - P_{wind} = T_{ro1}\omega_2 - T_{ri}\omega_1$$

(7.10)

where; P_{rated} is the rated power output to the power grid; P_{wind} is the wind power captured by the turbine blades. Clearly, only a partial scale converter is needed for this WECS and its power level depends on the designed speed range of the turbine blades. Like that of a doubly-fed induction generator, a synchronous speed is defined for the inner rotor of the DFDR-PM,

$$\omega_{1syn} = \frac{N_{ro}}{N_{ri}}\omega_2 = \frac{2\pi f_{sw}N_{ro}}{P_{sw}N_{ri}}$$

(7.11)

where f_{sw} and P_{sw} are respectively the frequency and the pole-pair number of the secondary winding. Accordingly, the speed below/above the synchronous speed is defined as subsynchronous/supersynchronous. The system working principle is simply introduced as follows.

1) When the inner rotor is rotating at the synchronous speed, P_{con} is 0, which means no power is flowing through the converter and the primary winding. The primary winding needs to be fed with dc current and no effective electromotive force is induced in it.

2) During subsynchronous operation, P_{con} is positive. The primary winding helps to drive the outer rotor and it extracts power from the grid through the converter as shown in Fig. 7.6(a).

3) During supersynchronous operation, *Pcon* is negative. More power is supplied by the inner rotor than the rated power needed by the outer rotor. The extra power goes to primary winding for generation. Both the primary winding and the secondary winding inject power to the grid. The power flow is shown in Fig. 7.6(b).

(a)

(b)
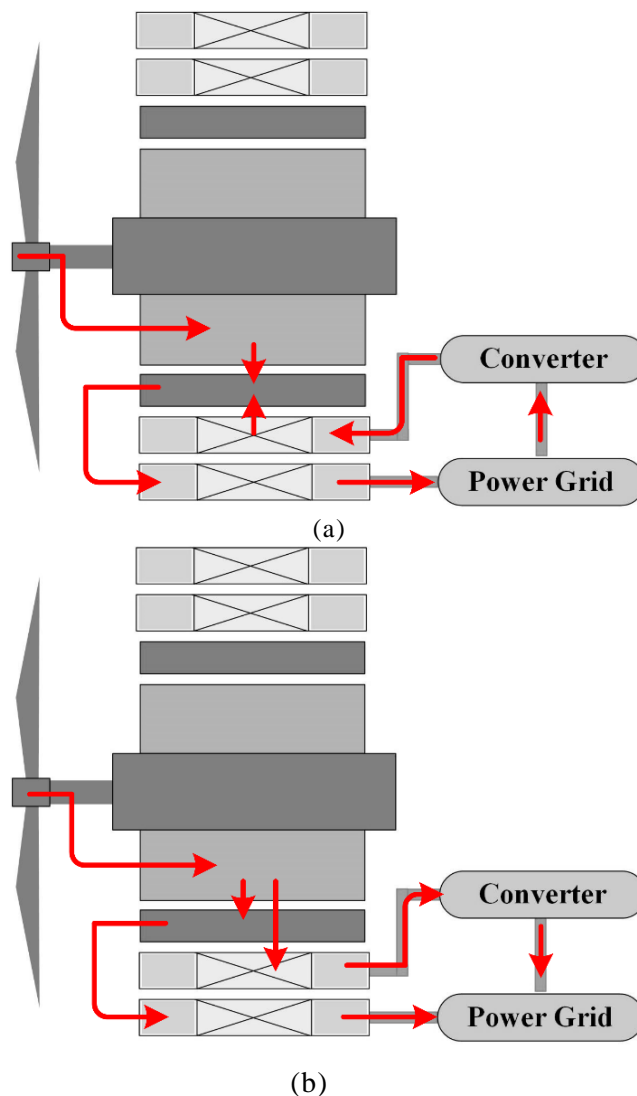
Fig. 7.6. Power flow in the WECS during (a) subsynchronous operation and (b) supersynchronous operation.

7.3.2 Preliminary Design Consideration

In view of the fact that the DFDR-PM is essentially a combination of an E-CVT and a generator, the performances of both of them have to be considered. For convenience, the two components are referred to as E-CVT part and generator part, respectively.

Considering that T_{ro1} and T_{ro2} need to cancel each other, the E-CVT part and the generator part should have similar torque capability. As these two parts have the same rotor diameter, they should also have similar electrical load. As a result, in this design, the slot room is evenly divided by the primary winding and the secondary for the sake of heat dissipation.

Since the torques of the rotors are reversely proportional to their pole-pair numbers as shown in Eq. 7.9, only the torque of the outer rotor needs to be considered for the design of the E-CVT part and the torque of the inner rotor can be decided accordingly.

The cogging torque in a FM machine is decided by the cogging torque factor which is the greatest common devisor between the pole-pair numbers of the two rotors [G11], [G15]. In the proposed DFDR-PM machine, the cogging torque factor is 1 with the designed pole combination and its cogging torque is expected to be relatively small.

For the design of a conventional synchronous machine, the following famous sizing equation is usually used,

$$S = 11 K_w \cdot \bar{B} \cdot A \cdot D^2 \cdot l \cdot n \tag{7.12}$$

where; S is the output power in W; K_w is the winding factor; $\bar{B}$ is the mean flux density in the airgap in T; A is the electrical loading in A/m; D

is the airgap diameter; l is the core length; and n is the rotational speed [G16]. For the DFDR-PM machine, although two windings are used, they do not affect each other except for the saturation problem since their pole-pair numbers are different. So Eq. (7.12) can still be used to decide the preliminary geometric parameters with only the generator part considered.

The ratio of PM width to steel width in the rotor has been investigated in [G17]. To achieve the best flux modulation effect, this ratio should be roughly 0.5~0.6. In the proposed DFDR-PM, the rotor PM and steel segments have the same width.

To have a general idea of the effect of the geometrical parameters on the torque performance of the DFDR-PM, a parametric analysis is first done before optimization. The analyzed variables are:

H_{ri}, radial length of the PM in the inner rotor;

H_{ro}, radial length of the outer rotor;

R_s, inner radius of the stator;

H_y, radial length of the stator yoke.

W_t, width of the stator teeth.

For each variable, its effects on T_{ro1} and T_{ro2} are analyzed separately using static two-dimensional (2-D) FEM. The excitation current is fixed at the maximum torque point during the analysis. The analysis results are shown in Fig. 7.7.

1) As is analyzed in Section 7.3.1, the inner rotor only interacts with the primary winding and the change of H_{ri} does not have significant influence on the torque of the generator part. For the E-CVT part, the change of H_{ri} affects its MMF and the flux modulation effect. H_{ro2} can be maximized at certain H_{ri} value.

2) To increase T_{ro2}, H_{ro} is required to be large enough, which is similar to the situation in a conventional PM machine. However, for the E-CVT part which is basically a FM machine, the increase of H_{ro} not only increases the MMF, but also decreases the radius of the inner airgap and affects the flux modulation effect. So a compromise is needed for the design of H_{ro}.

3) The effects of R_s on T_{ro1} and T_{ro2} are similar. The increase of R_s increases the airgap radius, which is a positive element for improving the torque. However, it also compresses the slot area, which decreases the electrical load considering a constant current density.

4) The effects of H_y and W_t are similar. The increase of them compresses the slot area, but lowers the flux density in the stator core. To improve the torque performance, they need to be designed with a compromise considering the electrical load and the saturation problem.
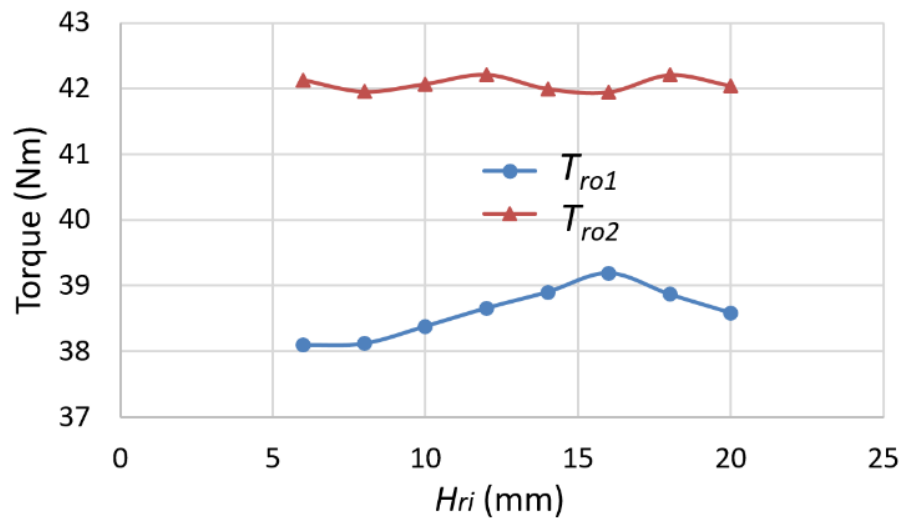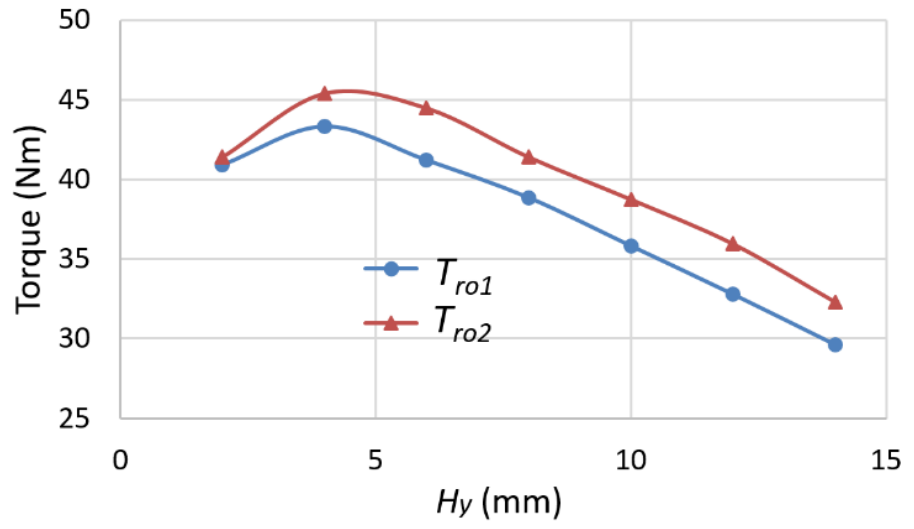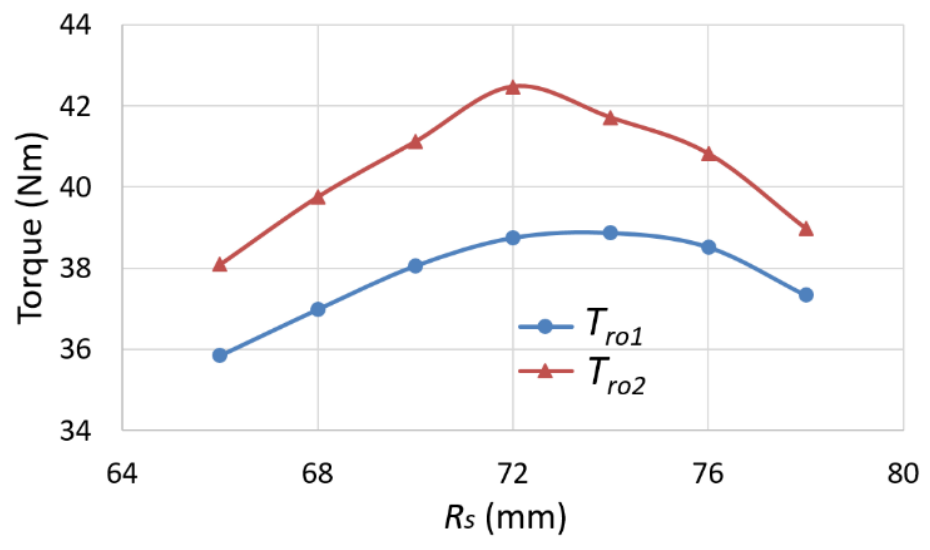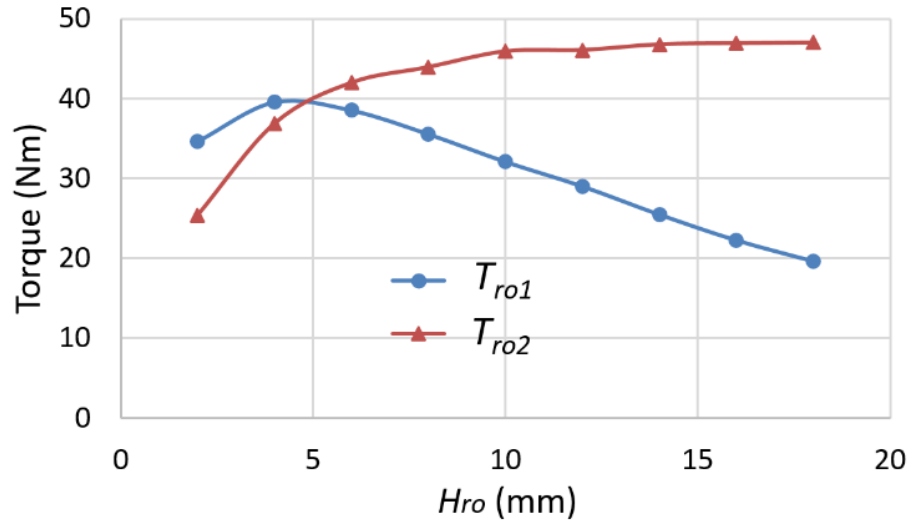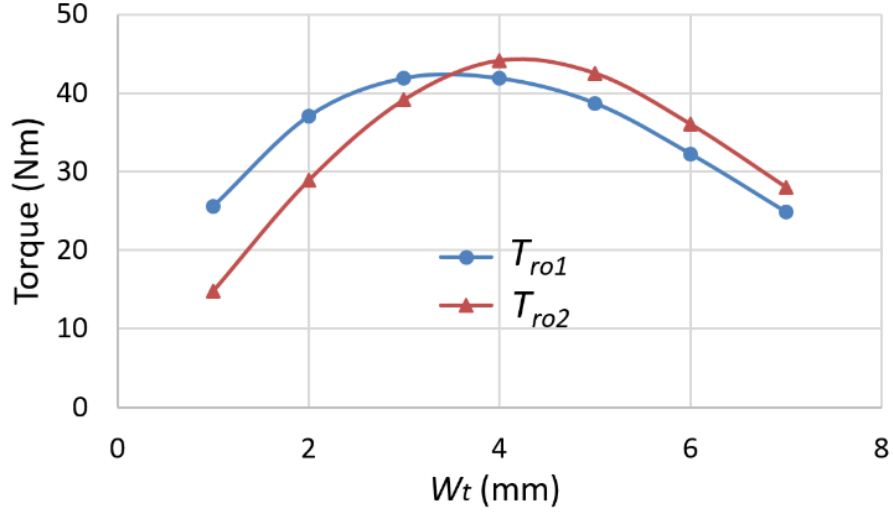
Fig. 7.7. Effect of geometric parameters on torque.

7.3.3 Optimal Design

An optimization of the DFDR-PM is conducted based on genetic algorithm (GA) and FEM. The aim is to maximize the torque capability of the system with both the E-CVT part and the generator part considered. As the torque components due to two windings need to balance each other on the outer rotor, both of them are important and their maximum values should be similar. The fitness function is,

$$F(H_{ri}, H_{ro}, R_s, H_y, W_t) = T_{ro1} \cdot T_{ro2}$$

(7.13)

The following constraints are used for the optimization.

1) The outer geometry is fixed. The outer diameter of the stator is fixed at 216 mm and the stack length is fixed at 65 mm.

2) The lengths of the outer airgap and the inner airgap are both fixed at 1 mm.

3) The current density in the conductor is limited within 5.5 A/mm2. The slot fill factor, which is the ratio of the cross section area of conductors to the slot area, is 55%.

115

For each element, T_{ro1} and T_{ro2} are respectively computed using one transient FEM analysis. Unlike the parametric analysis in which the windings are excited separately, to have the saturation issue considered, the two windings are excited at the same time in the optimization. For the calculation of T_{ro1}, the locked-rotor torque angle curve is first computed with the primary winding excited with ac current and the secondary winding excited with dc current. By averaging the maximum value and the minimum value in the torque angle curve, the torque component due to the secondary winding can be removed and T_{ro1} is calculated. The torque T_{ro2} can be calculated in a similar way by exciting the primary winding with dc current and the secondary winding with ac current. A flowchart of the optimization process is shown in Fig. 7.8.

The optimization is conducted with the following considerations: a population of 30 elements; the maximum generation number of 20; crossover probability of 0.8; mutation probability of 0.1.

To improve the GA convergence performance, for each generation, if the best element is worse than the best element of its previous generation, its worst element will be replaced by the previous best element. The fitness variation during the optimization process is shown in Fig. 7.9. Although the average fitness of the population goes up and down, the best fitness keeps increasing. The optimized variables are: $H_{ri} = 15.8$ mm, $H_{ro} = 6.1$ mm, $R_s = 73.3$ mm, $H_y = 4.1$ mm, $W_t = 3.9$ mm. Through the optimization, the slot area is designed to be relatively large. This is due to the arrangement of placing both windings in one stator. The other specifications of the DFDR-PM are listed in Table 7.1.
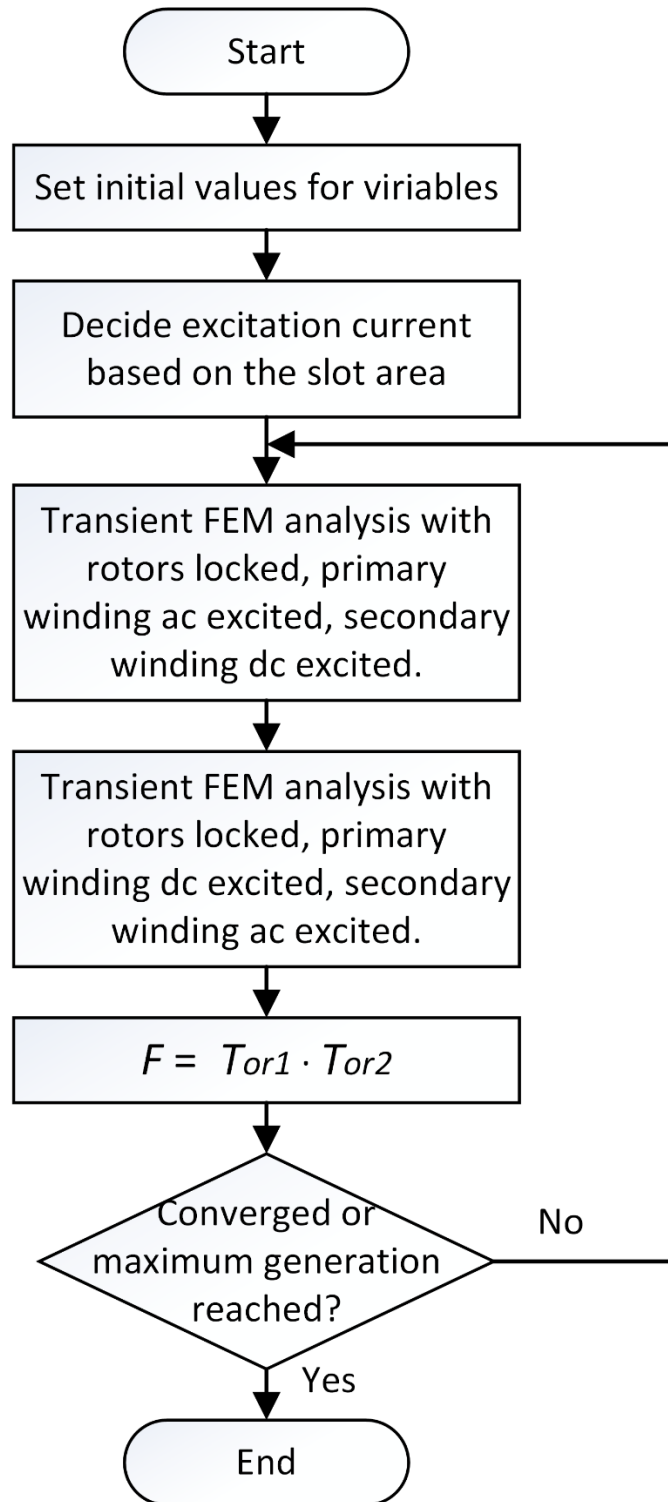
Fig. 7.8. Flowchart of the optimization process.

TABLE 7.1
SPECIFICATIONS OF THE DFDR-PM

Quantity	Value
Number of phases	3
Rated frequency	50 Hz
Rated power	420 W
Rated output phase voltage	13.5 V(rms)
Rated output phase current	10.4 A(rms)
Synchronous inner rotor speed	176.5 rpm
Rated inner rotor torque	27 Nm
Outer radius of stator	108.0 mm
Inner radius of stator	74.7 mm
Outer airgap length	1.0 mm
Inner airgap length	1.0 mm
Radial length of outer rotor	6.1 mm
PM length of inner rotor	15.8 mm
PM pole-pair number in outer rotor	28
PM pole-pair number in inner rotor	17
Number of primary stator winding pole pair	11
Number of secondary stator winding pole pair	28
Number of stator slots	48
Number of turns for primary winding	30
Number of turns for secondary winding	30
Stack length	65 mm
Stator and rotor core material	M19_24G
Magnetic remanence	1.2 T
Rated efficiency at synchronous speed	70 %
Power density	7.0×10^2 kW/m^3
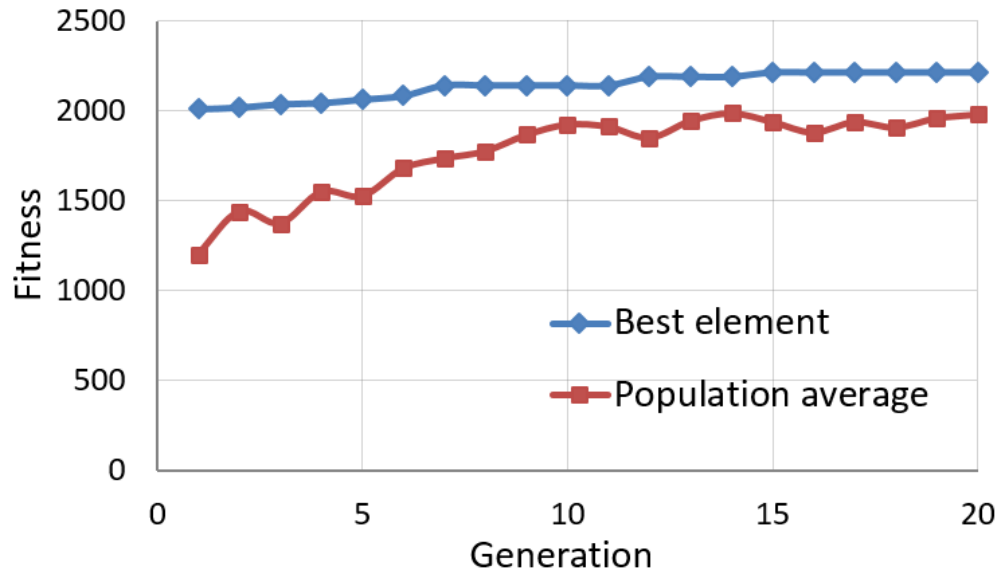
Fig. 7.9. Fitness variation during the optimization process.

7.3.4 Performance Validation

To validate the performance of the proposed machine, besides FEM simulation, a prototype is also made and tested as shown in Fig. 7.10 and Fig. 7.11. The inner rotor of the prototype is connected to a servo motor through a torque transducer. The primary winding is connected to the controller and the secondary winding is connected to resistive load.

<div style="text-align:center">(a)</div>

<div style="text-align:center">(b)</div>
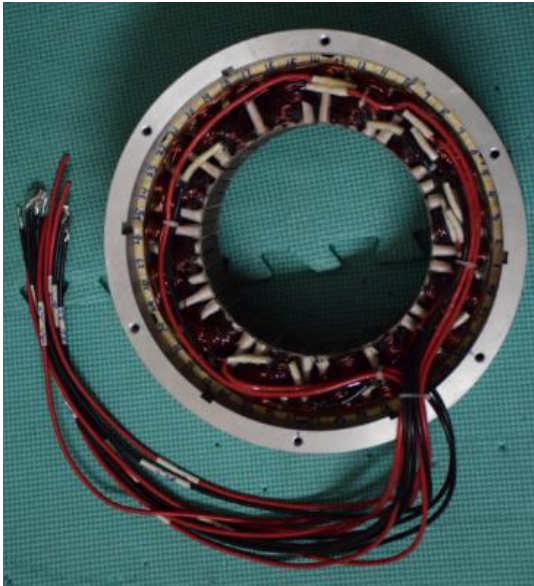
<div style="text-align:center">(c)</div>

<div style="text-align:center">(d)</div>

Fig. 7.10. (a) The inner rotor; (b) the outer rotor; (c) the stator; (d) the whole prototype of the DFDR-PM.
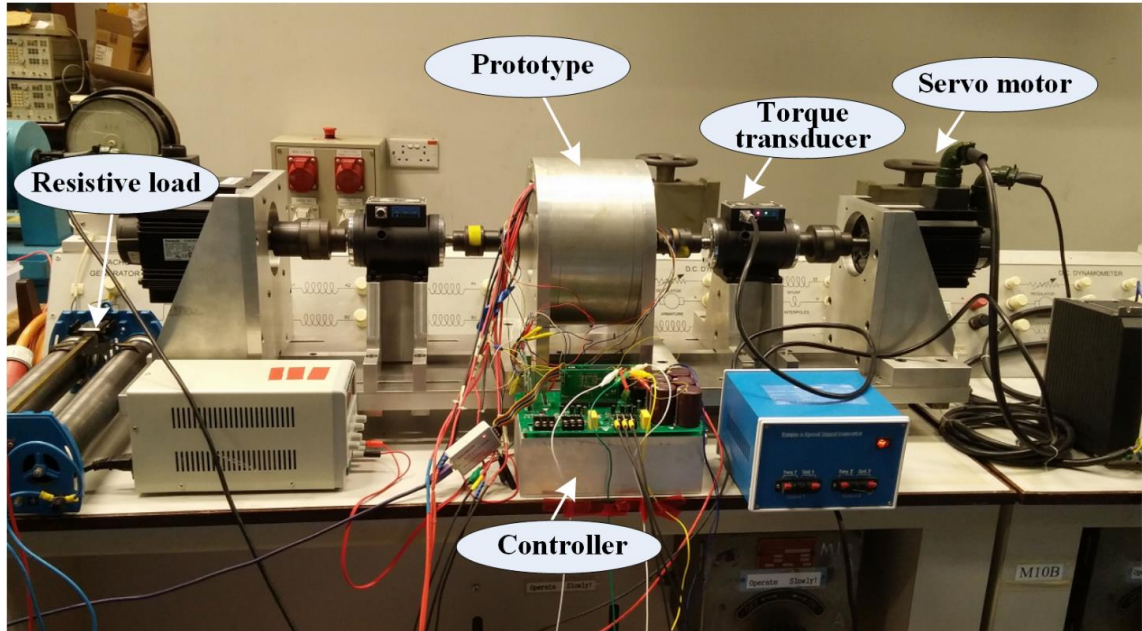
Fig. 7.11. The test bed.

A. Field and Back-EMF

Using FEM, the PM field is computed. The airgap flux density and the corresponding spectra are depicted in Fig. 7.12. Besides the largest fundamental components N_{ri} and N_{ro}, four harmonic components $2N_{ri}$, $2N_{ro}$, $N_{ro} - N_{ri}$, and $N_{ro} + N_{ri}$ are also significant. This FEM results agree well with the theoretical analysis given in Section 7.3.1. Under the rated load, the magnetic flux density and the flux lines are plotted in Fig. 7.13. The maximum flux density is about 2 T which is acceptable for the silicon steel used.
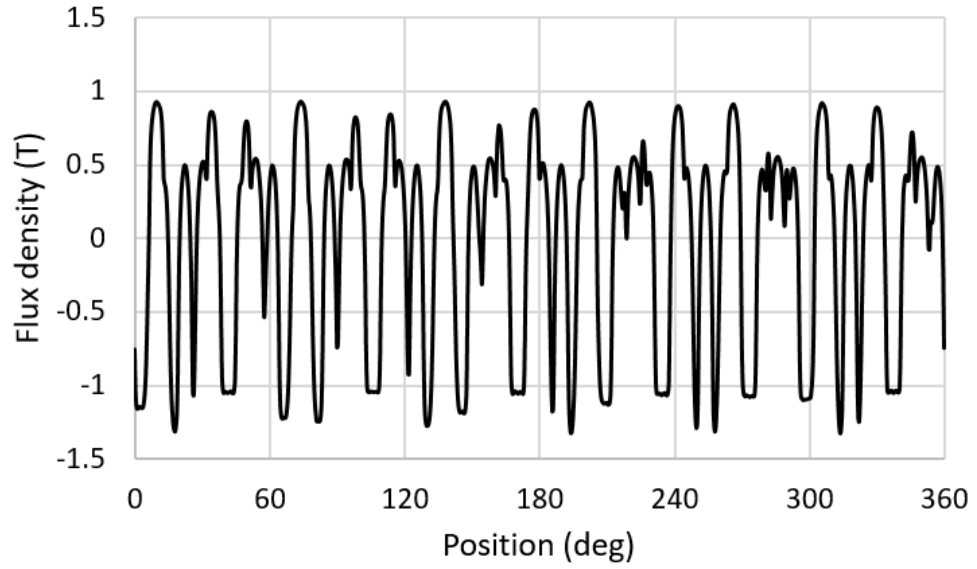
(a)
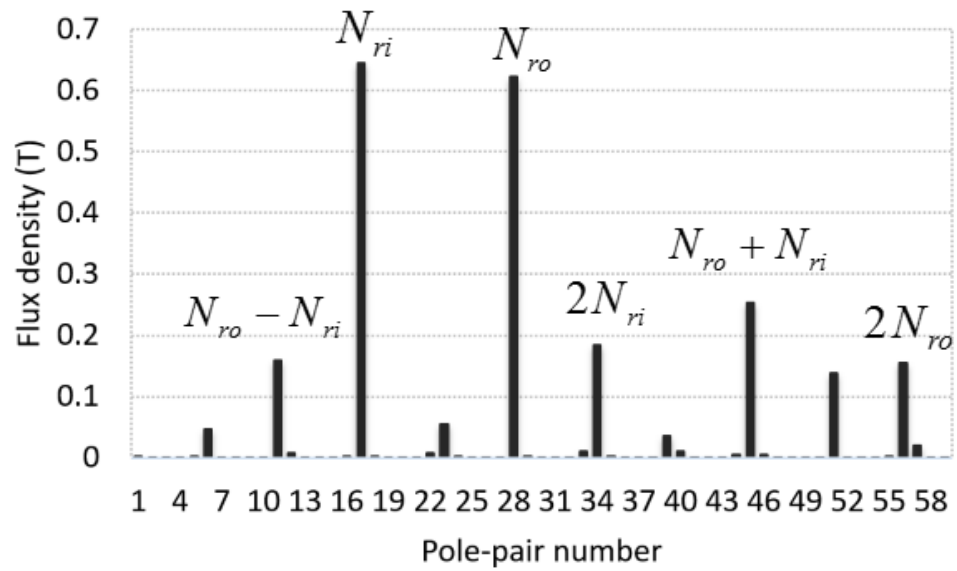
(b)

Fig. 7.12. (a) The PM flux density in the airgap and (b) the corresponding spectra.
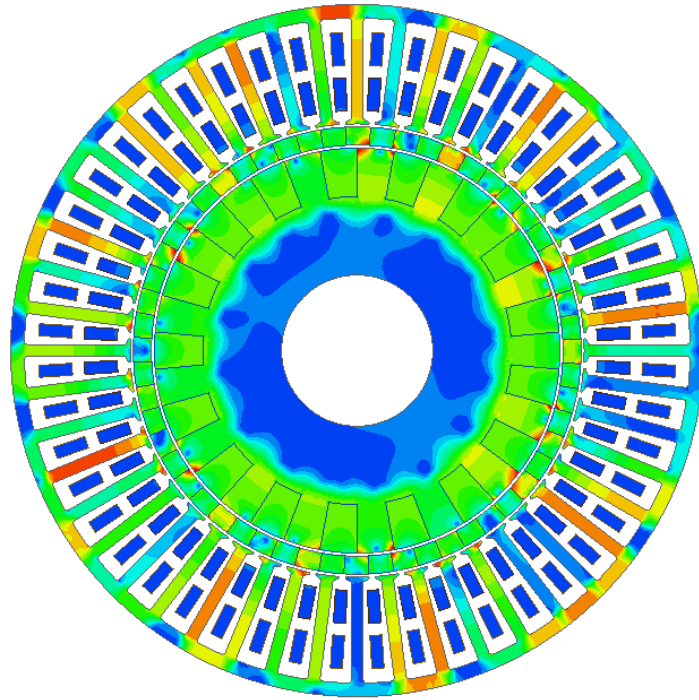
(a)
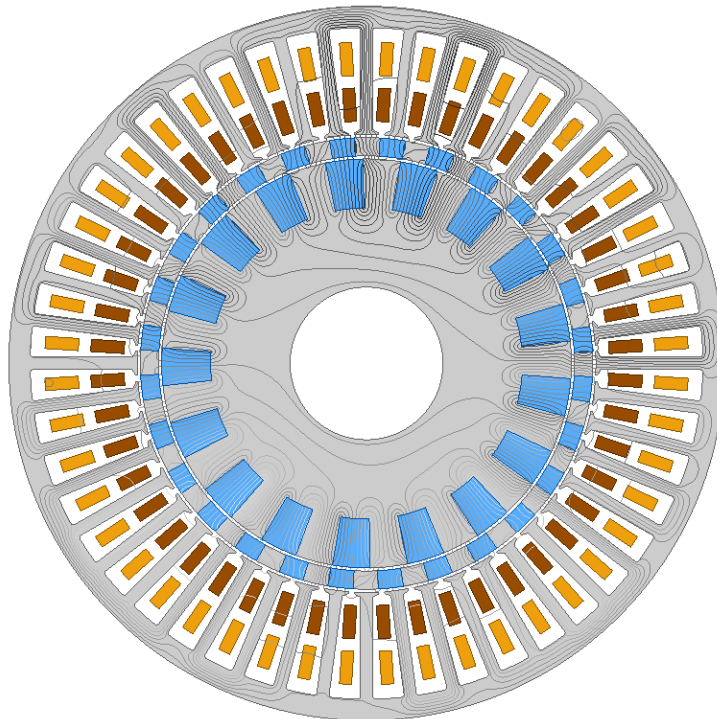
(b)

Fig. 7.13. (a) The flux density map, and (b) the flux line plot at the rated load.

The back-EMFs in two sets of windings during subsynchronous and synchronous operation and the corresponding harmonic spectra are shown in Figs. 7.14 - 7.17. For subsynchronous operation, the speed of the inner rotor is set at 100 rpm.

a) For the subsynchronous operation, the frequency of the back-EMF in the primary winding is around 18.3 Hz, which corresponds with the theoretical analysis in Eq. 7.7. The back-EMF of the primary winding is less sinusoidal than that of the secondary winding. The reason is that the primary winding has a pole-pair number of N_{ro} - N_{ri}. It is shown in Fig. 7.12(b) that this harmonic component of the airgap flux has smaller amplitude than the N_{ro} component which is the fundamental component for the secondary winding. The asynchronous harmonics of the airgap flux cause more significant distortion for the primary winding back-EMF.

b) The experimental and FEM results are generally in agreement, especially for the secondary winding back-EMF. In Fig. 7.14(a), the experiment result has larger distortion than the FEM result. The possible reasons are the small ripples in the inner rotor speed during the test. Also, the back-EMF of the primary winding is easier to be affected since its magnitude is small.

c) During synchronous operation, the back-EMF in the primary winding is close to zero. The reason is that the speed of the effective harmonic component is zero according to Eq. 7.6.

d) When the speed of the inner rotor changes from subsynchronous to synchronous, the back-EMF in the secondary winding is constant while the back-EMF in the primary winding changes accordingly. In the WECS, when the current frequency of the primary winding is intentionally controlled to vary with the speed of the inner rotor, the outer rotor speed

can be kept constant and hence the output voltage can be kept constant. In this way, the WECS can be used for VSCF operation.

(a)

(b)

(c)
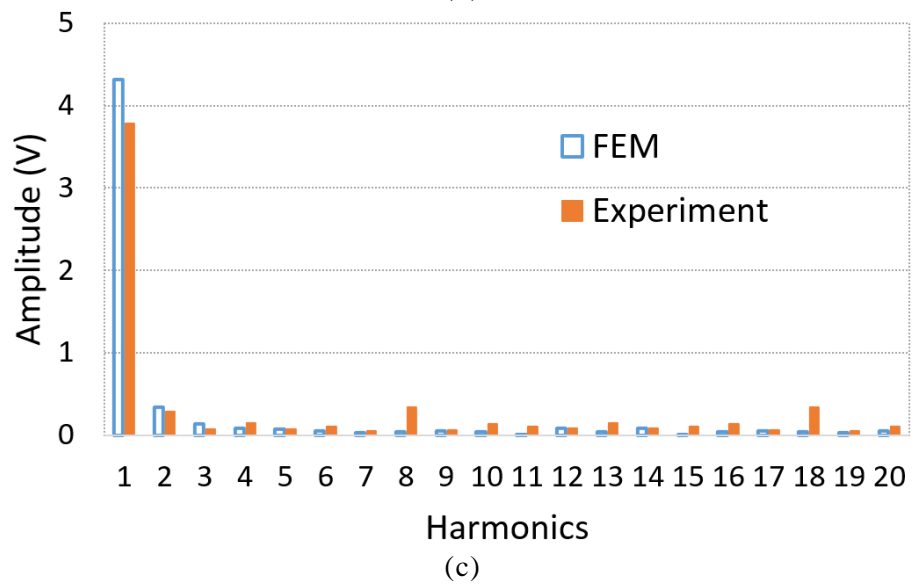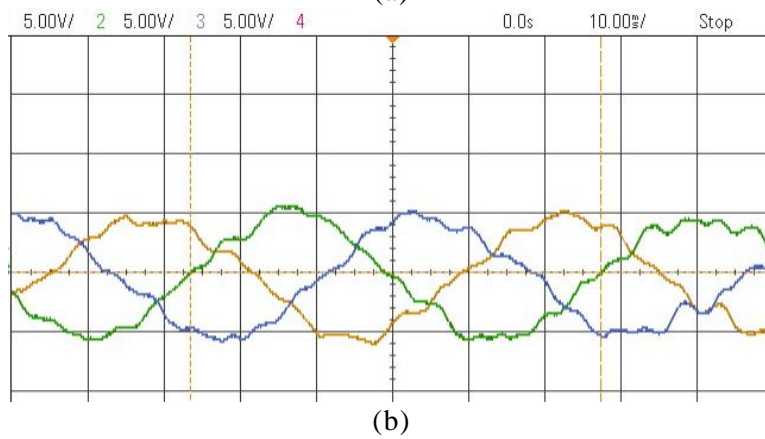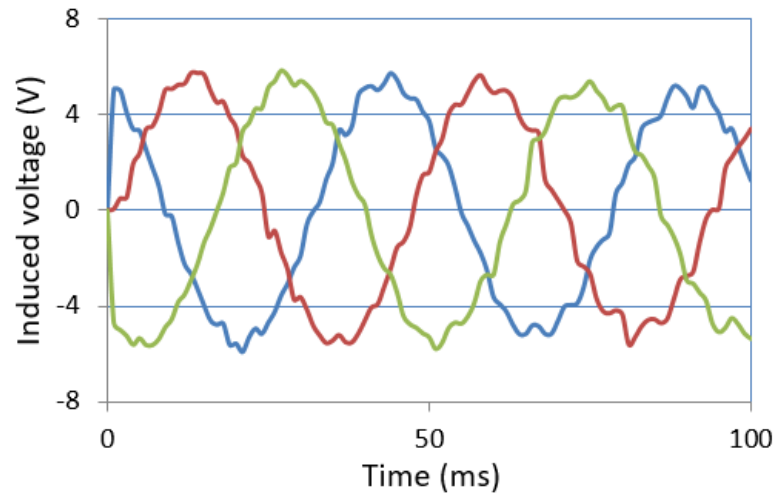
Fig. 7.14. The back-EMF during subsynchronous operation in the primary winding, (a) The FEM result, (b) the experiment result, and (c) the corresponding harmonic spectra.
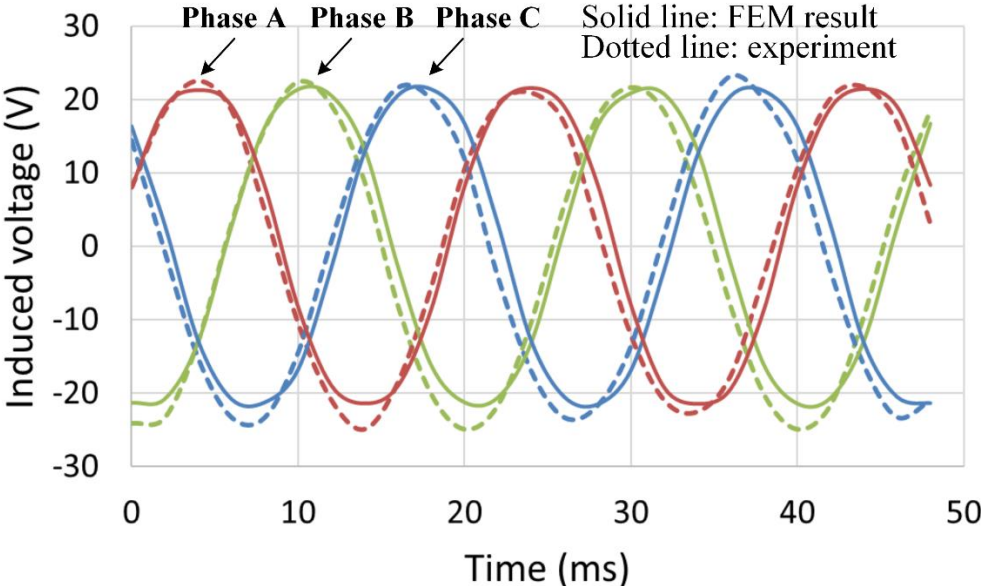
(a)
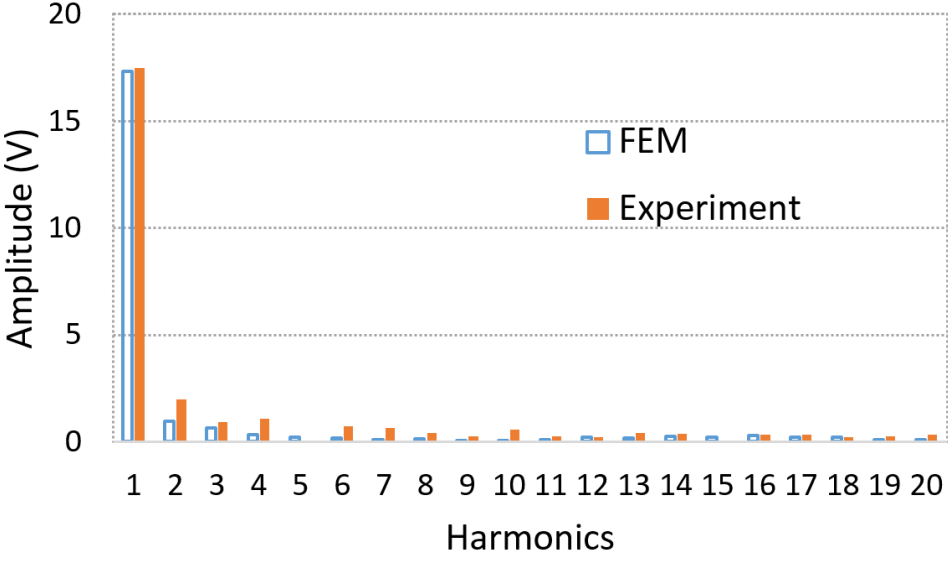
(b)

Fig. 7.15. (a) The back-EMF during subsynchronous operation in the secondary winding, and (b) the corresponding harmonic spectra.
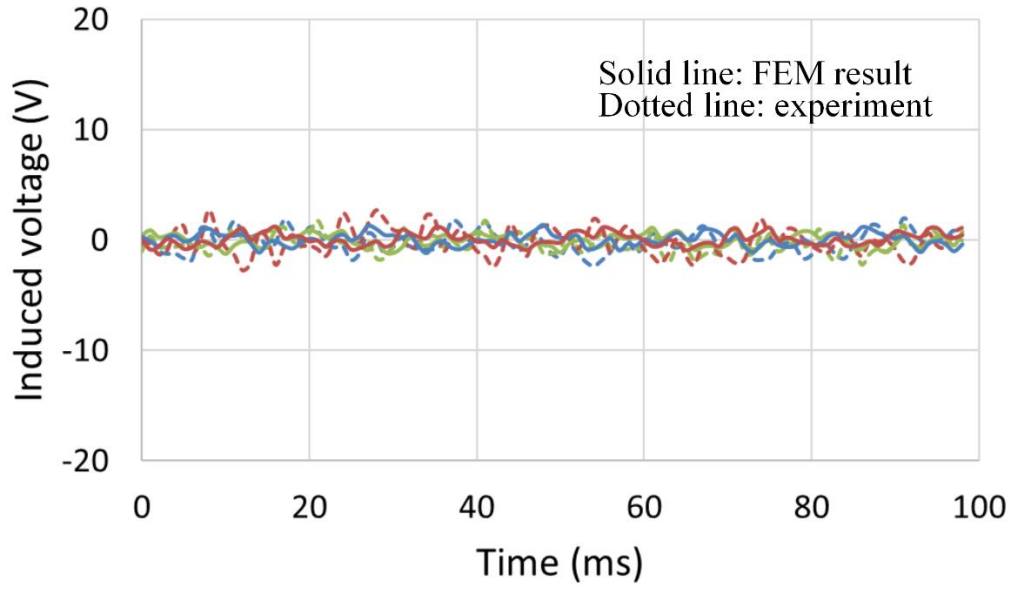
Fig. 7.16. The back-EMF during synchronous operation in the primary winding.
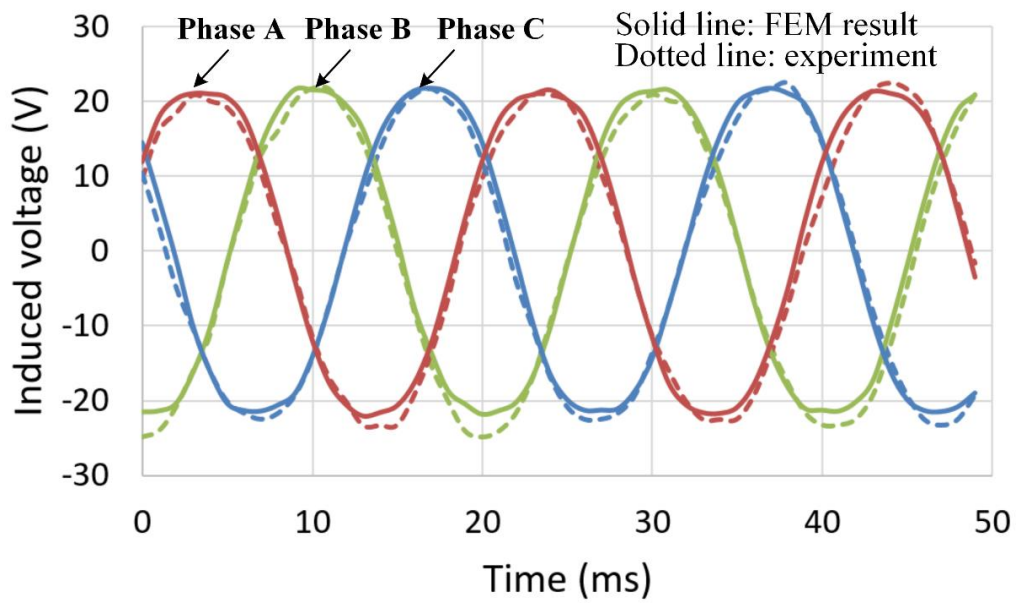
(a)
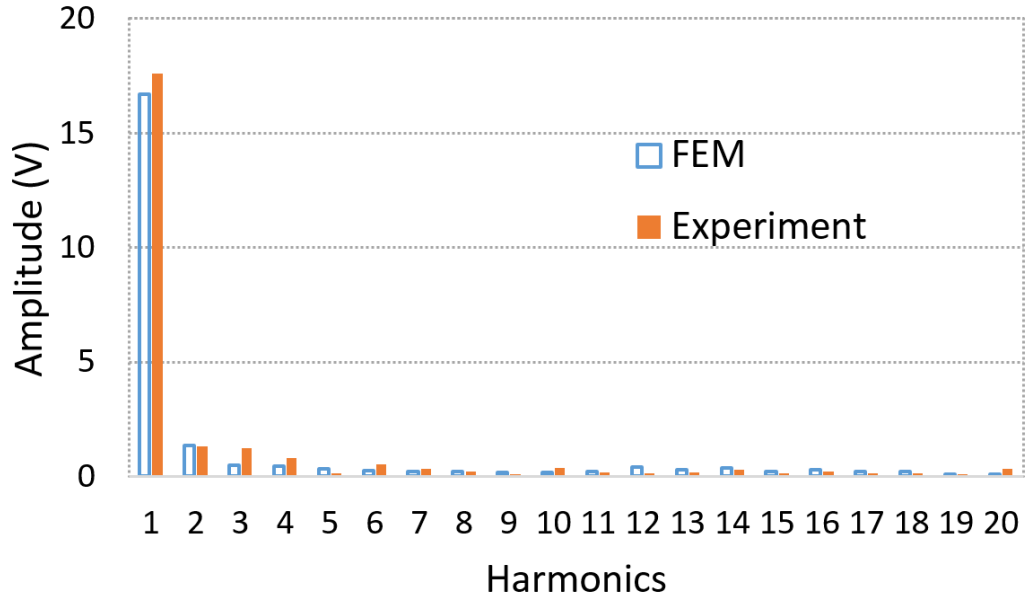
(b)

Fig. 7.17. (a) The back-EMF during synchronous operation in the secondary winding and (b) the corresponding harmonic spectra.

B. Operation under Load Conditions

In the beginning, the performances of the E-CVT part and the generator part are tested separately. For the test of the E-CVT part, the outer rotor is locked and the inner rotor is driven by the primary winding. At different inner rotor speeds and torque loads, the losses and efficiency are shown in Fig. 7.18. The copper loss is calculated simply by Joule's first law and it increases with the winding current. The sum of coreloss and the mechanical loss are measured by reducing the copper loss from the total loss. This part of losses increases with both the load torque and the rotor speed. For the generator part test, the outer rotor is driven by a servo motor and the secondary winding is connected to a resistive load. The losses and efficiency of the generator part are shown in Fig. 7.19.
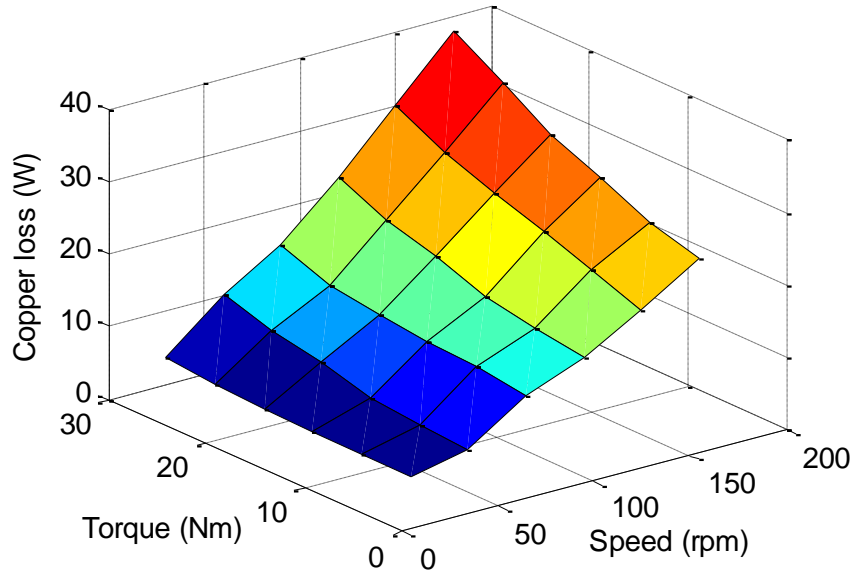
(a)
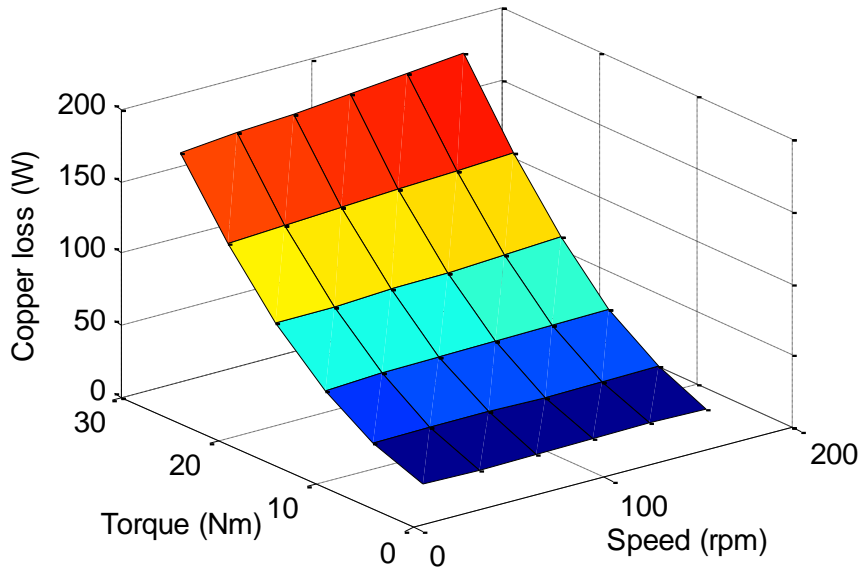
(b)
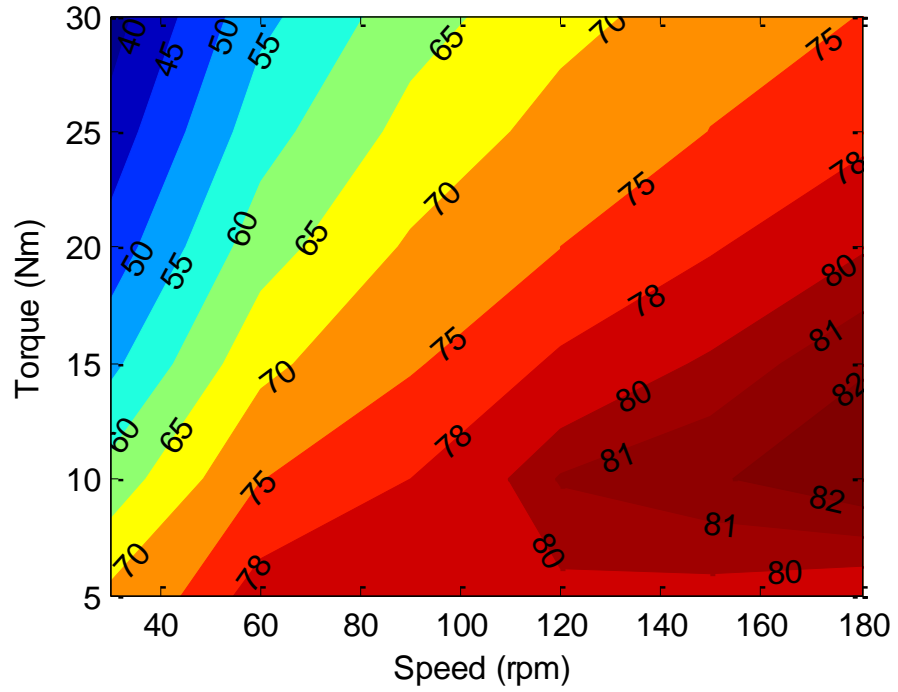
(c)

Fig. 7.18. (a) Coreloss and mechanical loss, (b) copper loss, and (c) efficiency of the E-CVT part at different inner rotor speeds and torque.
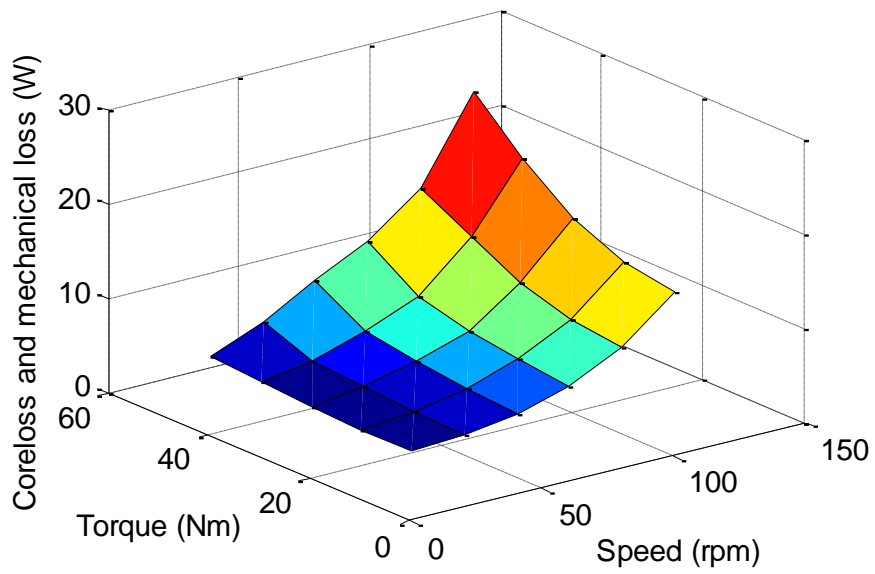
(a)
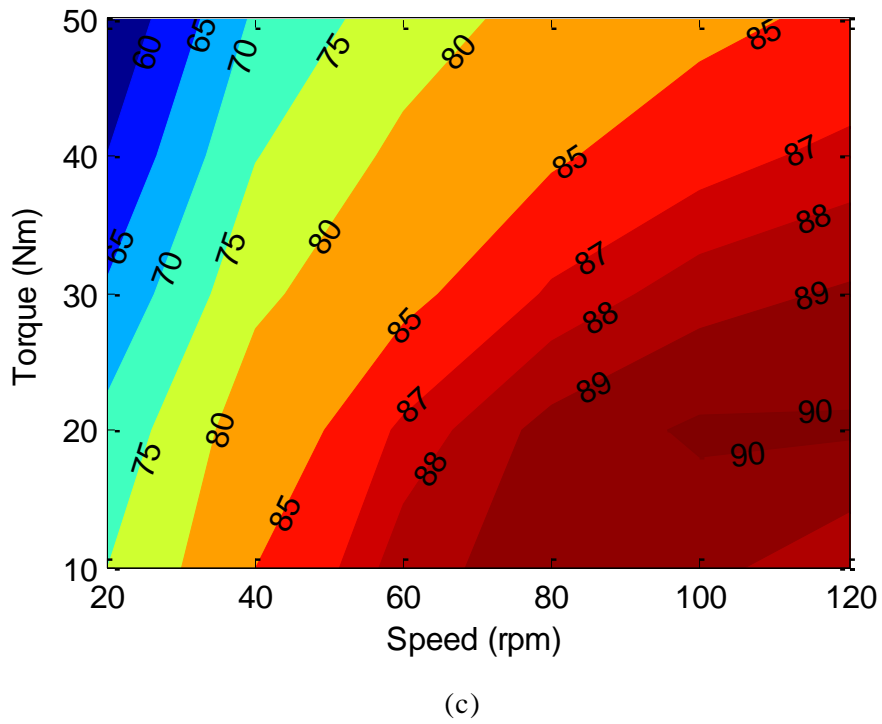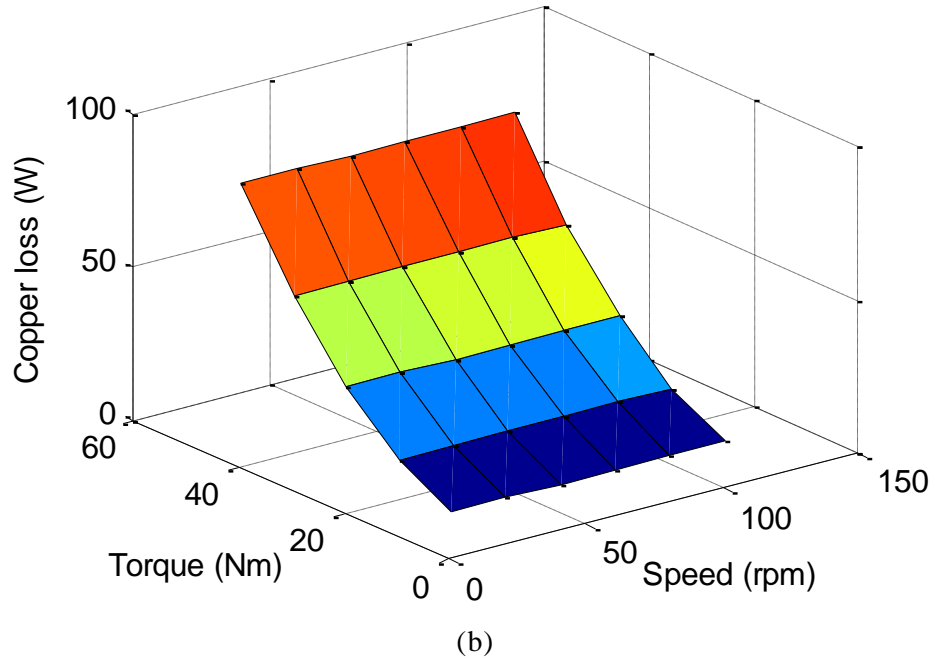
Fig. 7.19. (a) Coreloss and mechanical loss, (b) copper loss, and (c) efficiency of the generator part at different outer rotor speeds and torque.

For the test of the DFDR-PM, the secondary winding is connected to a resistive load. The inner rotor is driven by a servo motor at different

speeds while the outer rotor speed is kept constant, namely 107 rpm, by the primary winding. Assuming the efficiency of the converter to be 1, the losses and efficiency of the DFDR-PM under different input speeds and torques from the servo motor are shown in Fig. 7.18. The input power includes both the mechanical power from the servo motor and the electric power from the primary winding.

Note that as the two windings have different pole numbers, the two parts of DFDR-PM do not have significant influence on each other except for the saturation issue. Since the flux density is not high in this design as shown in Fig. 7.13(a), the saturation problem can also be neglected.

When the inner rotor is at 120 rpm and the outer rotor is at 107 rpm stably under the rated load, the torque from the outer rotor is measured in comparison with FEM analysis results as shown in Fig. 7.21.

a) As we have considered the cogging torque factor for the design of the pole number combination, the torque ripple is generally acceptable.

b) For the outer rotor, the torque due to the primary winding and the torque due to the secondary winding are canceling each other, which makes it a floating rotor.

c) The electromagnetic torque of the inner rotor is around 27 Nm. This torque is to be cancelled out by the mechanical torque from the wind blades in the WECS. In this experiment, it is balanced by the servo motor instead.
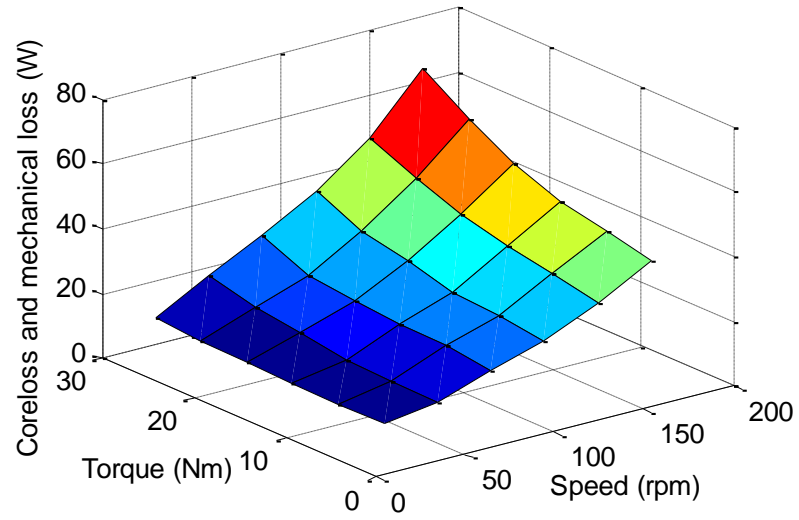
(a)
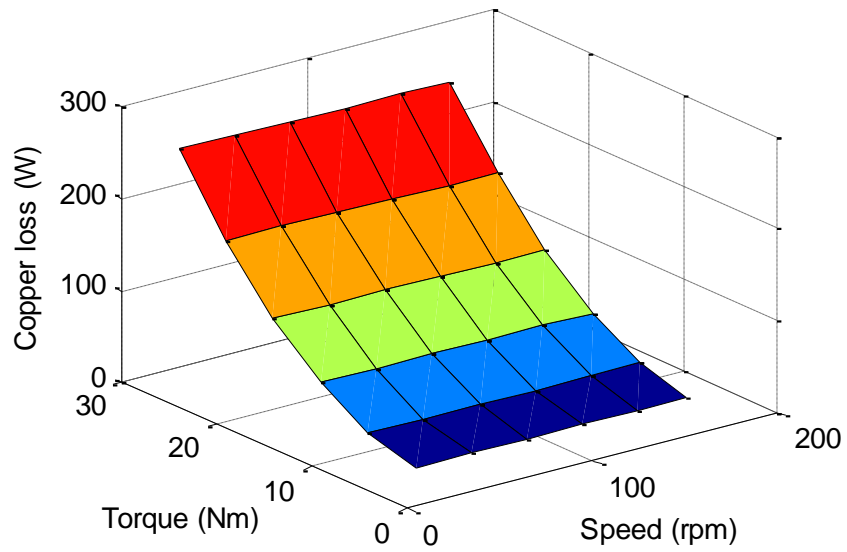
(b)
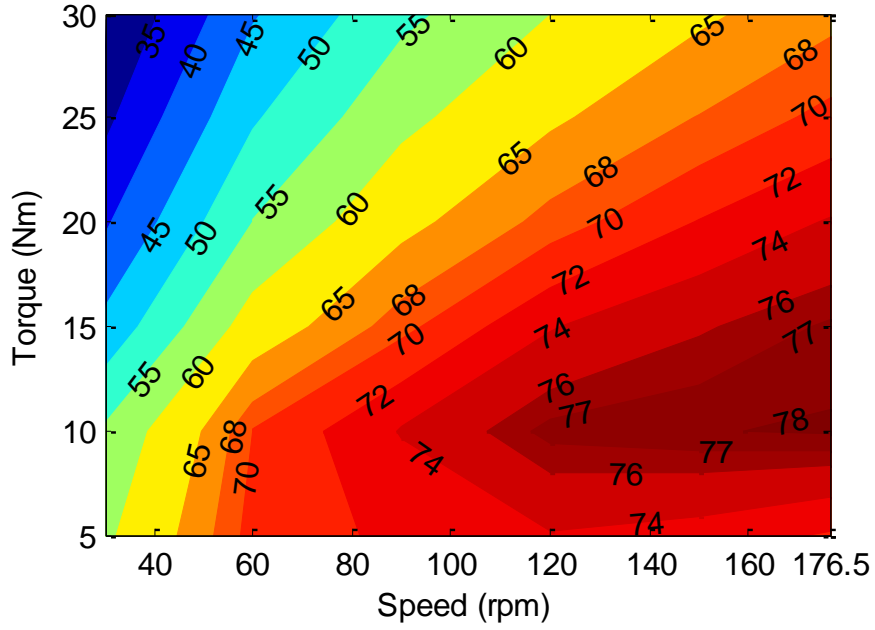
(c)

Fig. 7.20. (a) Coreloss and mechanical loss, (b) copper loss, and (c) efficiency of the DFDR-PM at different inner rotor speeds and torque.
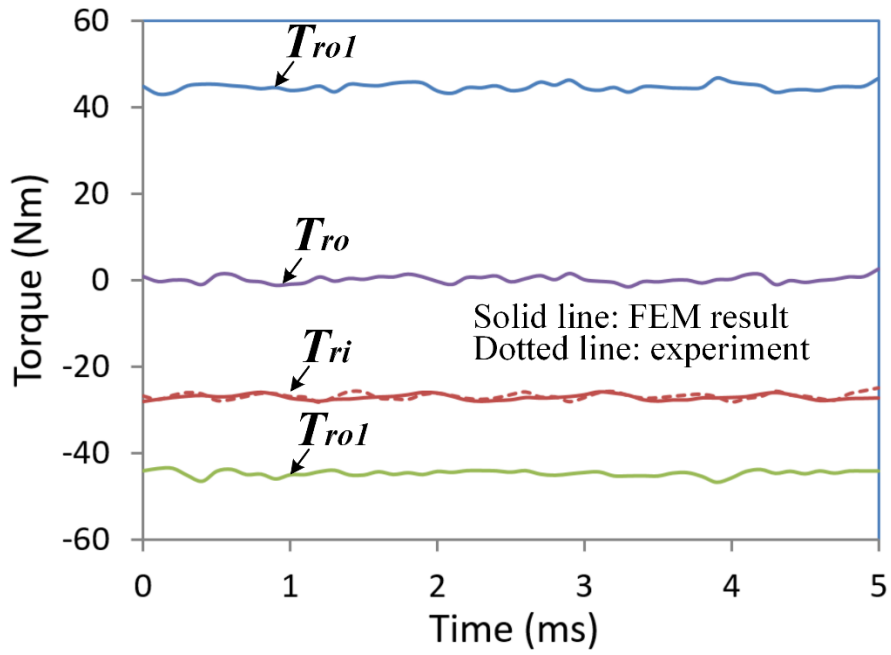
Fig. 7.21. Electromagnetic torque of two rotors.
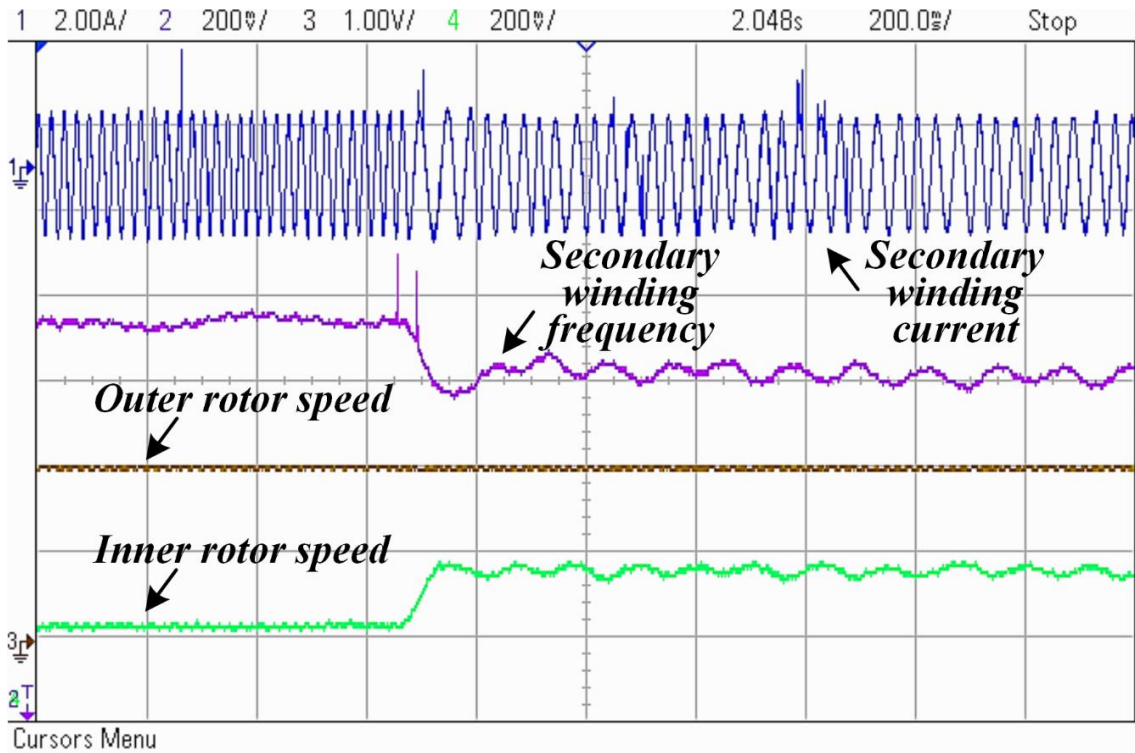
Fig. 7.22. System dynamics when the inner rotor speed changes.

A simple test for the dynamics of the system in VSCF operation is also conducted as shown in Fig. 20. Obviously, when the inner rotor speed increases, the frequency of the controlled current in the secondary winding decreases so that the speed of the outer rotor is kept constant.

7.4 Conclusion

A novel WECS concept based on E-CVT is proposed for VSCF wind power generation. The basic idea is to realize variable-speed operation by compensating the power from the wind turbine. Utilizing the flux modulation effect among the windings and rotors, the frequency of the output voltage is decoupled with the wind turbine speed. By artfully integrating a flux modulation machine with a conventional PM machine,

this system realizes the speed matching and power generation within one single machine. Compared with previous WECS concepts, this system has the advantage of being gearless and brushless and it needs only a partial scale converter, which means to incorporate the merits of the popular DFIG system and direct drive PMSG system. The working principle and design of the core DFDR-PM are introduced. The performance of the DFDR-PM is validated by both FEM simulation and experimental results.

References – part G

[G1]   Annual market update 2014: Global Wind Report.

[G2]   H. Polinder, J. A. Ferreira, B. B. Jensen, A. B. Abrahamsen, K. Atallah, and R. A. McMahon, "Trends in wind turbine generator systems", *IEEE Trans. Emerg. Sel. Topics Power Electron*, vol. 1, no. 3, pp. 174-185, 2013.

[G3]   M. Liserre, R. Cardenas, M. Molinas, and J. Rodriguez, "Overview of multi-MW wind turbinesand wind parks", *IEEE Trans. Ind. Electron.*, vol. 58, no. 4, pp.1081 -1095, 2011.

[G4]   Yaramasu V., Bin Wu, Sen P.C., Kouro S., and Narimani M., "High-power wind energy conversion systems: State-of-the-art and emerging technologies," *Proc. IEEE*, vol.103, no.5, pp.740-788, May 2015.

[G5]   H. Gorginpour, H. Oraee, and R. A. McMahon, "Electromagnetic-thermal design optimization of the brushless doubly-fed induction generator", *IEEE Trans. Ind. Electron.*, vol. 61, no. 4, pp. 1710-1721, 2014.

[G6]   L. Greedy, *Review of Electric Drive-Train Topologies*. Bristol, U. K.: Garrad Hassan and Partners, May 2007, 11593/BR/01.

[G7]   E. Camm et al., "Characteristics of wind turbine generators for wind power plants", in Proc. IEEE Power Energy Soc. (PES) Gen. Meet., Calgary, AB, Canada, Jul. 2009, pp. 1–5.

[G8]   C. Rossi, P. Corbelli, and G. Grandi, "W-CVT continuously variable transmission for wind energy conversion system," in *Proc. IEEE Conf. Power Electron. Mach. Wind Appl.*, Jun. 2009, pp. 1–10.

[G9]   K. Atallah, J. B. Wang, S. D. Calverley, and S. Duggan, "Design and operation of a magnetic continuously variable transmission," *IEEE Trans. Ind. Appl.*, vol. 48, no. 4, pp. 1288–1295, Jul./Aug. 2012.

[G10]   X. Sun, M. Cheng, Y. Zhu, and L. Xu, "Application of electrical variable transmission in wind power generation system," *IEEE Trans. Ind. Appl.*, vol. 49, no. 3, pp. 1299–1307, May/Jun. 2013.

[G11]   K. Atallah, S. D. Calverley, and D. Howe, "Design, analysis and realization of a high-performance magnetic gear," *IEE Proc.—Electric Power Appl.*, vol. 151, no. 2, Mar. 2004, pp. 135–143.

[G12]   Z. Q. Zhu, Z. P. Xia, L. J. Wu and G. W. Jewell, "Influence of slot and pole number combination on radial force and vibration modes in fractional slot PM brushless machines having single and double layer windings," *ECCE 2009*, Sept 20-24. 2009, pp. 3443-3450.

[G13]   B. Prieto, M. Martinez-Iturralde, L. Fontan and I. Elosegui, "Analytical calculation of the slot leakage inductance in fractional-slot concentrated-winding machines", *IEEE Trans. Ind. Electron.*, vol. 62, no. 5, pp. 2742-2752, May. 2015.

[G14]   S. Niu, S. L. Ho, and W. N. Fu, "Design of a Novel Electrical Continuously Variable Transmission System Based on Harmonic Spectra Analysis of Magnetic Field," *IEEE Trans. Magn.*, vol.49, no.5, May 2013, pp.2161-2164.

[G15]   Z. Q. Zhu and D. Howe, "Influence of design parameters on cogging torque in permanent magnet machines," *IEEE Trans. Magn.*, vol. 15, no. 5, May 2000, pp. 407–412.

[G16]   M. G. Say, *Performance and design of AC machines*, Pitman, London, 1970, ISBN: 273 40199 8.

[G17]   B. Kim and T. A. Lipo, "Operation and Design Principles of a PM Vernier Motors", *IEEE Trans. Industry Applications*, vol. 50, No. 6, 2014, pp. 3656-3663.

Chapter 8

Summary, contributions and recommendations

In this thesis, the design, analysis, and application of a new electric machine concept, namely the FM machines, are studied. At first, the historical development of different types of FM machines is reviewed. A comprehensive insight into the flux modulation effect is then taken by analyzing a magnetic gear model, after which a unified theory of FM machines is proposed. The theory is then used to derive different FM machines and explain their working principles. The general design principles of different components in FM machines are briefly introduced. A quantitative comparison among different FM machines is conducted to investigate their pros and cons, after which the potential applications of these machines are identified accordingly. As an example, a DFRM and a doubly-fed dual-rotor FM machine are proposed for EV propulsion and wind energy conversion, respectively. Prototypes of these two machines are made and tested for validation.

The main merits of FM machines can be summarized as follows. 1) Flexible pole design. As the pole numbers can be different for the rotor and the stator winding, the FM machines are particularly suitable for low speed applications where high pole numbers are needed. 2) Capability of offering multi-mechanical / electrical port. The existence of FMPs naturally offers an additional mechanical port when they are used as a rotor. It is also possible to add an extra electrical port in relation to the

PM rotor without using the flux modulation effect. The FM machines are hence an attractive choice for power splitting, which makes them suitable to be used in HEV and wind energy conversion. 3) Capability of realizing a robust reluctance rotor structure with PM housed in the stator.

The main drawback of FM machines is that, due to flux modulation, the flux leakage increases and their power factors are usually not as high as those of the conventional PMSMs, which increases the copper loss.

The following areas are recommended for future research. 1) FM machines with single rotor are considered in the performance comparison in this thesis. The performance of multi-rotor designs can be further studied. 2) FM machines with axial flux, transverse flux, or linear configurations need to be studied. 3) A common method for the improvement of power factor is worth investigating. 4) Simple single-objective GA is used for optimization in this thesis. Other algorithms and multi-objective optimization of the FM machines can be investigated. 5) The potential of FM machines for more applications needs to be studied, such as in robotics, wave energy harvesting, and railway transportation.